NAVAL POSTGRADUATE SCHOOL
MONTEREY, CALIFORNIA

THESIS

TEMPORAL EFFECTS OF SHIPTRACKS
ON CLOUDS

by

Andrew Brown III

March, 1995

Thesis Advisor: Philip A. Durkee

Approved for public release; distribution is unlimited.

DISCLAIMER NOTICE

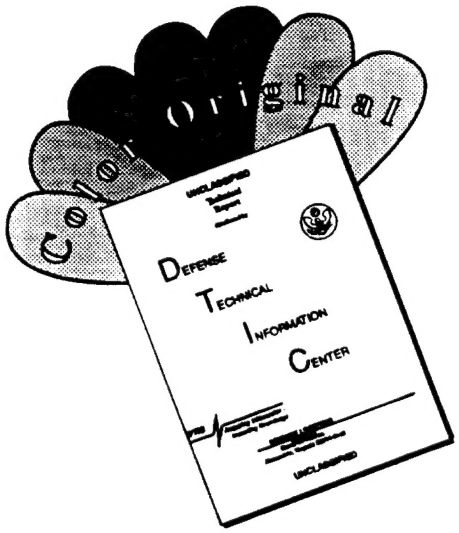

THIS DOCUMENT IS BEST QUALITY AVAILABLE. THE COPY FURNISHED TO DTIC CONTAINED A SIGNIFICANT NUMBER OF COLOR PAGES WHICH DO NOT REPRODUCE LEGIBLY ON BLACK AND WHITE MICROFICHE.

REPORT DOCUMENTATION PAGE

Form Approved OMB No. 0704-0188

1. AGENCY USE ONLY *(Leave blank)*	2. REPORT DATE	3. REPORT TYPE AND DATES COVERED
	March 1995	Master's Thesis

4. TITLE AND SUBTITLE TEMPORAL EFFECTS OF SHIPTRACKS ON CLOUDS

5. FUNDING NUMBERS

6. AUTHOR(S) Andrew Brown III

7. PERFORMING ORGANIZATION NAME(S) AND ADDRESS(ES)
Naval Postgraduate School
Monterey CA 93943-5000

8. PERFORMING ORGANIZATION REPORT NUMBER

9. SPONSORING/MONITORING AGENCY NAME(S) AND ADDRESS(ES)

10. SPONSORING/MONITORING AGENCY REPORT NUMBER

11. SUPPLEMENTARY NOTES The views expressed in this thesis are those of the author and do not reflect the official policy or position of the Department of Defense or the U.S. Government.

12a. DISTRIBUTION/AVAILABILITY STATEMENT
Approved for public release; distribution is unlimited.

12b. DISTRIBUTION CODE

13. ABSTRACT *(maximum 200 words)*

The physical and optical characteristics of 27 shiptracks are analyzed using AVHRR satellite data. Channel 1 (.63μm), and channel 3 (3.7μm), are utilized to determine the temporal variations in shiptrack albedo and track width. In most cases, shiptracks mirror the trend of albedo changes exhibited by the ambient clouds in which they are formed. Under special circumstances, shiptrack albedo increases when ambient cloud albedo decreases due to cloud thinning. Shiptrack widths show uniformity of growth, with rapid growth rates of 4-6 km/hr in the near-source region, decreasing to 1-2 km/hr in the far field. Maximum width ranges from 10 to 12 kilometers. Predicted growth rates based on a parameterization of the standard deviation of plume concentration correlate well with observed track width values.

14. SUBJECT TERMS Shiptrack, AVHRR, aerosol, albedo, plume concentration			15. NUMBER OF PAGES 133
			16. PRICE CODE
17. SECURITY CLASSIFICATION OF REPORT Unclassified	18. SECURITY CLASSIFICATION OF THIS PAGE Unclassified	19. SECURITY CLASSIFICATION OF ABSTRACT Unclassified	20. LIMITATION OF ABSTRACT UL

NSN 7540-01-280-5500

Standard Form 298 (Rev. 2-89)
Prescribed by ANSI Std. 239-18 298-102

Approved for public release; distribution is unlimited.

TEMPORAL EFFECTS OF SHIPTRACKS
ON CLOUDS

by

Andrew Brown III
Lieutenant Commander, United States Navy
B.A., San Diego State University, 1982

Submitted in partial fulfillment
of the requirements for the degree of

MASTER OF SCIENCE IN METEOROLOGY AND OCEANOGRAPHY

from the

NAVAL POSTGRADUATE SCHOOL
March 1995

Author: _____
Andrew Brown III

Approved by: _____
Philip A. Durkee, Thesis Advisor

_____
Kenneth L. Davidson, Second Reader

_____
Robert L. Haney, Chairman
Department of Meteorology

ABSTRACT

The physical and optical characteristics of 27 shiptracks are analyzed using AVHRR satellite data. Channel 1 (.63μm), and channel 3 (3.7μm), are utilized to determine the temporal variations in shiptrack albedo and track width. In most cases, shiptracks mirror the trend of albedo changes exhibited by the ambient clouds in which they are formed. Under special circumstances, shiptrack albedo increases when ambient cloud albedo decreases due to cloud thinning. Shiptrack widths show uniformity of growth, with rapid growth rates of 4-6 km/hr in the near-source region, decreasing to 1-2 km/hr in the far field. Maximum width ranges from 10 to 12 kilometers. Predicted growth rates based on a parameterization of the standard deviation of plume concentration correlate well with observed track width values.

TABLE OF CONTENTS

ACKNOWLEDGEMENTS

I would like to thank Dr. Philip A. Durkee of the Department of Meteorology at the Naval Postgraduate School for his support and guidance through this entire project. I would also like to thank Drs. Kenneth L. Davidson and Robert L. Haney for their insightful review and comment of this manuscript. I owe a special debt of gratitude to Mr. Chuck Skupniewicz and Mr. Kurt Nielsen whose technical expertise kept me from running aground time after time. Finally, I want to thank my wife, Debbie, and children, Andrew, Aaron, and Heather, for their unfailing love and support during this project. I would never have finished without it.

I. INTRODUCTION

Shiptracks have been observed in satellite images since the early 1960s when the early Television and Infrared Operational Satellites (TIROS) became operational (Connover, 1966). Initially detected in the visible portion of the spectrum, these "anomalous cloud lines" were suspected to have been caused by additional aerosol particles produced by ships (Connover, 1966; Twomey, 1968). The introduction of the Advanced Very High Resolution Radiometer (AVHRR) sensor onboard the NOAA polar orbiting satellites revealed that many more shiptracks were observable in the near-infrared at 3.7μm (channel 3 of the AVHRR) than previously noted in the visible imagery. This is clearly evident in Figures 1 and 2 which show shiptracks in channel 1 and channel 3, respectively, for the same image.

Perhaps the least understood aspect of shiptracks is exactly which combination of effluents generated by the ship contribute to track formation. Possibilities include: particles emitted directly from the ship's track; sea salt particles generated in the ship's wake; and particles produced after the oxidation of sulfur dioxide or another of the gases emitted by the ship. Figure 3 illustrates possible mechanisms for shiptrack production. More recent studies have furthered the understanding of the influence of ships on pre-existing clouds (Coakley et al, 1987) and have strengthened the correlation between ships and these "anomalous cloud lines" (Radke et al, 1989). Measurements from aircraft in a ship influenced cloud showed that cloud microphysical effects were important for the formation of tracks observed at 3.7μm wavelength (Radke et al, 1989: King, 1990). These aircraft measurements indicated that stack emissions from a ship passing under stable stratoform clouds served as a source of cloud condensation nuclei (CCN) which increased the number of water droplets and reduced the average droplet size. Cloud reflectance at 3.7μm is driven solely by water droplet radius, assuming cloud thickness greater than 100m. It is this decrease in droplet radius size that produces the increase in

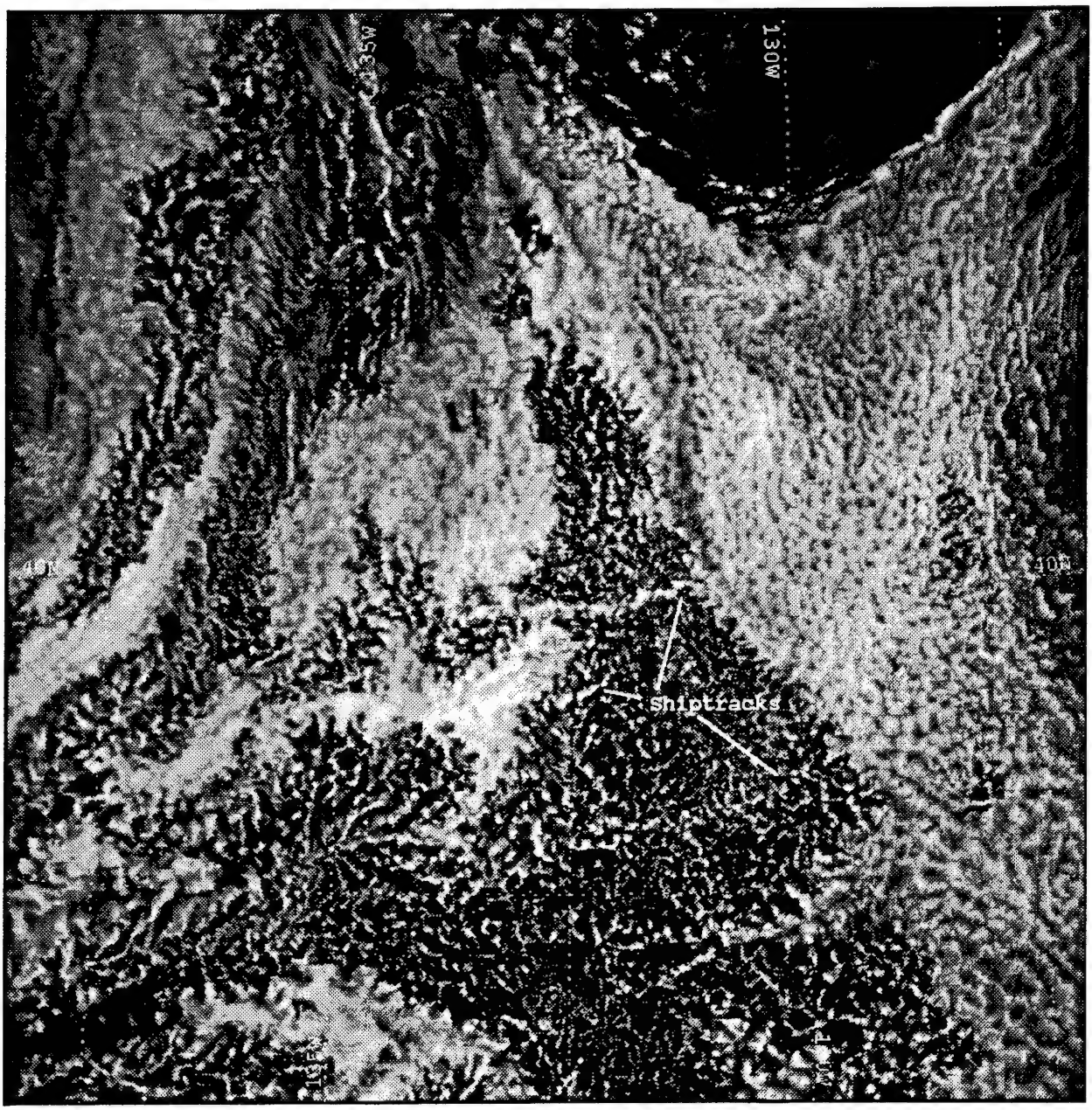

Figure 1. NOAA 09 1753 UTC 27 June 1994 Ch.1 Satellite Imagery Depicting Shiptrack Features.

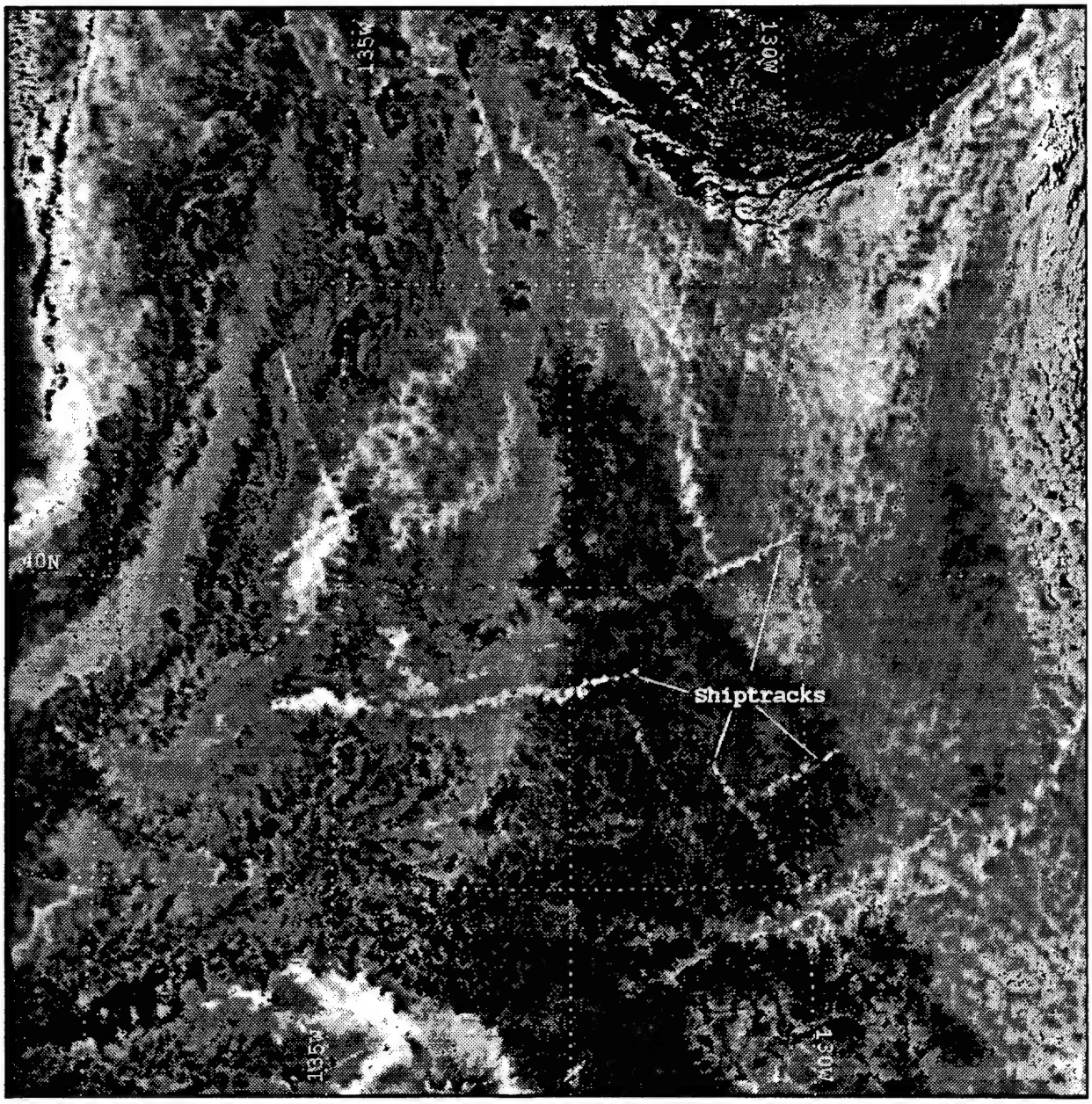

Figure 2. NOAA 09 1753 UTC 27 June 1994 Ch.3 Satellite Imagery Depicting Shiptrack Features. Notice how many more are discernable in Ch.3 than in Ch.1 (Figure 1).

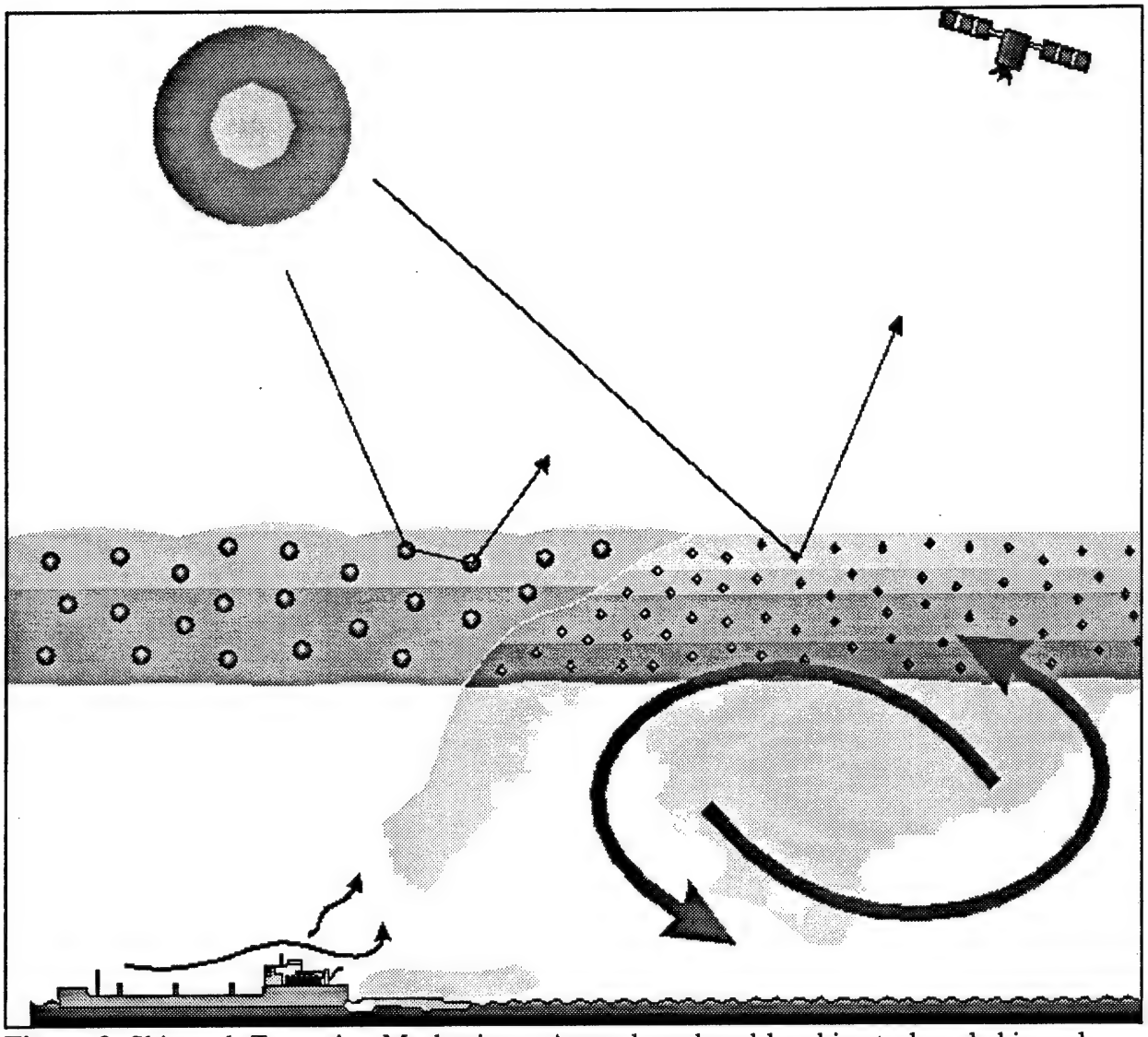

Figure 3. Shiptrack Formation Mechanisms. Aerosol produced by ship stack and ship wake are introduced into the Marine Atmospheric Boundary Layer (MABL). Large, curved arrows represent turbulent mixing in the MABL. Thin, linear arrows represent solar radiation at 3.7μm. Increased reflection of solar radiation at this wavelength from ship-influenced cloud is due to greater scattering by smaller radius water droplets formed by ship-produced aerosol. Lower reflection from uncontaminated cloud is due to greater absorption by larger radius water droplets at 3.7μm.

cloud albedo which is observed at 3.7μm wavelength. Hence, shiptrack features become much more evident in channel 3 imagery.

As observations of shiptracks increases, a clearer understanding of the processes behind shiptrack formation becomes an item of keen interest. The fact that a ship's stack emissions can leave a record of its passage under broad stratoform cloud regions (subject to nearly constant satellite surveillance) has significant tactical implications. One motivation for studying the physical processes involved is to be able to predict and perhaps prevent shiptrack occurrence. A more fundamental motivation is to understand how anthropogenic aerosols modify the reflectivity of clouds, and thus the earth's radiation balance. The perturbation of cloud albedo by anthropogenic aerosols is an indirect radiative effect which may have important consequences in terms of global climate (Charlson et al, 1987; Charlson et al, 1992; Albrecht, 1989).

Not all ships cause shiptracks. Throughout the world's shipping areas shiptracks are prevalent in some geographic locations and absent in others. Tracks which appear on a satellite image in an area conducive to their formation may disappear on a subsequent image only to reappear on a later one. There clearly must be a combination of ambient conditions necessary in the marine atmosphere before a specific ship will form a shiptrack.

Previous thesis studies on the shiptrack phenomenon have dealt with radiative characteristics of shiptracks formed in different ocean basins (Millman, 1992), effects of shiptracks as they are advected through different cloud transition regions (Evans, 1992), correlating shiptracks with specific ships (Pettigrew, 1992), shiptracks associated with specific propulsion types (Mays, 1993), and marine atmospheric boundary layer conditions conducive to shiptrack formation (Trehubenko, 1994; Brenner 1994). The objective of this thesis is to observe and describe the evolution of shiptrack physical and optical characteristics over time in order to further our understanding of the phenomenon. It will mark the first study in which multiple shiptracks over successive images associated with single ships are analyzed. This is an important undertaking because it will provide insight on how radiative characteristics of shiptracks from the same ship change when that ship

transits through changing environments. It will also give an indication of the dispersive nature of the environment through dilution of aerosol as each segment of track ages. This will hopefully lead to clues on the predictability of shiptrack characteristics in forecasted environmental conditions.

Chapter II will provide background, outline the method of approach of the study and will describe the data collection and analysis process. Chapter III will present the results of specific case studies conducted and Chapter IV will state conclusions and provide recommendations for further study.

II. METHODOLOGY

A. DATA

1. General

a. Monterey Area Shiptrack Experiment

The primary data source used in this analysis was satellite imagery collected during the Monterey Area Ship Track (MAST) experiment (CNO Project K-1420) conducted off the west coast of the U.S. in June, 1994. The MAST experiment was a joint U.S.-U.K. effort to analyze the shiptrack phenomenon and test hypotheses grouped in the following four categories: 1) aerosol/cloud interactions and detailed microphysics; 2) boundary layer perturbations by ships; 3) cloud dynamics; and 4) background environmental conditions. A detailed overview of the MAST experiment objectives can be found in the MAST Science Plan (Durkee, 1994).

The satellite imagery used for this study is from the Advanced Very High Resolution Radiometer (AVHRR) onboard the NOAA 9/10/11/12 satellites. These polar orbiting satellites are approximately 860 kilometers above the earth's surface, with the AVHRR continuously recording 2048 samples per scan line at pass center. The sensor scans upwelled radiation, both emitted and reflected energy, over five wavelength channels centered at 0.63μm, 0.86μm, 3.7μm, 11μm, and 12μm. This scanning geometry produces a pixel resolution of 1 km by 1 km at nadir. Up to 10 passes per day were obtained from this suite of four satellites, providing nearly constant surveillance of the MAST area. The greatest gap in coverage was between 4 to 6 hours.

Channel 3 of the AVHRR (3.7μm) was the primary channel used to determine low cloud reflectance. As discussed earlier, channel 3 reflectance is dependent upon droplet size only, while channel 1 reflectance is driven by droplet size, liquid water content, and cloud thickness. Raw reflectance data for channels 1 and 3 were processed to focus on reflectance values for clouds in the lower atmosphere, specifically in the Marine Atmospheric Boundary Layer (MABL) where shiptracks form and persist.

Initial satellite analysis after the MAST experiment revealed a cloud brightening bias resulting from anisotropic reflectance. The changing geometry of satellite, sun, and reflecting surface causes relative changes in shiptrack radiative characteristics from one image to the next. In order to make a temporal analysis meaningful, absolute reflectance of shiptracks must be compared. Applying a correction factor (anisotropic reflectance factor) removes this reflectance bias for each pixel. This process is explained in further detail in Brenner, 1994.

b. Climate

The northeastern Pacific is dominated by high pressure in the late spring and summer months. The presence and strength of the subtropical anticyclone creates stable conditions over the area with extensive stratus fields capped by a strong subsidence inversion. The MAST experiment was conducted in June to exploit these conditions which are extremely favorable for shiptrack formation.

2. Shiptrack Data Base

One objective of the experiment was to create a master shiptrack database, cataloging specific details of shiptrack and associated ship characteristics. To that end, satellite passes from each day during the experiment were reviewed for existence of shiptracks. Once these features were identified , a 1000 by 1000 kilometer subscene was created (or several, depending on the number and location of observed shiptrack-like features) to begin a process of shiptrack "extraction" from the satellite image. This is a multi-step process to create a file that contains the radiative signature of the shiptrack and the surrounding ambient cloud.

At the heart of the process is a shiptrack extraction algorithm developed at the Naval Postgraduate School by Nielsen and Durkee (1992). The shiptrack is first mapped by defining latitude/longitude points along its length. The algorithm linearizes the shiptrack then creates a 61 km swath about the track and assigns the centerline to the brightest pixels along the entire length. The algorithm then looks laterally out from the centerline to find the steepest reflectance gradient, which represents the edge of the track. At one kilometer beyond this gradient on both sides of the centerline, the next five pixels'

reflectance values are averaged to produce the ambient cloud brightness for a 1 km length of track. This process is continued for each 1 km segment over the length of the track.

3. Correlation of Shiptracks with Specific Ships

Over 1300 shiptracks were observed during the 30 day MAST period. Of those, 637 shiptracks were extracted using the process described above. Each extracted shiptrack was given a filename keyed to the sub-region from which it was mapped and sequenced according to the number within the sub-region. A master file of the "heads" of each extracted track (the exact beginning of the shiptrack) was compiled and coded to aid in the future correlation of ships to shiptracks. These "head" positions were further correlated one to another over successive satellite passes if they appeared to move in a linear fashion just as a ship would move along its transit path. These paths of shiptrack "heads" could then be compared to actual ship transit paths to determine possible correlations.

In order to correlate specific ships with individual shiptracks observed, it was necessary to obtain ship position data for all shipping types in the area for the month of June. As a first step in that direction, synoptic weather reports from ships during June 1994 were obtained from the Fleet Numerical Meteorology and Oceanography Center (FNMOC), Monterey, California. FNMOC maintains a database of these reports which include ship position, course and speed, and various meteorological and oceanographic parameters. Computer files of these reports were created for each synoptic hour (UTC hours of 0000, 0600, 1200, and 1800) of each day during the period of study. These files were then converted to latitude/longitude point files and superimposed on satellite images whose pass times were near the synoptic hour. Typically the passes occurred within 30 minutes of the hour and often within ten minutes.

As a starting point, position reports were superimposed on near-hour passes to determine if a reporting ship was in close proximity to an identified shiptrack. Figure 4 shows ship positions for 1800 UTC on 26 June, 1994, superimposed on the NOAA 09 AVHRR Ch.3 satellite image for 1800 UTC on the same day. Shiptrack features appear to emanate from several ship's reported positions. This is the first indication that particular ships are associated with specific shiptracks. Using a parallel approach, the shiptrack

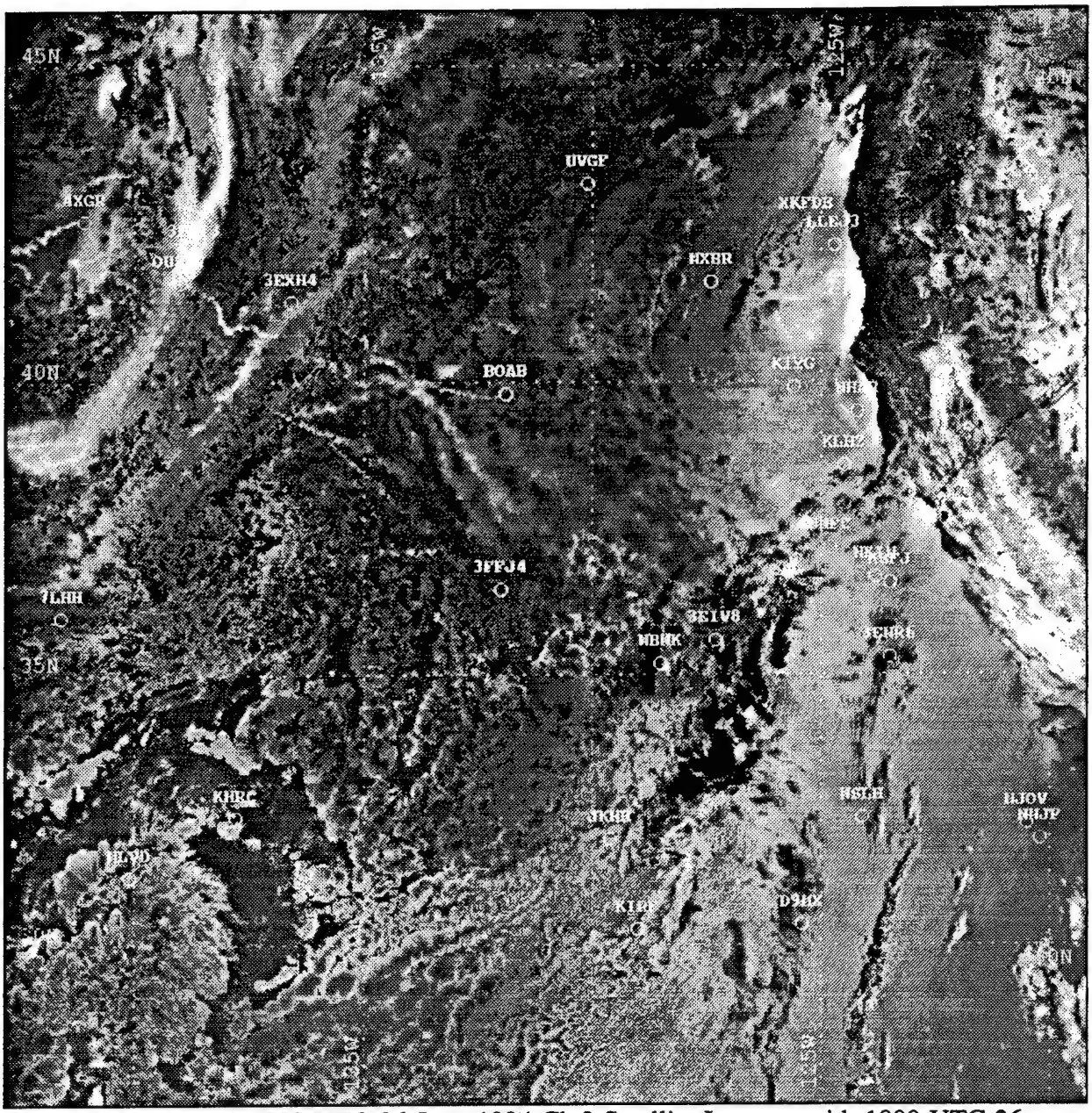

Figure 4. NOAA 09 1800 UTC 26 June 1994 Ch.3 Satellite Imagery with 1800 UTC 26 June 1994 ship positions superimposed. Ship position data from FNMOC synoptic weather reports.

"head" positions were compared with all synoptic reports. They were screened by proximity in time and distance as possible correlations. If the heads were within three hours and 1 degree of latitude they were considered reasonable candidates. Once these potential correlations were made, the investigation continued by superimposing a plot of all a particular ship's reported positions, thereby constructing a record of the ship's movement on the image. By comparing this record with the geometry of the shiptrack in question it was possible to correlate the track with that ship or eliminate it as a possibility.

To illustrate, the exhaust plume is first advected away from the ship in the direction of the relative wind. The satellite image of the shiptrack should therefore reveal an indication of the direction of the relative wind near the emitting ship. Calculating the relative wind from the ships reported true wind and its course and speed then comparing it with the observed relative wind from the satellite image should indicate whether or not the ship could produce the shiptrack. Ships report true wind within one degree and one knot. Course and speed are coded as single digit values that decode as a range of courses and speeds. At 1800 UTC on June 26, container ship Tai He (callsign BOAB) was reporting true winds from 330 at 13 knots, with course and speed reported as southeasterly at about 18 knots. Figure 5 illustrates that by plotting limits of possible course/speed combinations within the reported range and using vector addition, several possible relative winds result. Comparing the geometry of the shiptrack associated with Tai He with these possibilities, it is apparent that this ship is a good candidate for generating the shiptrack in question. Figure 6 shows the same satellite image as in Figure 4 with the addition of a plot of position reports for Tai He from 25-30 June. Notice that the shiptrack extending to the west from Tai He's 26 1800 UTC position matches very well with expected relative winds. This step being successful, a final check was made by superimposing the shiptrack heads positions that were screened earlier. Figure 7 indicates a favorable comparison of these points with the ship's dead reckoned position and raised the confidence level significantly that Tai He indeed produced this shiptrack.

Once the ship-to-shiptrack correlations were compiled, the resulting database was

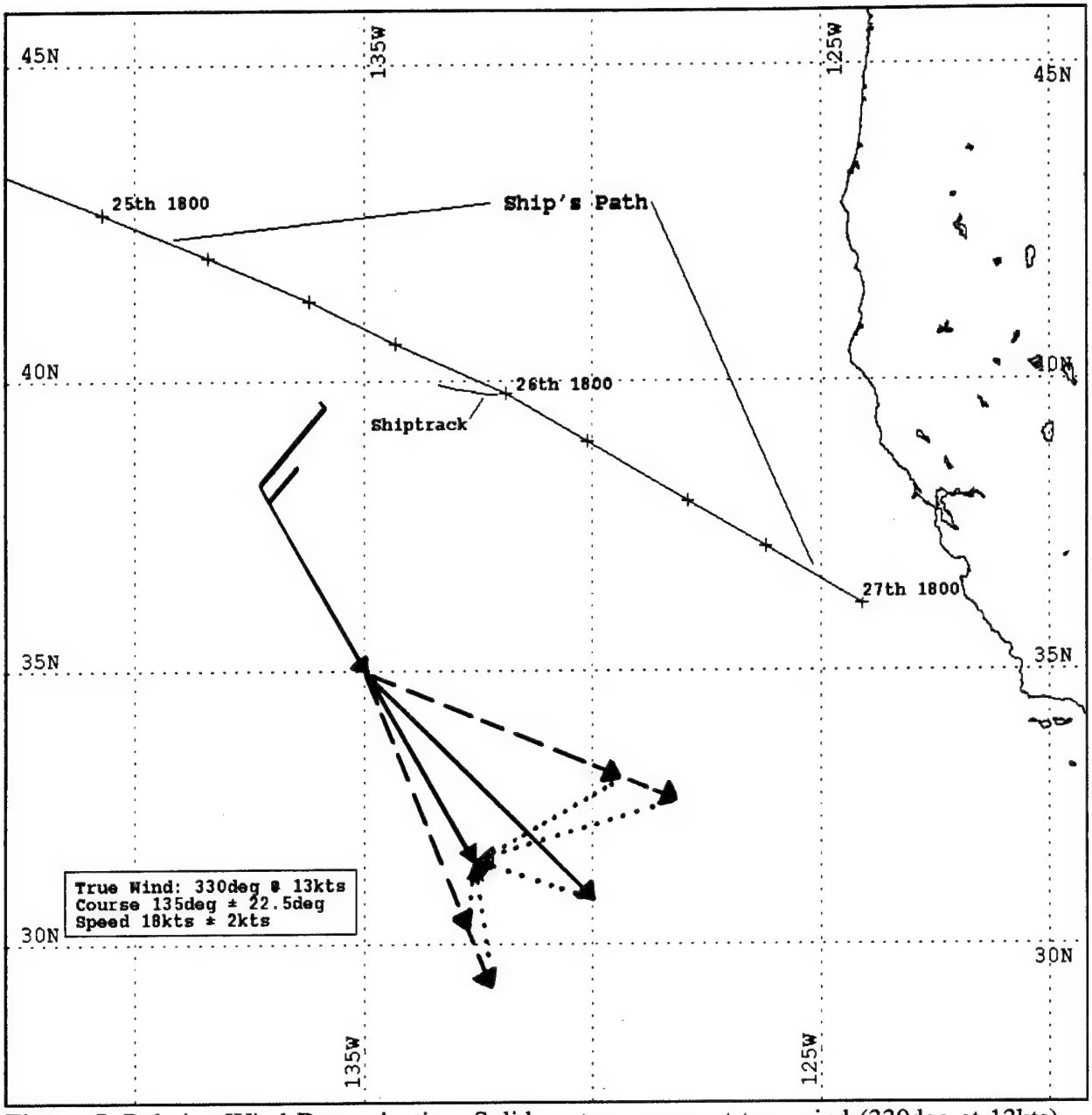

Figure 5. Relative Wind Determination. Solid vectors represent true wind (330deg at 13kts) and mean course and speed (135deg at 18kts). Dashed vectors represent course and speed range about the mean reported value. Dotted vectors represent resultant, or relative, wind solutions. The curvilinear feature labeled "shiptrack" extends from the 1800 UTC position of container ship Tai He (callsign BOAB) seen in Figure 4. Comparing resultant vectors with shiptrack indicates actual relative wind from the east.

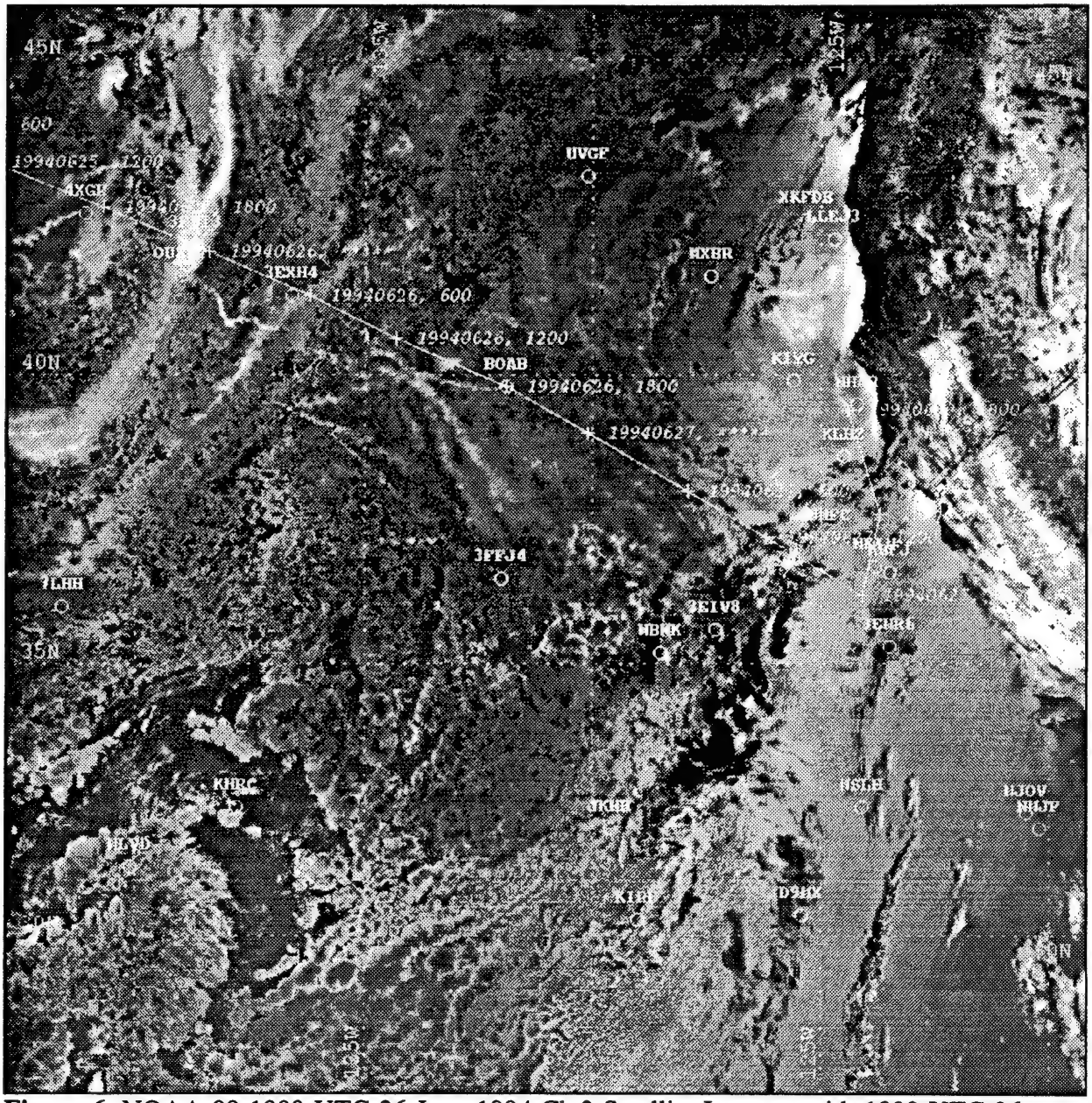

Figure 6. NOAA 09 1800 UTC 26 June 1994 Ch.3 Satellite Imagery with 1800 UTC 26 June 1994 ship positions and Container Ship Tai He (BOAB) Transit History superimposed. Ship data from FNMOC synoptic weather reports.

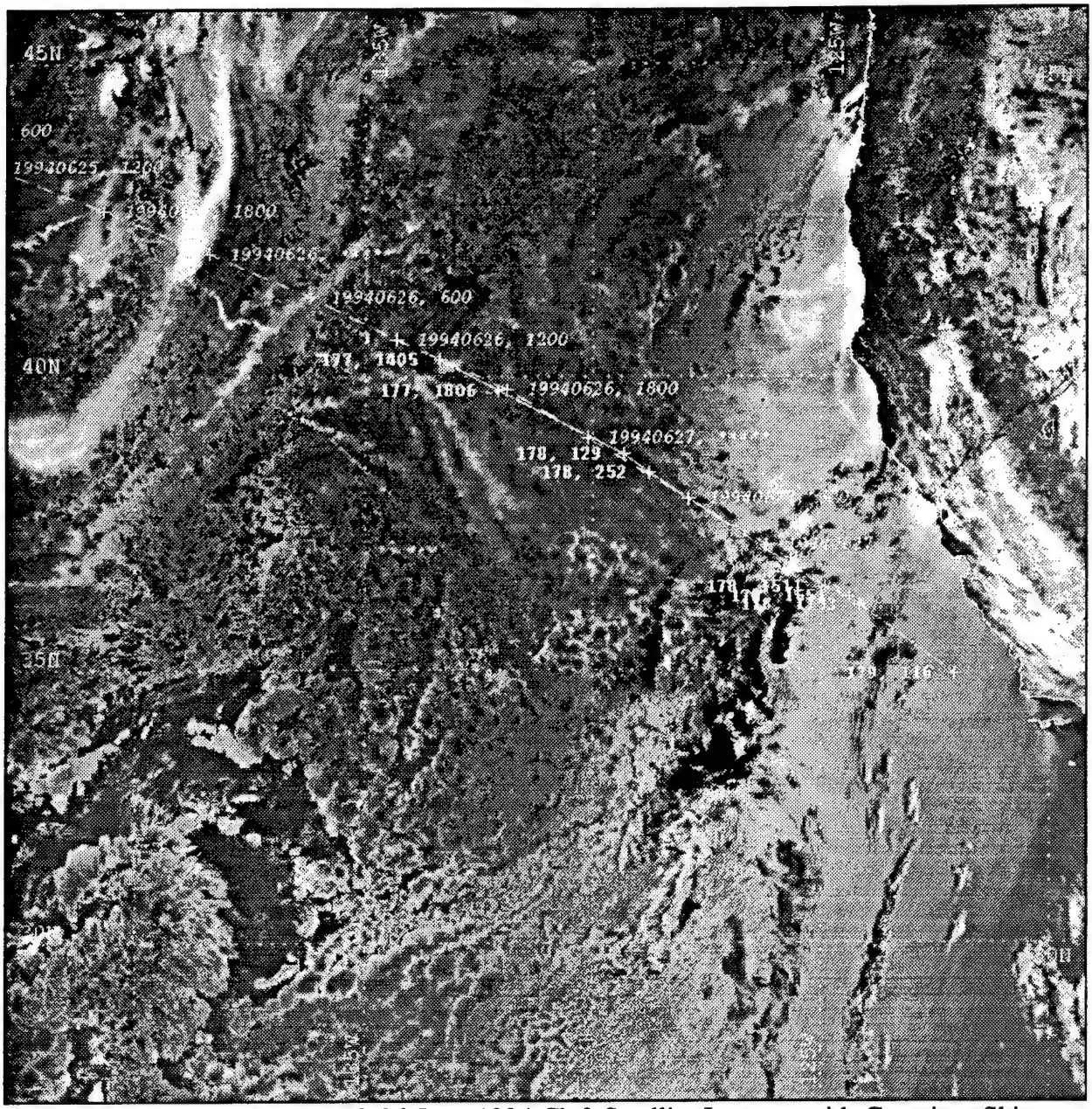

Figure 7. NOAA 09 1800 UTC 26 June 1994 Ch.3 Satellite Imagery with Container Ship Tai He (BOAB) Transit History (dashed line, italic date/time) and Shiptrack Head Positions (solid line, bold julian day, time) superimposed. Shiptrack head positions mark the exact beginning of a shiptrack, which is within 5 to 15 km from the emitting source. Comparison of vessel path to shiptrack head path over several image times indicates a very close correlation between the two. Ship data from FNMOC synoptic weather reports.

scanned for ships with multiple correlations along their path of actual movement. It was from this set of multiple correlations that six cases were chosen for analysis.

B. ANALYSIS

1. Overview

The six ships selected for this study were all commercial vessels. Table 1 is a listing of those ships with a brief summary of their individual characteristics. The

Ship Name	Callsign	Ship Type	Fuel	Weight (tons)	Length (m)	June Dates	No. Tracks
Tai He	BOAB	Container	Oil	35963	236	26-28	7
Zim America	4XGR	Container	Oil	37209	236	27-28	4
Century Highway	8JNP	Vehicles Carrier	Oil	46186	186	13-15	6
Hercules Highway	JKOW	Vehicles Carrier	Oil	46815	179	13-15	6
Sea-Land Consumer	WCHF	Container	Steam	23763	219	12-13	4
Manulani	KNIJ	Container	Steam	23785	219	12-13	4

Table 1. Case Study Ship Characteristics

selection criteria was based solely on the ship being associated with multiple shiptracks. The ships paired nicely due to their common transit lanes. Tai He and Zim America transited toward the Southern California area along nearly the same path within 24 hours of each other. Century Highway and Hercules Highway were within three hours of each other on a southeastward transit toward Panama. Sea-Land Consumer and Manulani were within three hours of each other transiting from the Southern California region to Hawaii.

The ships within each of these three track pairs were also similar in their size and engineering plants. Tai He, Zim America, Century Highway and Hercules Highway were oil-burning; Sea-Land Consumer and Manulani were steam driven. This coupling presented an excellent opportunity to observe shiptrack characteristics from similar ships as they transited through similar environments at different times.

2. Radiative and Physical Characteristics

An analysis of the radiative characteristics of these shiptracks and surrounding ambient cloud can be performed with the extraction process now completed. The quantities evaluated in this study include: 1) average ambient cloud and shiptrack reflectance in channels 1 and 3; 2) the reflectance difference between shiptrack and ambient cloud in channels 1 and 3; 3) the percent change of the reflectance difference between ambient cloud and track for channels 1 and 3; and 4) track width.

The average reflectance for ambient cloud and shiptrack yields information on the modification of the cloud by ship effluent. By the process of smaller water droplet formation described earlier, the track should appear more reflectant than the surrounding ambient cloud through the length of the track until through dispersion it becomes indistinguishable from the background. Track width should give insight into the dispersion characteristics and should get larger with distance down track. Previous studies indicate that track widths grow rapidly over the first few kilometers from the source, then stabilize at some distance down track from emitting source (Gifford, 1980; Mikkelsen, 1983). Comparing shiptrack width growth patterns with predicted patterns should reveal insight into the behavior of the shiptrack as it is influenced by both true and relative wind. The dispersion characteristics will be affected by the moving nature of the source. Reflectance difference between shiptrack and cloud should decrease with the age of the shiptrack through the same dispersive mechanisms. The percent change for the reflectance difference between track and cloud should show fairly constant values since shiptrack radiative characteristics are dependent upon the pre-existing cloud in which they form.

a. Time Since Emission

Analysis of radiative characteristics and physical widths of individual shiptracks as a function of their time since emission, or age, are displayed in the Appendix. Time since emission is defined as distance downtrack divided by the relative wind speed. For example, a track segment 50 km downtrack experiencing a relative wind of 10 km/hr through the period is 5 hours old.

Comparison of width characteristics for a group of shiptracks produced by the same ship will be presented in each case study. Widths will be shown in composite plots as a function of time since emission in order to view differences in trends. Predicted values for shiptrack width growth will also be shown on these plots.

Shiptrack width growth can be predicted by considering the dispersion of the concentration of the ship produced aerosol particles within the plume. Assuming a neutrally stable, well-mixed marine atmospheric boundary layer, plume growth for a stationary platform can be parameterized by (Skupniewicz and Schacher, 1986)

$$\sigma_y = \sigma_{y_{ref}} \left[\frac{x}{x_{ref}}\right]^{\alpha}$$

where σ_y is the standard deviation of the plume concentration and x is the distance down-plume. α, σ_{ref}, and x_{ref} are all parameters based on assumed stability (positive, negative, or neutral). This can be adjusted for a moving source by using the ratio of true wind speed to relative wind speed as a correction factor. Specifically,

$$\sigma_y = \sigma_{y_{ref}} \left[\frac{x}{x_{ref}} \frac{U_{true}}{U_{rel}}\right]^{\alpha}$$

Assuming a Gaussian distribution of concentration within the plume, the width can be defined as the distance between the maximum reflectance gradients on either

side of the plume centerline. Previous studies (Gifford, 1980; Mikkelsen, 1983) have shown that σ_y is proportional to the lateral position of the reflectance, decreasing with increasing distance down-plume. This approximation holds so long as the plume is clearly visible. Observational evidence obtained in these previous studies also indicates that predicted values of width are less than those observed visually.

The track width analysis above does not account for the effects of absolute concentration of ship produced aerosol particles, but considers only the turbulent dispersion effects on plume width. These dispersion effects can be analyzed with channel 3 AVHRR data because of the tight relationship between reflectance and aerosol (aerosol affects CCN, which affects droplet size, which determines reflectance) as shown by aircraft measurements in ship influenced clouds (Radke et al, 1989).

b. Time of Emission

Composites of the radiative characteristics for all shiptracks associated with a particular ship, as a function of time of emission, will be presented in each case study. Time of emission is defined as image time minus the time since emission, yielding a timeline over which radiative characteristics of each shiptrack in a series of images can be compared. Each segment is emitted at a given time and shows up in subsequent images as an older piece of track. This depiction illustrates how a segment of track evolves from one image to another.

c. Shiptracks at Night

Channel 3 radiative characteristics of shiptracks at night are based solely on emission of electromagnetic radiation at 3.7μm. Daytime shiptrack images show reflected energy as well as emitted (being in the near infrared). Therefore, radiative characteristics of night shiptracks were not evaluated. However, since they are "visible" in the imagery, the physical track width characteristic was evaluated.

III. RESULTS

A. CASE STUDIES

1. Tai He (Callsign BOAB)

Tai He is an oil burning container ship 236 meters in length, displacing 35,963 tons. Shiptracks associated with this vessel were first observed on 26 June 1994 at 1800 UTC (1100 local). Figures 8 through 15 show the movement of this shiptrack through seven satellite images over a period of 31 hours. Based on the ship's synoptic weather reports Tai He was on a southeasterly heading at a speed of between 16 and 20 knots. True winds were reported out of the northwest from 10 to 20 knots producing relative winds from the east. All Tai He shiptracks in these successive images generally correlated well with the reported conditions. Table 2 lists Tai He's reported conditions. Note that

Date/Time YYMMDD HHMM	**Position** LAT/LON	**Course/Speed** DEG/KTS	**True Wind** DEG/KTS	**Rel Wind** DEG/KTS
940626 1800	39.8n/131.9w	135/18	330/13	100/07
940627 0124	38.6n/129.3w	135/18	020/13	090/17
940627 0246	38.2n/129.0w	135/18	000/14	085/13
940627 1511	36.6n/124.8w	135/18	350/18	065/11
940627 1651	36.4n/124.0w	135/18	340/16	070/08
940627 1753	36.2n/123.8w	135/18	330/14	095/06
940628 0116	34.9n/122.2w	135/18	340/18	060/08

Table 2. Position and Wind Reports for Tai He (BOAB).

course and speed are mean values for the coded range reported. Relative wind is based on this mean reported value. Potential error in the relative wind calculation becomes apparent when comparing it with the direction of the shiptrack plume seen in the satellite imagery. The 27 June 1753 UTC shiptrack is a good example. The relative wind direction

calculated from the reported ships course and true wind is 095 degrees. The satellite image, Figure 14, suggests that it is closer to 010 degrees. The cause is most likely an error in the reported true wind. An increase in true wind speed of only 8 knots would produce a relative wind of 015 degrees at 6 knots which is close agreement with the orientation of the shiptrack.

a. Radiative Characteristics

Analysis of the radiative characteristics of these shiptracks yield some interesting results. Figure 16 indicates an increasing trend in ambient cloud reflectance values as Tai He transits toward the continent--into stratus that is increasingly contaminated with continental aerosol. This affects the stratus in much the same way as ship-stack effluent does. The injection of continental, man-made aerosol particles into the marine environment effectively increases cloud reflectance at 3.7μm by forming smaller droplet radii. Hence their is an increasing trend in channel 3 reflectance values, shown in Figure 17. Shiptracks in the 27 0246 UTC and 27 1511 UTC show the effects of the shiptrack extraction algorithm's difficulty in resolving radiative characteristics at low sun angles. The resulting plots for these two times show up as outliers to the general trend of the data). The departure from this trend is seen in a drop in ambient reflectance from 12% at 27 1651 UTC to 10% at 27 1753 UTC, with an increase in shiptrack reflectance from 13% to 15% during the same interval. In order to explain this anomaly, it is necessary to inspect the ambient and shiptrack reflectance trends in more detail.

Figures 18 and 19 show the delta percent change for channel 3 and channel 1 (DPC3 and DPC1), respectively, between shiptrack and ambient cloud for all seven shiptracks as a function of their time of emission. The large and variable DPC3 and DPC1 values for 26 1800 UTC reveal the broken nature of the stratus at this location. DPC3 values for 27 0124 UTC show the same trend but are not quite as large. The remainder of the plots are clustered around the 20% DPC3 value, with the exception of the 27 1753 UTC track. This shiptrack shows an unexpected 20% increase in percent change from the ambient cloud that is evident along the entire length of the track. Peaks in the reflectance are due to intersections with other shiptracks in the area. From the

ambient and shiptrack reflectance values for 27 1753 UTC, Figures 16 and 17 again, it is apparent that the ambient values decreased while the track values increased. This runs counter to expectations. The shiptrack reflectance trend should mirror that of the ambient cloud in which it is formed. Inspection of the imagery for both passes in channel 3 and channel 1 reveals that the stratus is undergoing a change from the earlier image to the later. Keeping in mind that local time is 0951 to 1053, it is clear that the stratus is thinning, a typical late morning event in the early summer months in this region. Recall that at 3.7μm wavelength, reflectance is dependent upon droplet size only *assuming cloud thickness is greater than 100m.* In thin cloud, reflectance is lowered as a result of more transmittance of 3.7μm energy through the cloud. The shiptrack cloud does not undergo this thinning process. One possible explanation is that as relative humidity decreases in the general environment, a general decrease in water droplet size results which enhances track reflectance. This accounts for the absolute increase in track reflectance and an absolute decrease in the reflectance of the ambient cloud.

b. Track Width

Widths for each of Tai He's shiptracks are plotted as a function of their time of emission (i.e., age) as shown in Figure 20 (values are widths averaged over each 10 km segment of track). The overall trend in the plots shows an initially rapid growth rate of approximately 5-6 km/hr then decreasing to a maximum width of 10 to 12 km 100 km to 200 km down track. The slight decrease in width at the end of each track is a result of the broken cloud environment and the effects of diffusion causing difficulty in determining the edge of the track. The peaks in the 27 1651 UTC and 28 0116 UTC tracks reflect increased width in the vicinity of intersections with other shiptracks. The 27 0246 UTC and 27 1511 UTC plots again indicate the difficulty the algorithm has with resolving low sun angle geometries.

This general trend matches well with predicted plume width in the growth region of the track (shown as the smooth curves in Figure 20). Beyond the maximum plume width a linear correlation between observed and predicted widths is not expected (Gifford, 1980; Mikkelsen, 1983). Variations in predicted growth are determined by the

ratio of true wind to relative wind, which corrects for the movement of the ship (see discussion of plume dispersion, p. 17). Also affecting this variation is the magnitude of the relative wind. Since the plot is a function of the time since emission, distance down track must be converted to time by dividing by the relative wind. The larger the magnitude of the relative wind, the smaller the rate of growth.

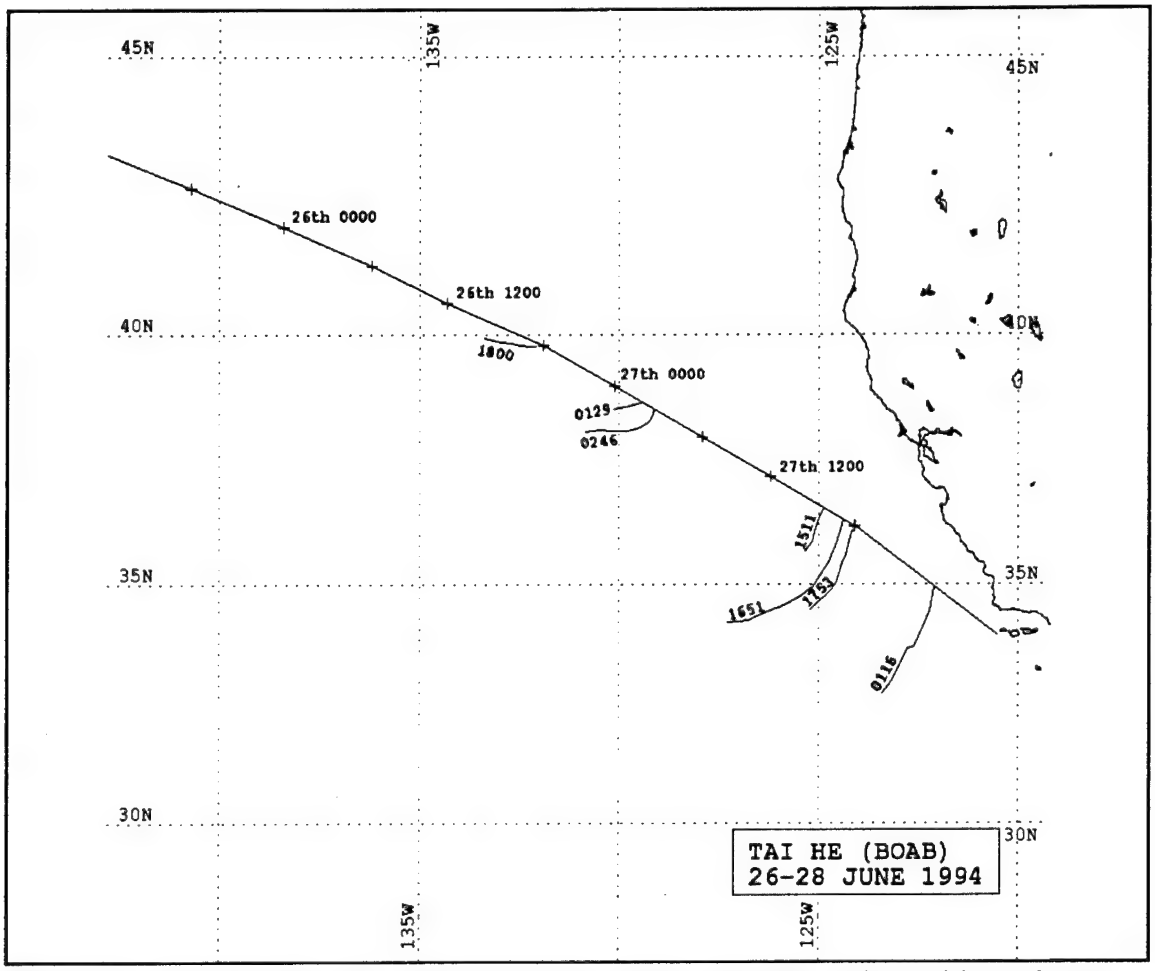

Figure 8. Transit History for Container Ship Tai He (BOAB). Ship positions shown with day and time. Associated shiptracks are denoted by curved lines extending from transit path with satellite pass times indicated on individual tracks.

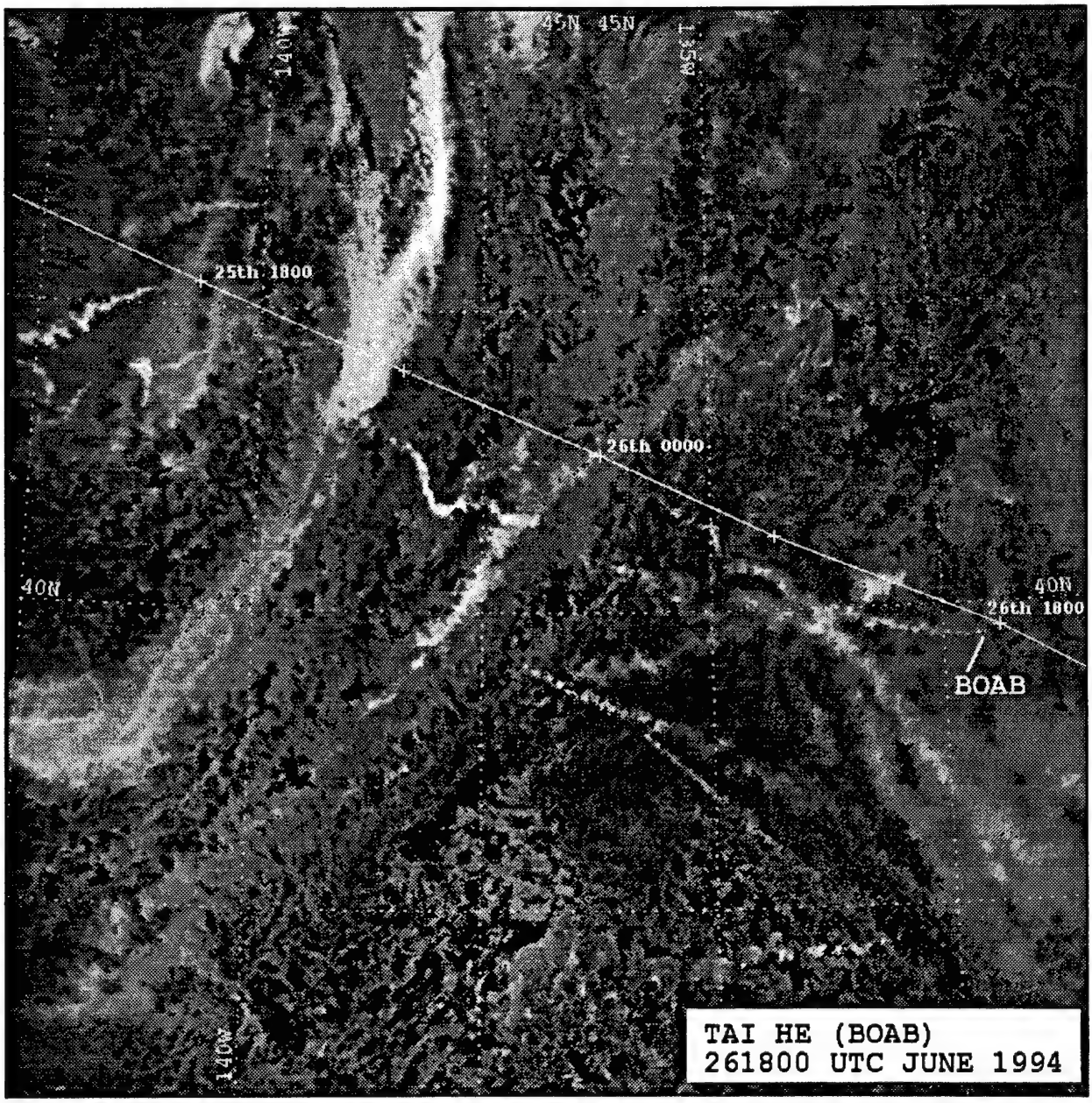

Figure 9. NOAA 09 1800 UTC 26 June 1994 Ch.3 Satellite Imagery Depicting Shiptrack Produced by Container Ship Tai He (BOAB). Solid line denotes Tai He position history based on synoptic weather reports. Shiptrack location indicated by callsign BOAB.

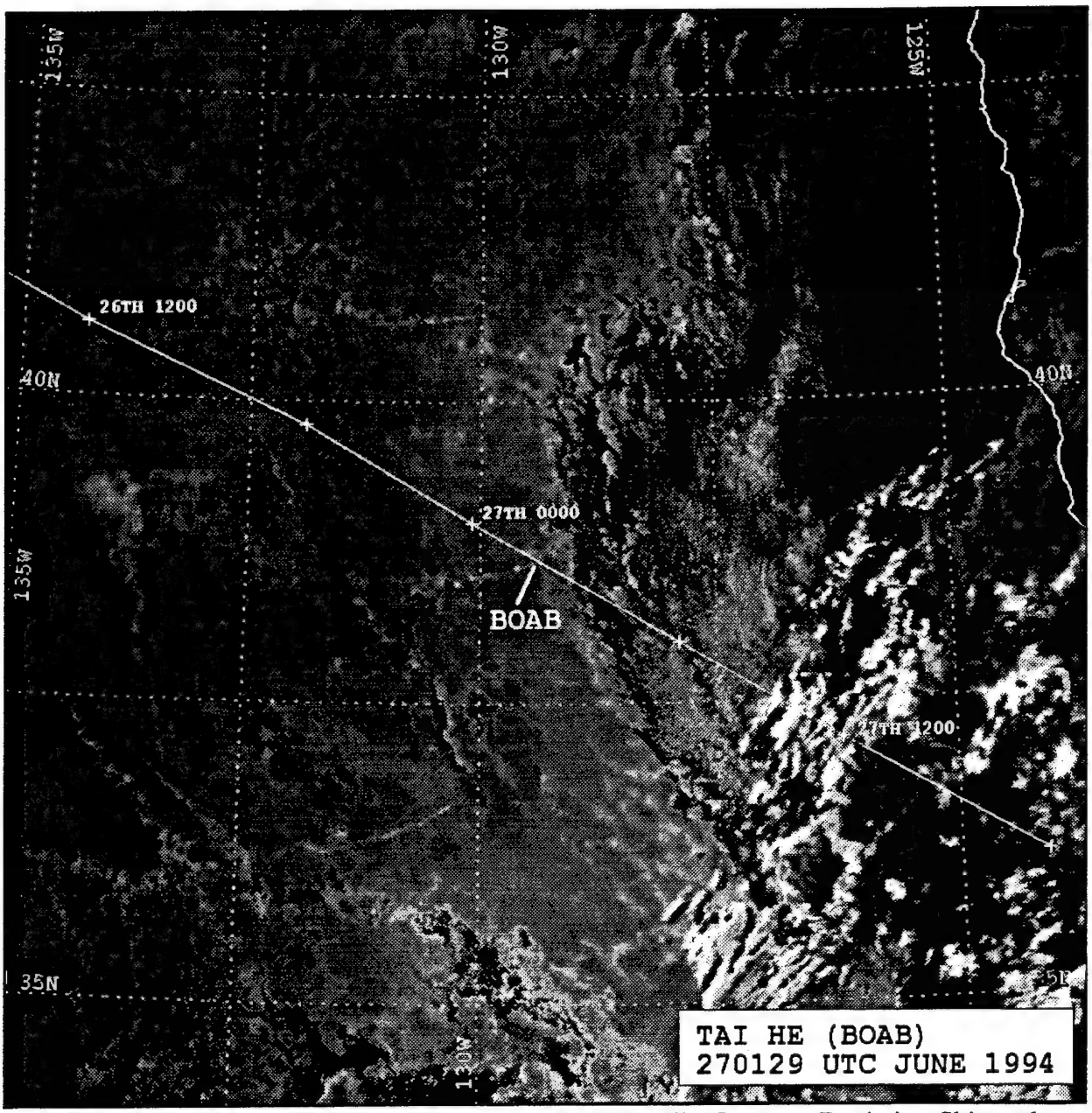

Figure 10. NOAA 11 0129 UTC 27 June 1994 Ch.3 Satellite Imagery Depicting Shiptrack Produced by Container Ship Tai He (BOAB). Solid line denotes Tai He position history based on synoptic weather reports. Shiptrack location indicated by callsign BOAB.

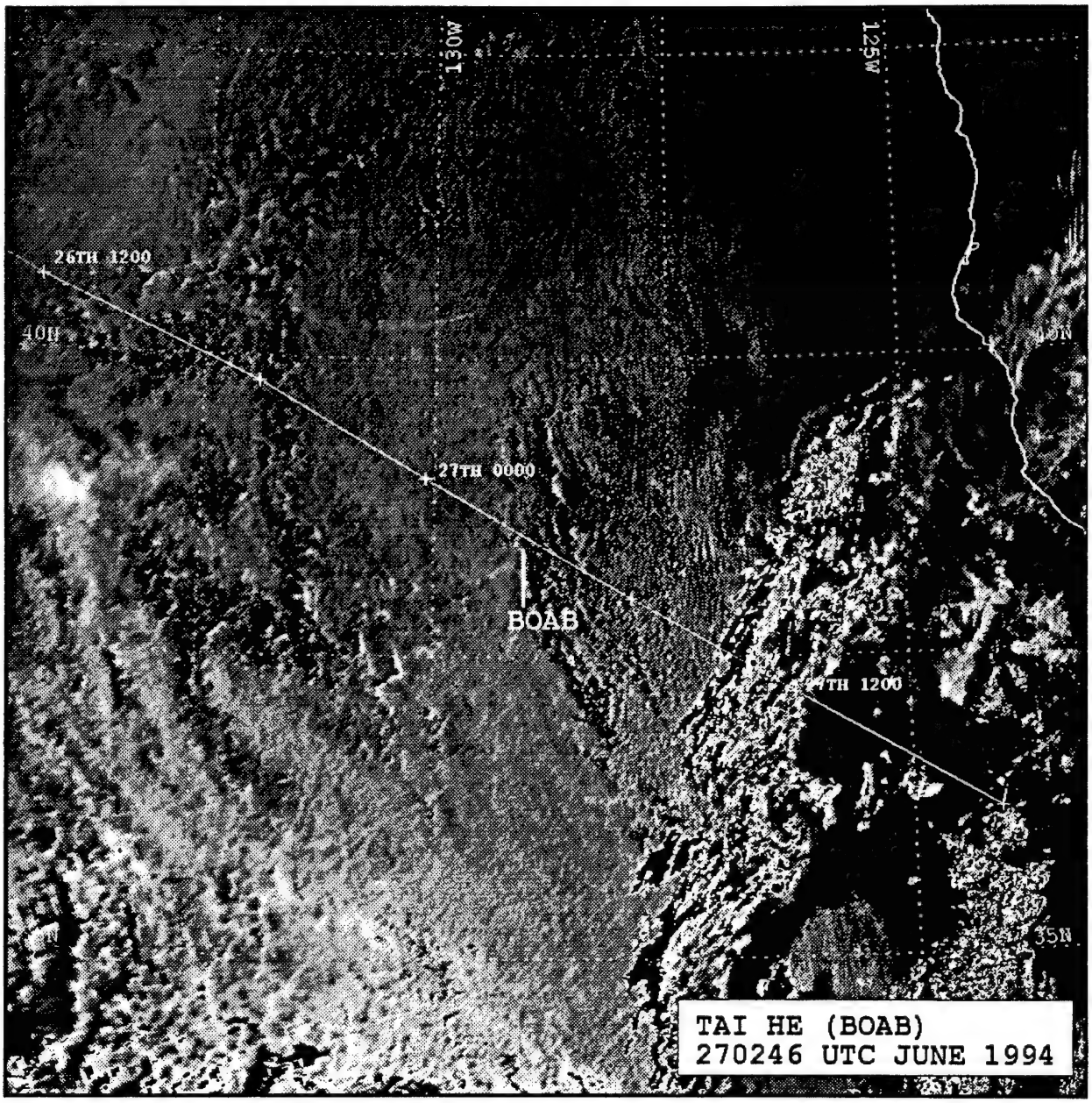

Figure 11. NOAA 12 0246 UTC 27 June 1994 Ch.3 Satellite Imagery Depicting Shiptrack Produced by Container Ship Tai He (BOAB). Solid line denotes Tai He position history based on synoptic weather reports. Shiptrack location indicated by callsign BOAB.

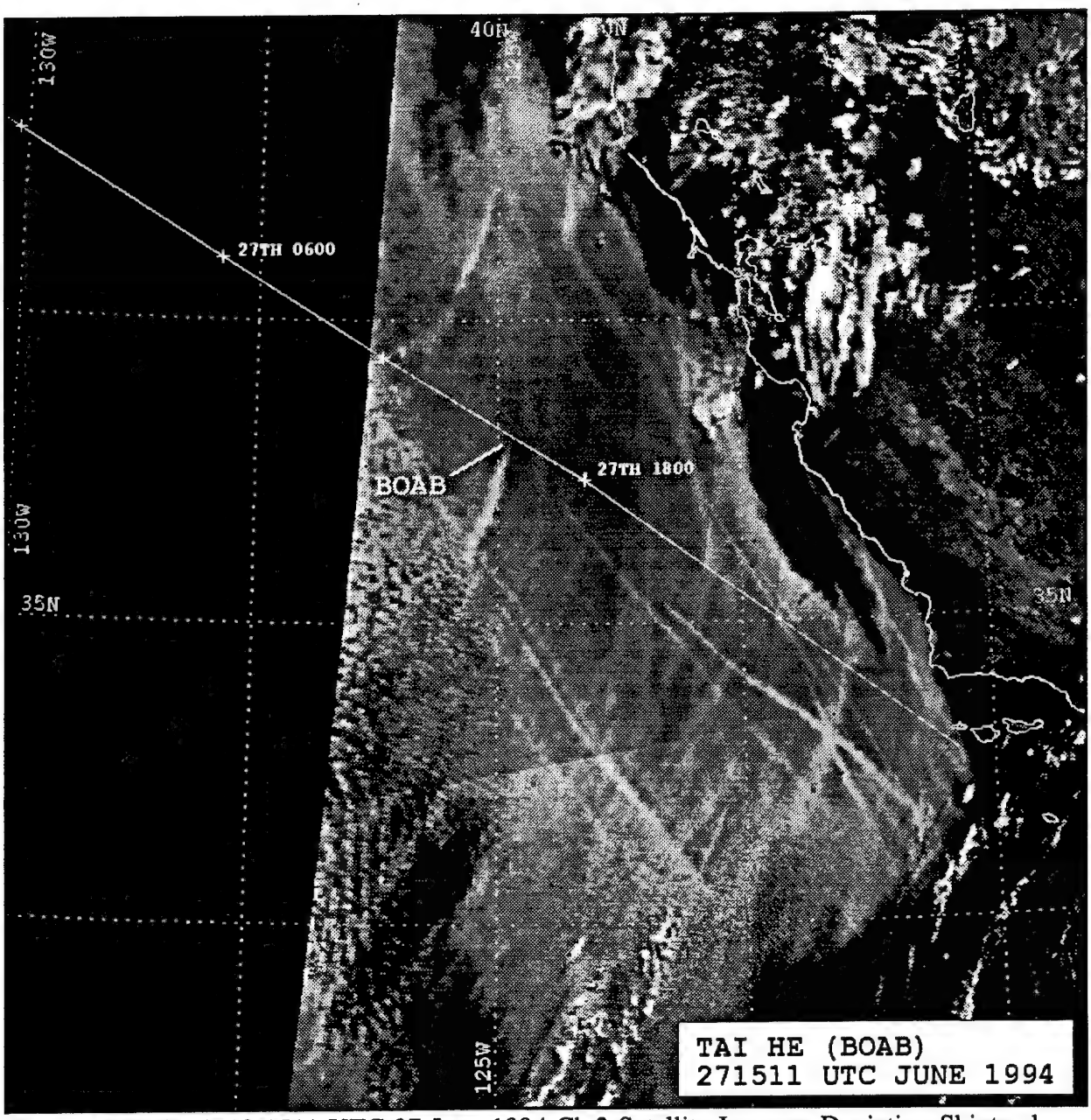

Figure 12. NOAA 12 1511 UTC 27 June 1994 Ch.3 Satellite Imagery Depicting Shiptrack Produced by Container Ship Tai He (BOAB). Solid line denotes Tai He Position history based on synoptic weather reports. Shiptrack location indicated by callsign BOAB.

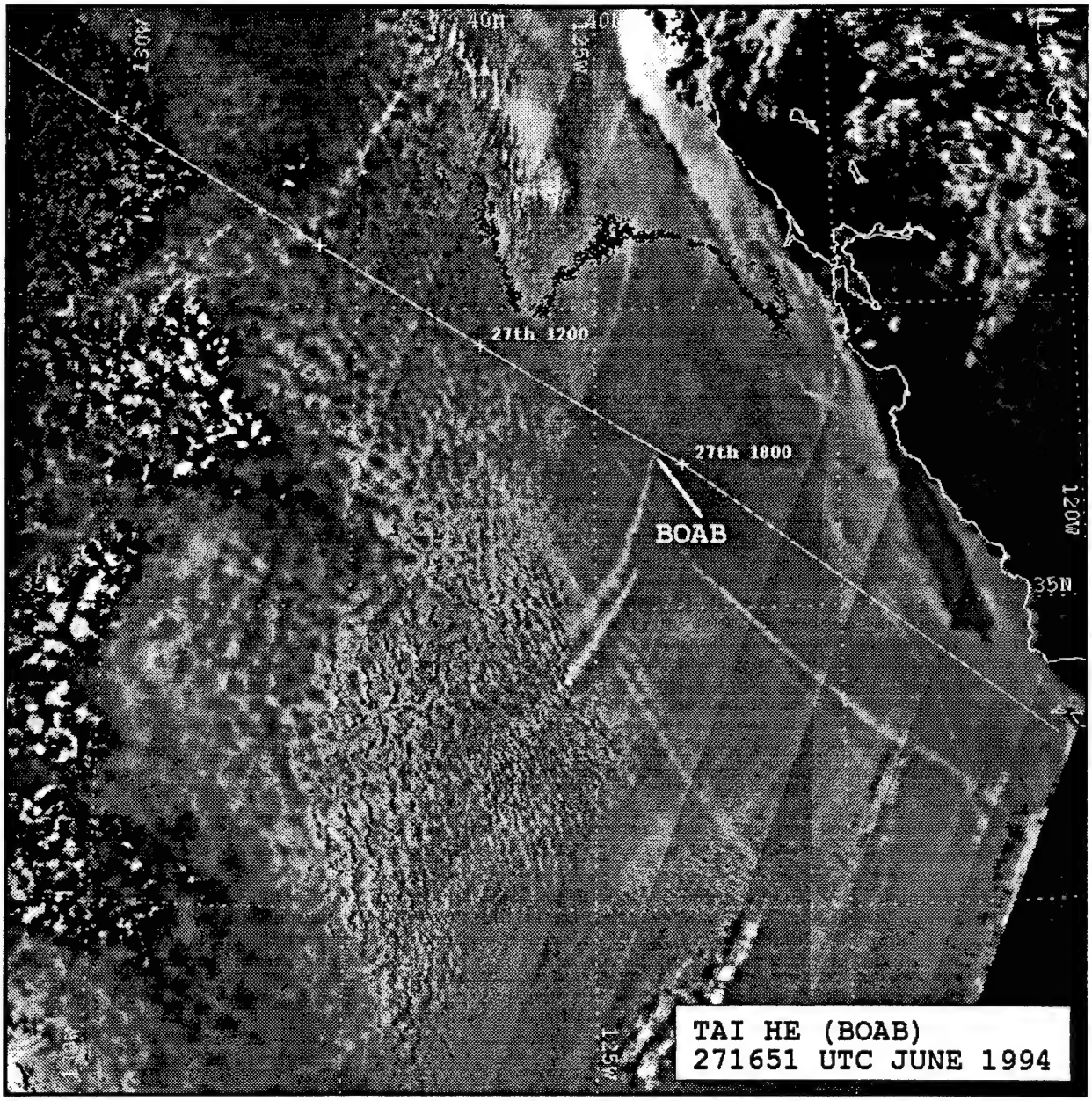

Figure 13. NOAA 12 1651 UTC 27 June 1994 Ch. 3 Satellite Imagery Depicting Shiptrack Produced by Container Ship Tai He (BOAB). Solid line denotes Tai He position history based on synoptic weather reports. Shiptrack location indicated by callsign BOAB.

Figure 14. NOAA 09 1753 UTC 27 June 1994 Ch. 3 Satellite Imagery Depicting Shiptrack Produced by Container Ship Tai He (BOAB). Solid line denotes Tai He position history based on synoptic weather reports. Shiptrack location indicated by callsign BOAB.

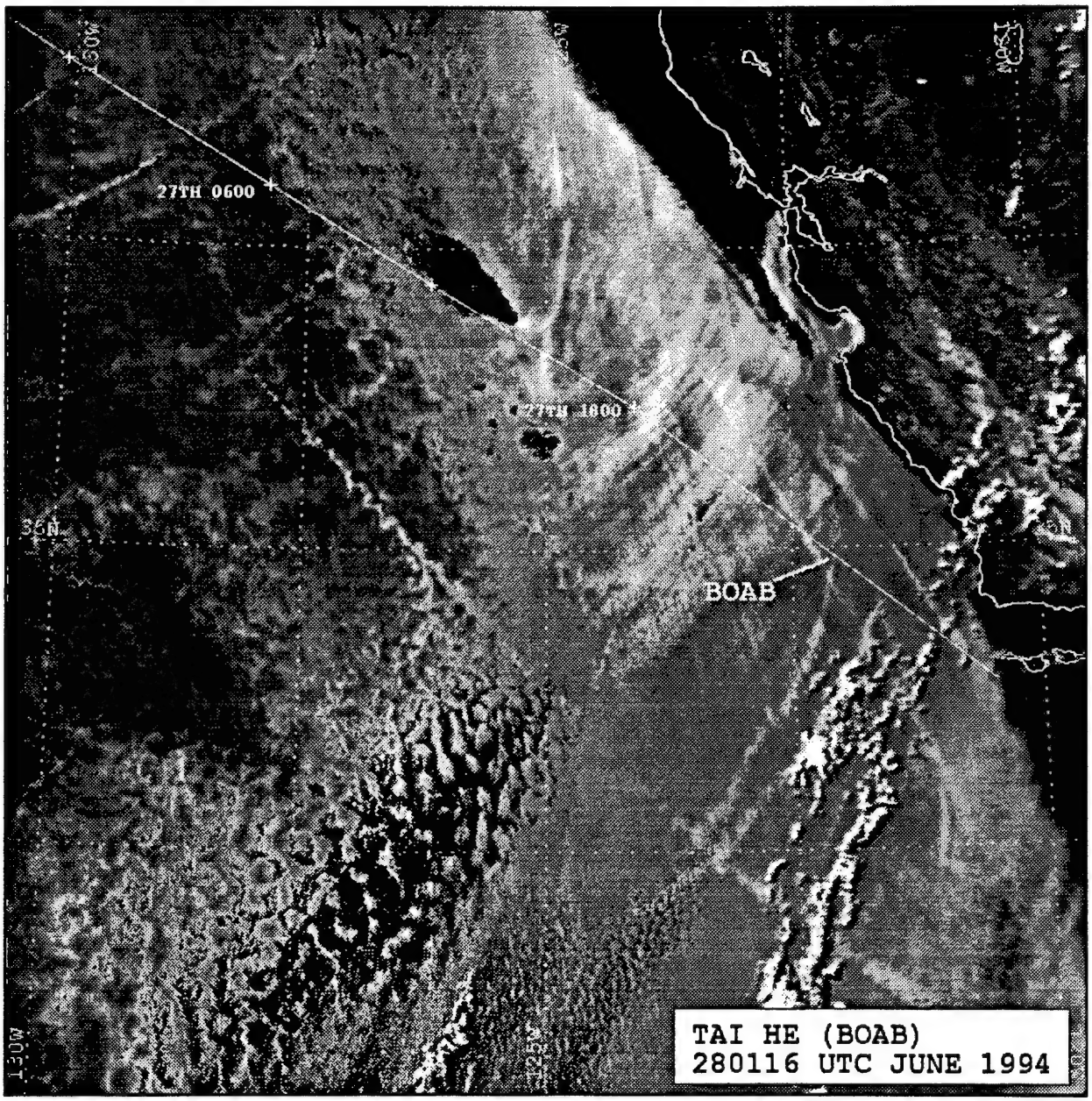

Figure 15. NOAA 11 0116 UTC 28 June 1994 Ch. 3 Satellite Imagery Depicting Shiptrack Produced by Container Ship Tai He (BOAB). Solid line denotes Tai He position history based on synoptic weather reports. Shiptrack location indicated by callsign BOAB.

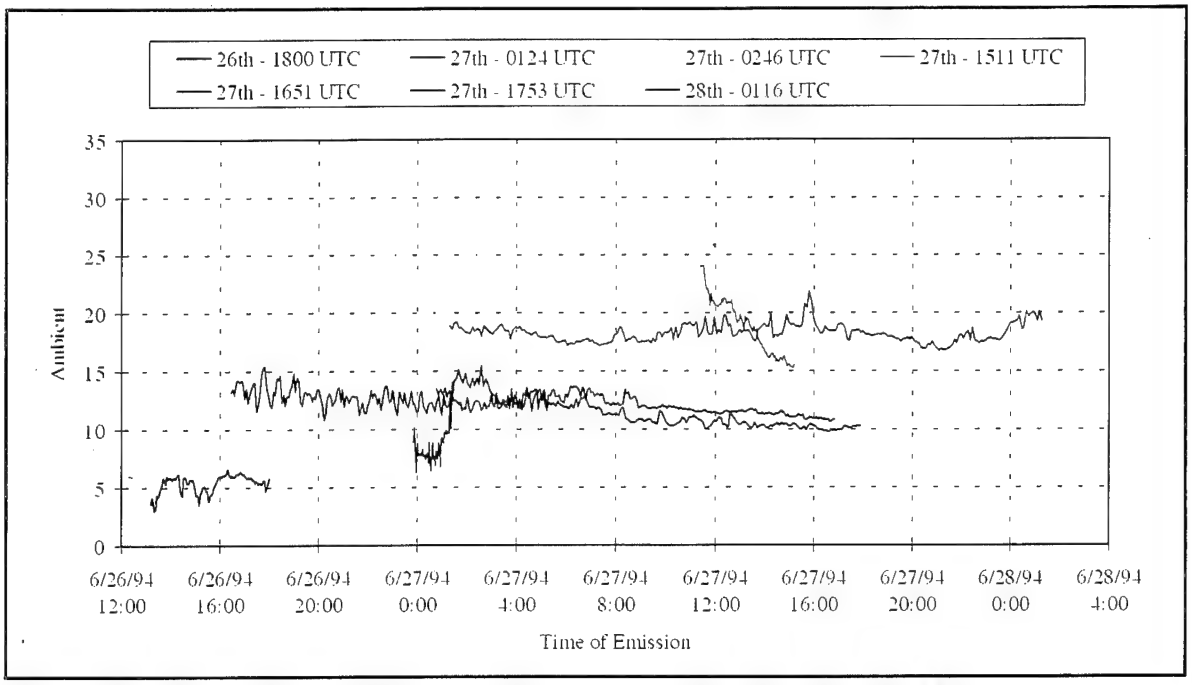

Figure 16. Ch.3 Ambient Reflectance for Container Ship Tai He (BOAB).

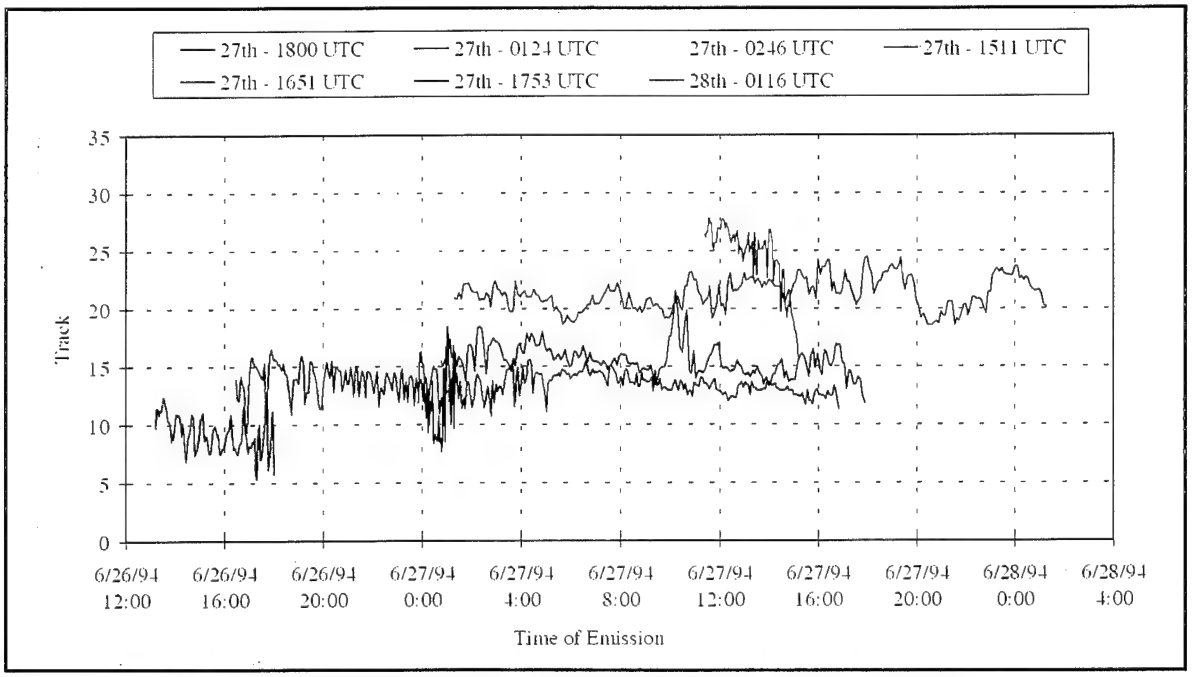

Figure 17. Ch.3 Shiptrack Reflectance for Container Ship Tai He (BOAB).

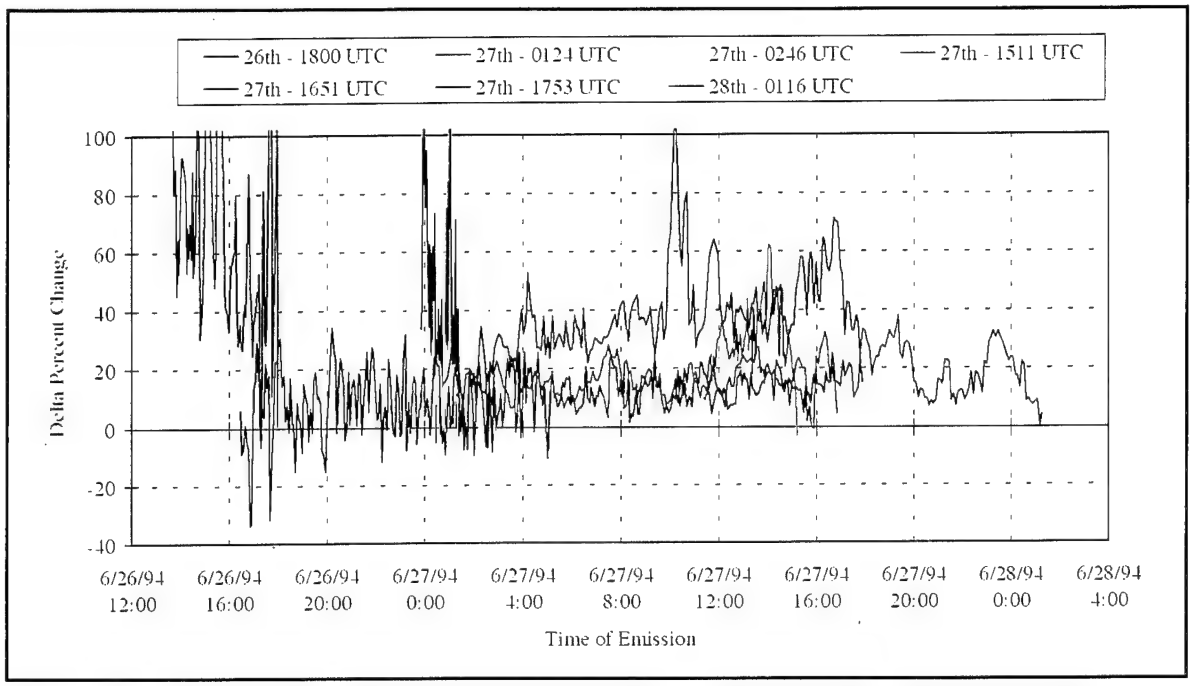

Figure 18. AVHRR Ch.3 Delta Percent Change for Container Ship Tai He (BOAB)

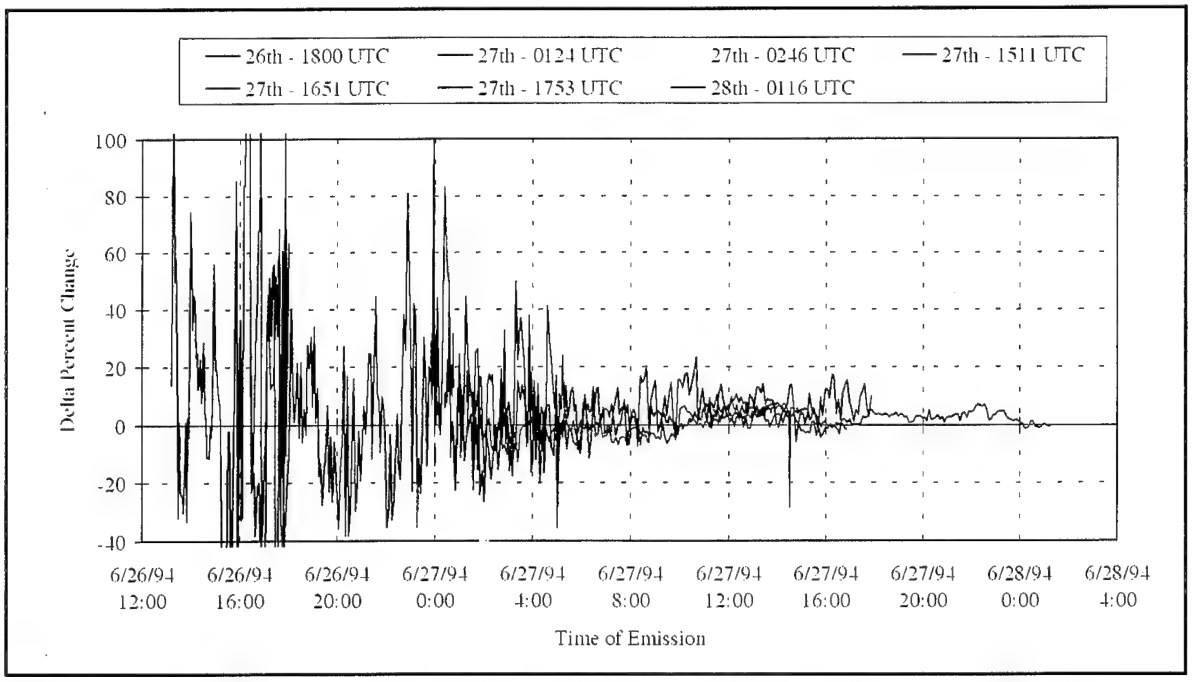

Figure 19. AVHRR Ch.1 Delta Percent Change for Container Ship Tai He (BOAB)

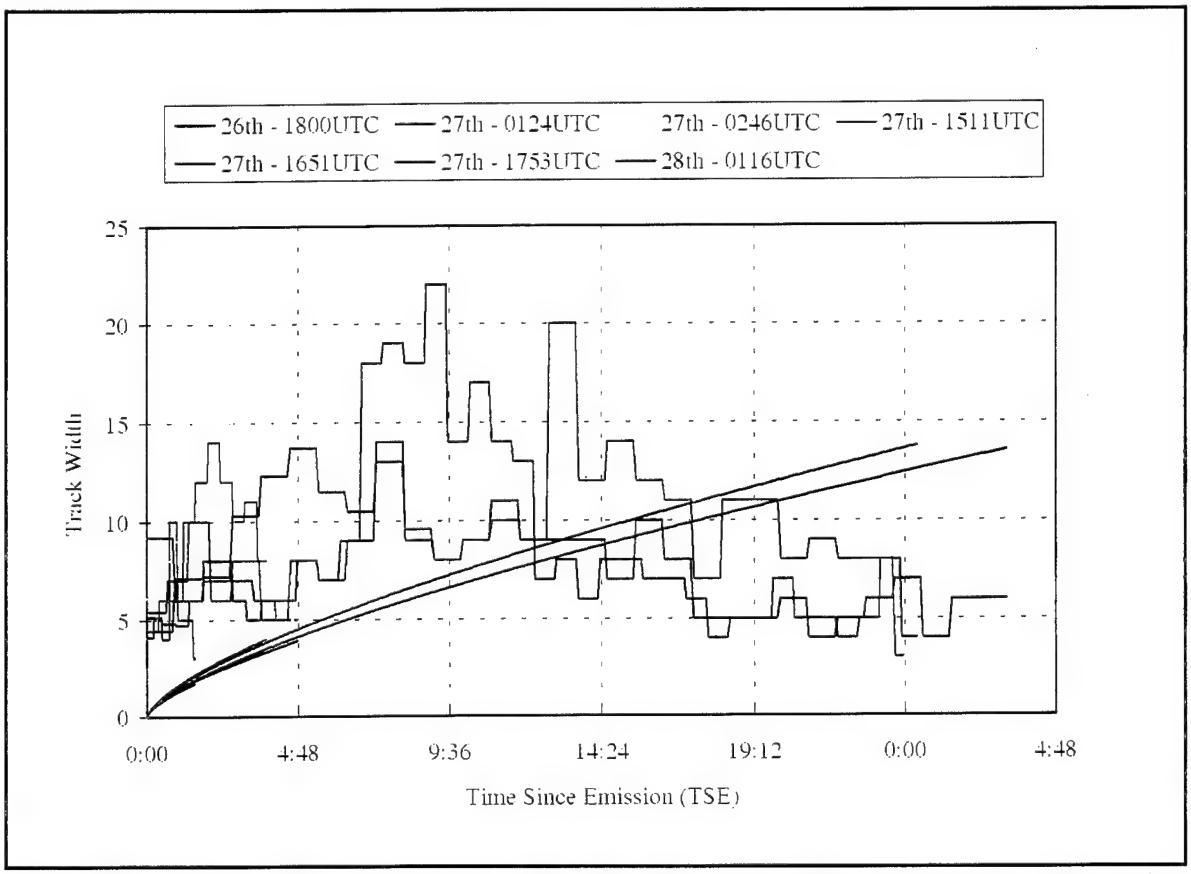

Figure 20. Average Widths for Tai He (BOAB) Shiptracks. Width is averaged over each 10 km segment of shiptrack. Smooth curves represent predicted growth based on twice the standard deviation of the plume concentration.

2. Zim America (Callsign 4XGR)

Zim America is an oil burning container ship 236 meters in length, displacing 37,209 tons. Shiptracks associated with this vessel were first observed on 27 June 1994 at 1753 UTC (1053 local). Figures 21 through 25 show the movement of this shiptrack through four satellite images over a period of 24 hours. Zim America was on a similar course to that of Tai He which transited the same area 24 hours earlier. Based on the ship's synoptic weather reports Zim America was on a southeasterly heading at a speed of between 16 and 20 knots. True winds were reported out of the northwest from 10 to 20 knots producing relative winds from the east. All Zim America shiptracks in these successive images correlated well with the reported conditions. Table 3 lists Zim America's reported conditions. Note that course and speed are mean values for the coded range reported. Relative wind is based on this mean reported value.

Date/Time YYMMDD HHMM	**Position** LAT/LON	**Course/Speed** DEG/KTS	**True Wind** DEG/KTS	**Rel Wind** DEG/KTS
940627 1753	39.2n/131.8w	135/18	010/20	065/18
940628 0116	38.2n/128.9w	135/18	000/30	035/21
940628 1629	35.8n/123.5w	135/18	340/22	035/09
940628 1740	35.6n/123.1w	135/18	340/22	035/09

Table 3. Position and Wind Reports for Zim America (4XGR).

a. Radiative Characteristics

Analysis of the radiative characteristics of Zim America's shiptracks yield results similar to Tai He's. Ambient and shiptrack channel 3 reflectance values (Figures 26 and 27) are increasing as the continent is approached. The channel 3 ambient reflectance values show a general increase from approximately 5% in the 27 1753 UTC track, to approximately 14% in the 28 1740 UTC track. Variability in reflectance values

for each track can be explained in the corresponding imagery. Lower relative values occur when there are breaks in the general cloud regime, with higher values in more uniform stratus regions. The reflectance increase of the 28 1740 UTC track (18%) from the 28 1629 UTC (17%) track is not as pronounced as was seen in the Tai He case which went from about 12% at 27 1651 UTC to approximately 16% at 27 1753 UTC. The ambient cloud decrease in reflectance is occurring again. However, the effect is also not as pronounced as in the Tai He case the previous day, with a 1% decrease for Zim America compared to a 2-3% decrease for Tai He. Shiptrack reflectance for the 28 1740 UTC track shows more of the expected trend, decreasing in value from approximately 20% at the head of the track, increasing to about 15% at an intersection with an older track remnant, then decreasing again to less than 15% at the shiptrack's end.

The trend in the DPC3 values (Figure 28) is indicating the same increase in ambient cloud reflectance toward the continent and increased continental CCN as that seen in the Tai He case. The large DPC3 values associated with the 27 1753 UTC track reflect the position of the head of the track in a broken stratus area moving into a smoother, more uniform stratus field for the remainder of the track. This trend toward higher continental CCN is again reflected in the steady decrease in DPC3 values to between 20% and 30% in subsequent tracks. DPC1 values (Figure 29) are between 2% and 5% showing broad fluctuations in the 27 1753 UTC and 20 0116 UTC tracks with less fluctuation in the more uniform stratus at 28 1629 UTC and 28 1740 UTC.

b. Track Width

The overall trend in track width growth is similar to the Tai He case. The initial rate of growth is somewhat greater (7-8 km/hr) but the trend is the same. Figure 30 shows maximum width once again at approximately 10 to 12 km. The predicted growth mirrors the actual values, indicating a steeper pattern than Tai He's. The values again are determined by the ratio of the true wind to the relative wind which is largest in the 28 1629 UTC and the 28 1740 UTC tracks. The magnitude of the relative wind in these two tracks is also greater than in the Tai He case, which results in larger growth rates.

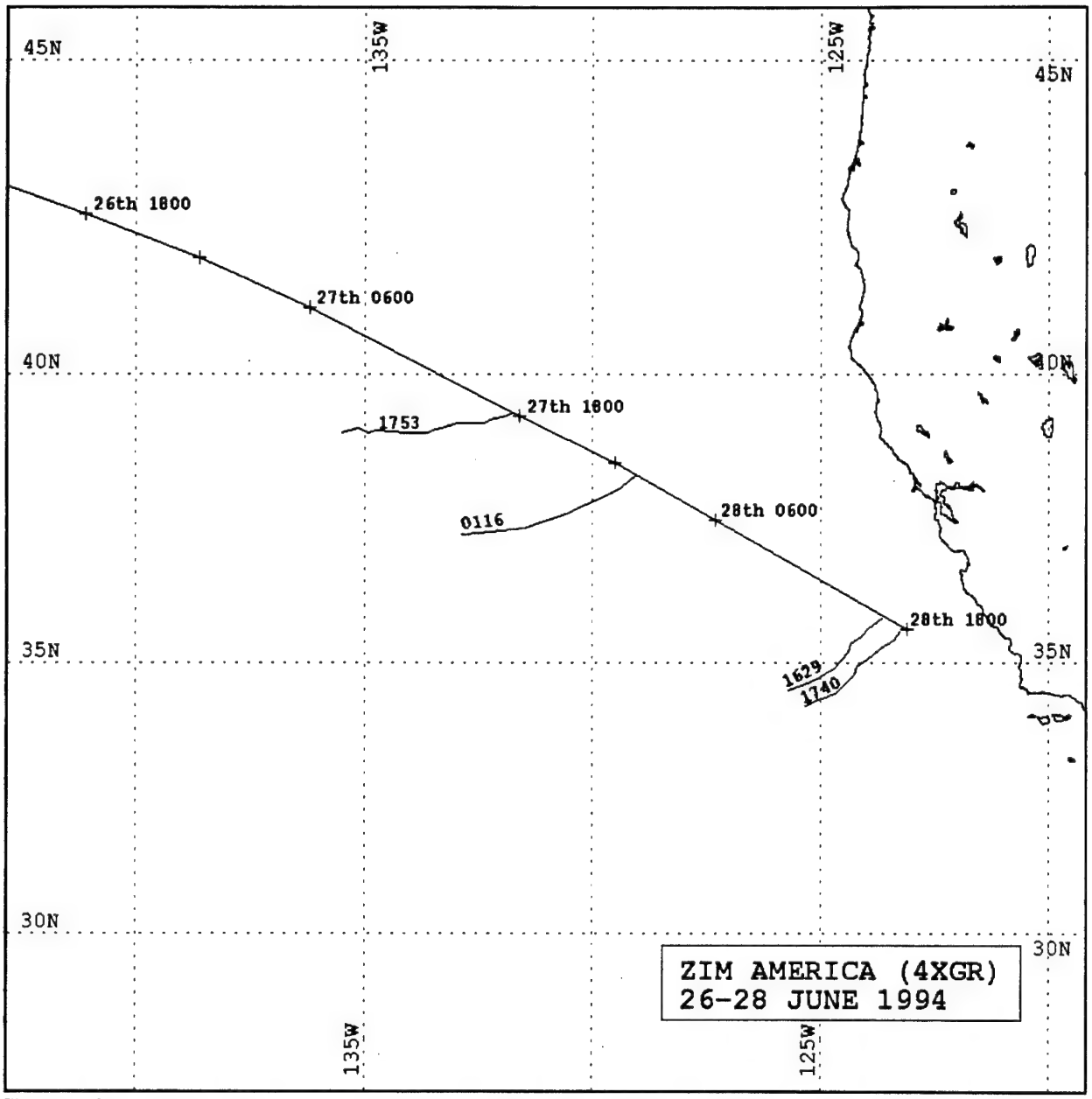

Figure 21. Transit History for Container Ship Zim America (4XGR). Ship positions shown with day and time. Associated shiptracks are denoted by curved lines extending from transit path with satellite pass times indicated.

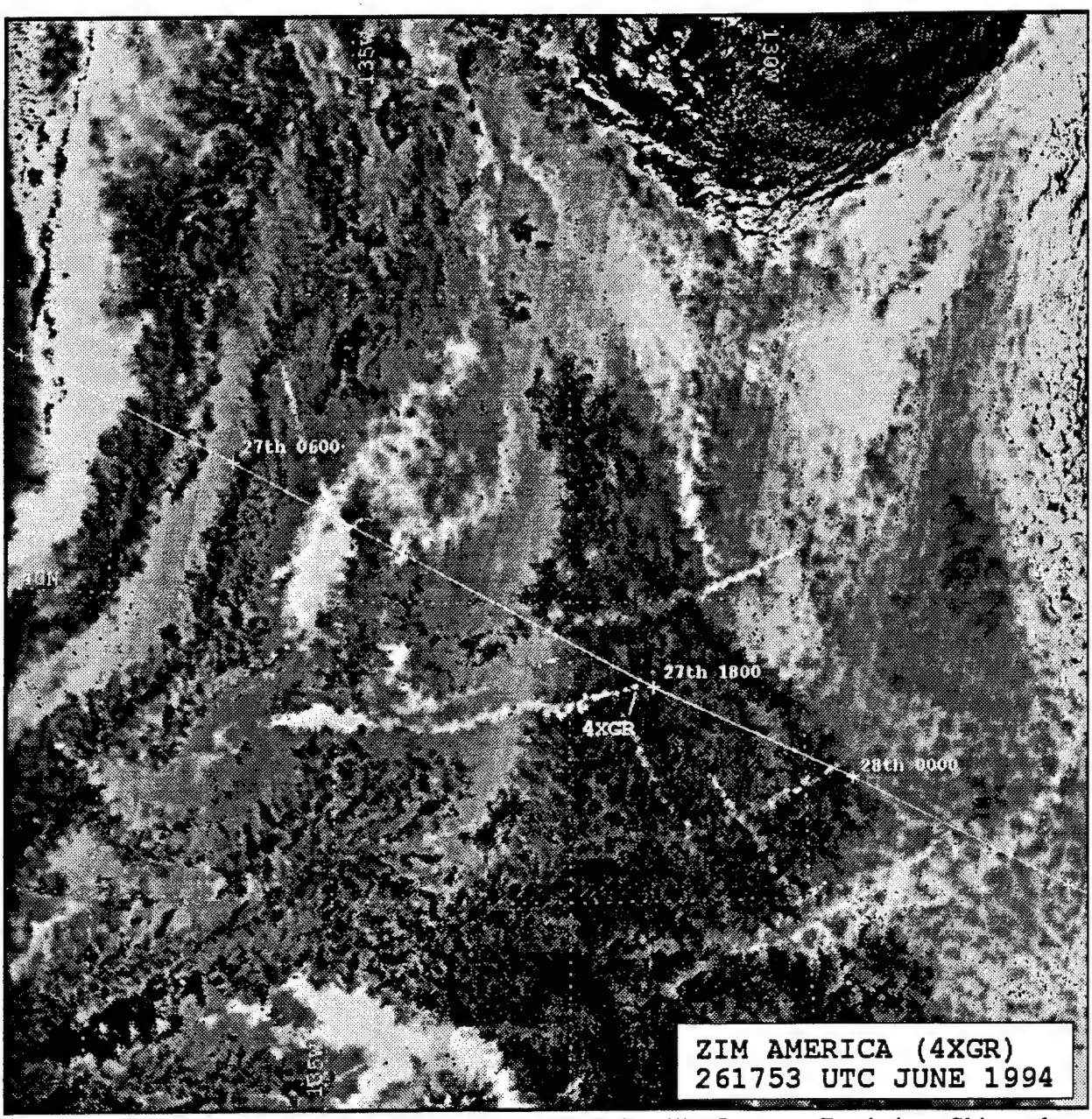

Figure 22. NOAA 09 1753 UTC 27 June 1994 Ch.3 Satellite Imagery Depicting Shiptrack Produced by Container Ship Zim America (4XGR). Solid line denotes Zim America position history based on synoptic weather reports. Shiptrack location indicated by callsign 4XGR.

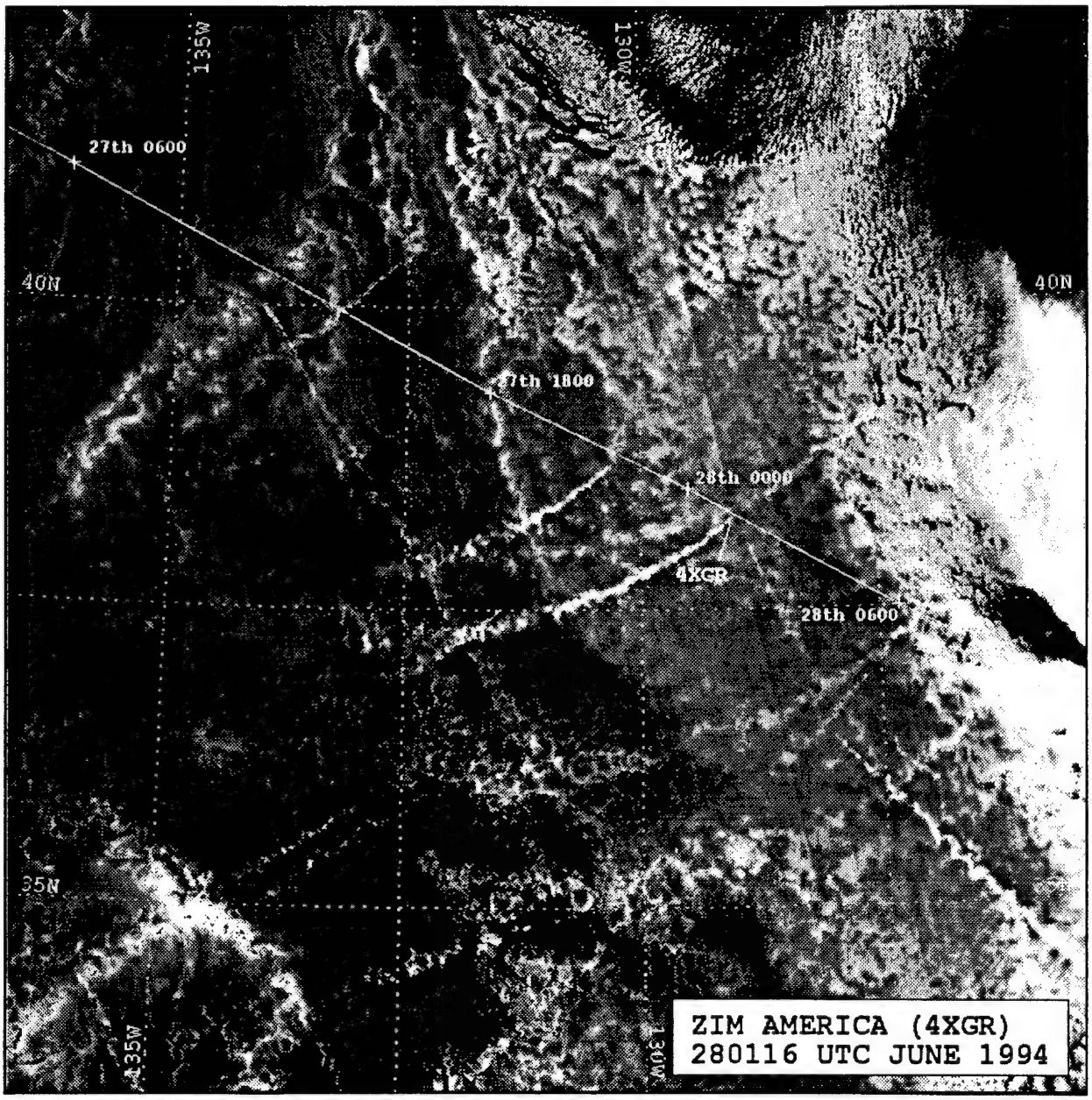

Figure 23. NOAA 11 0116 UTC 28 June 1994 Ch.3 Satellite Imagery Depicting Shiptrack Produced by Container Ship Zim America (4XGR). Solid line denotes Zim America position history based on synoptic weather reports. Shiptrack location indicated by callsign 4XGR.

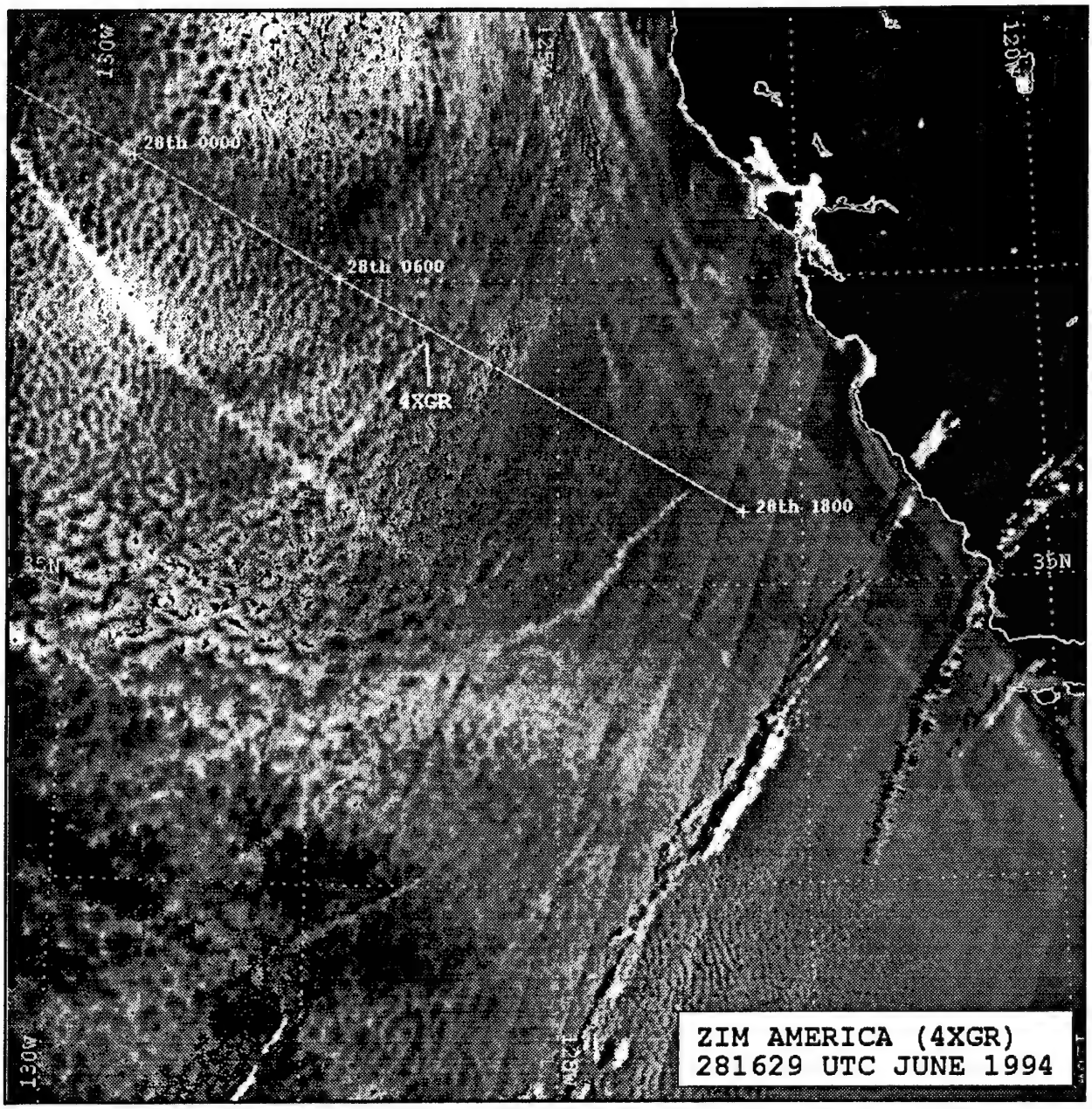

Figure 24. NOAA 12 1629 UTC 27 June 1994 Ch.3 Satellite Imagery Depicting Shiptrack Produced by Container Ship Zim America (4XGR). Solid line denotes Zim America position history based on synoptic weather reports. Shiptrack location indicated by callsign 4XGR.

Figure 25. NOAA 09 1740 UTC 28 June 1994 Ch.3 Satellite Imagery Depicting Shiptrack Produced by Container Ship Zim America (4XGR). Solid line denotes Zim America position history based on synoptic weather reports. Shiptrack location indicated by callsign 4XGR.

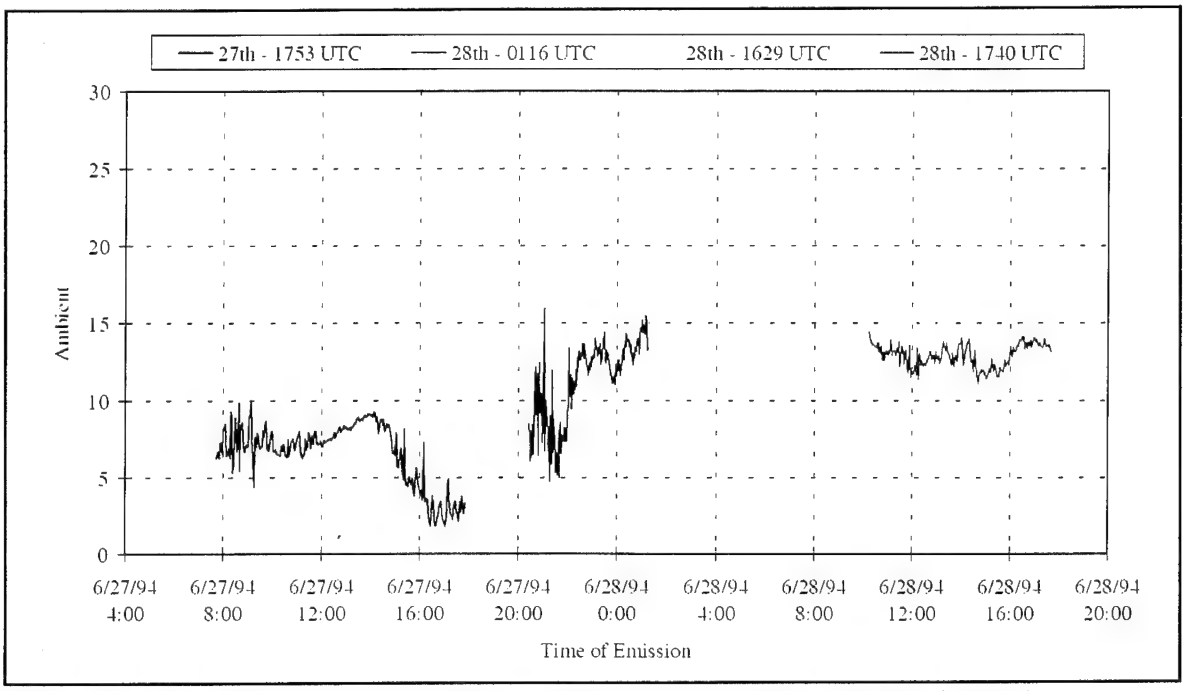

Figure 26. Ch.3 Ambient Reflectance for Container Ship Zim America (4XGR).

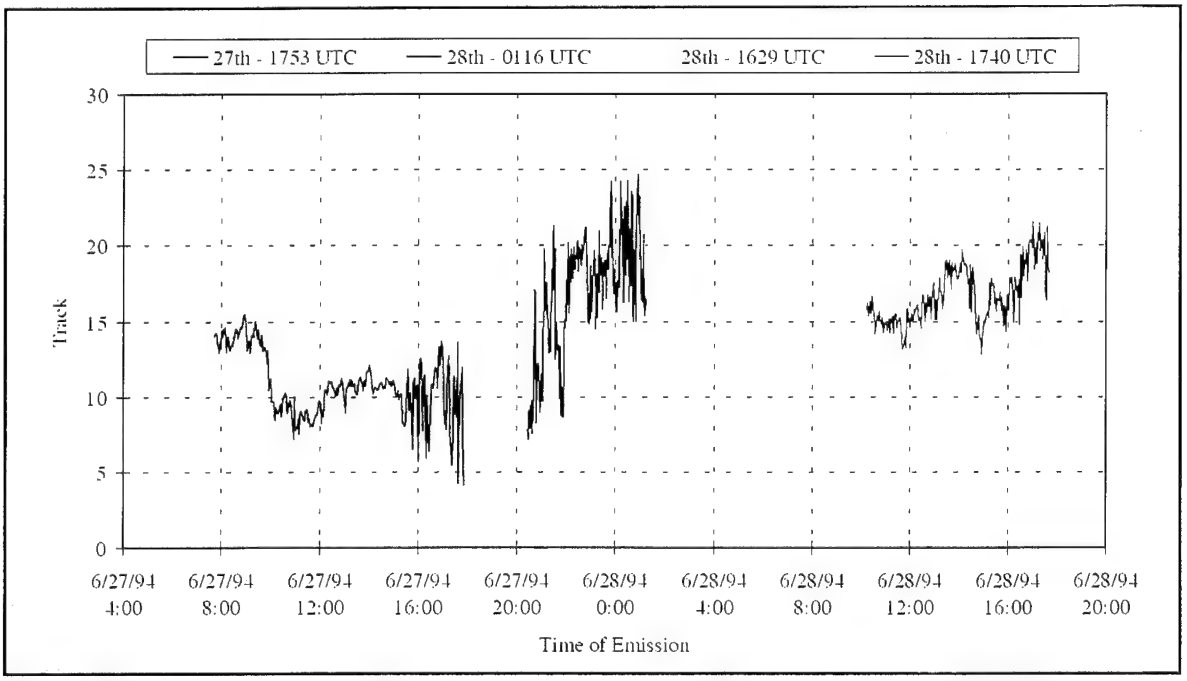

Figure 27. Ch.3 Shiptrack Reflectance for Container Ship Zim America (4XGR).

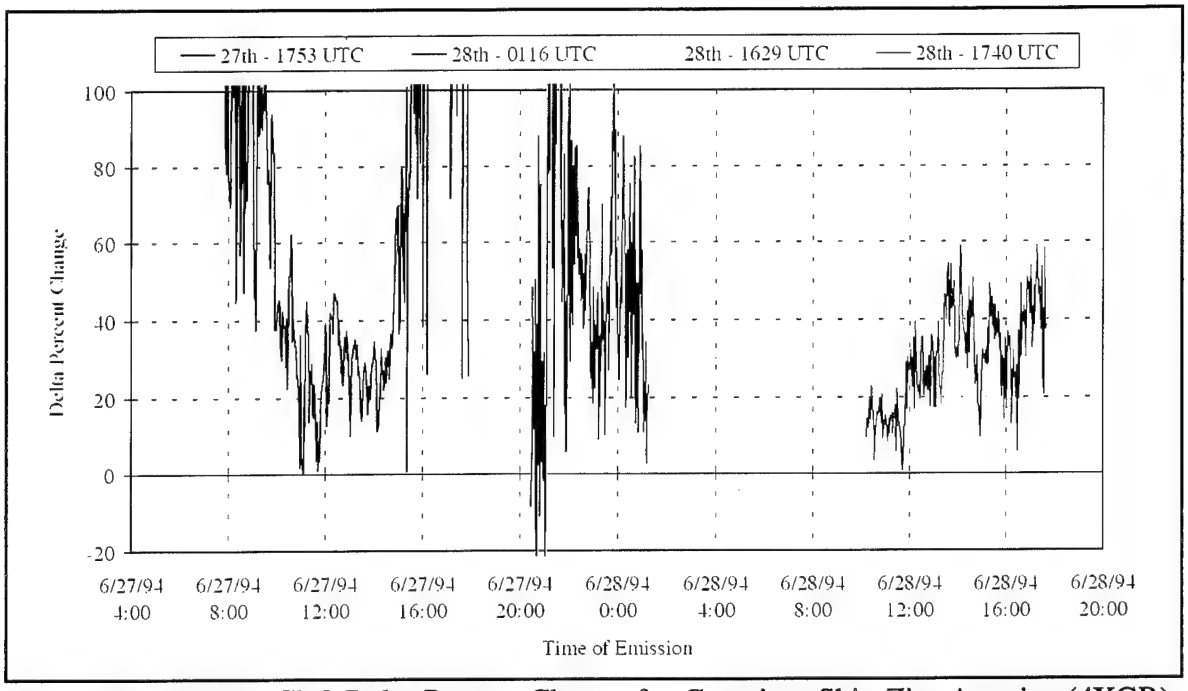

Figure 28. AVHRR Ch.3 Delta Percent Change for Container Ship Zim America (4XGR).

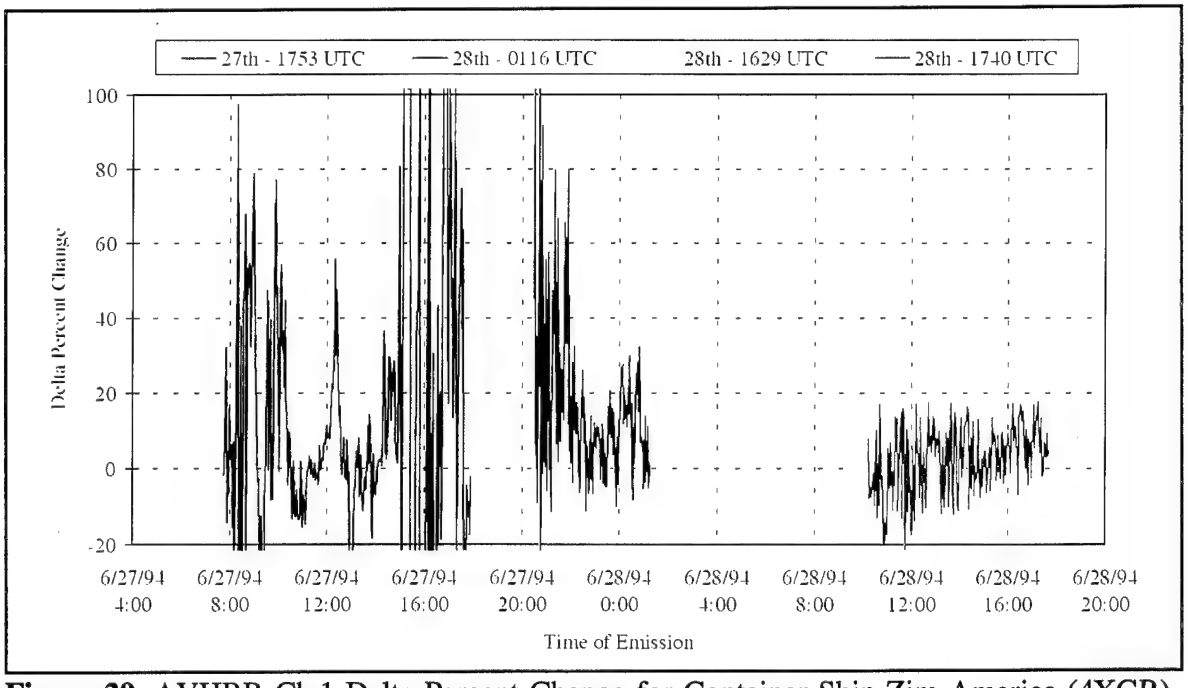

Figure 29. AVHRR Ch.1 Delta Percent Change for Container Ship Zim America (4XGR).

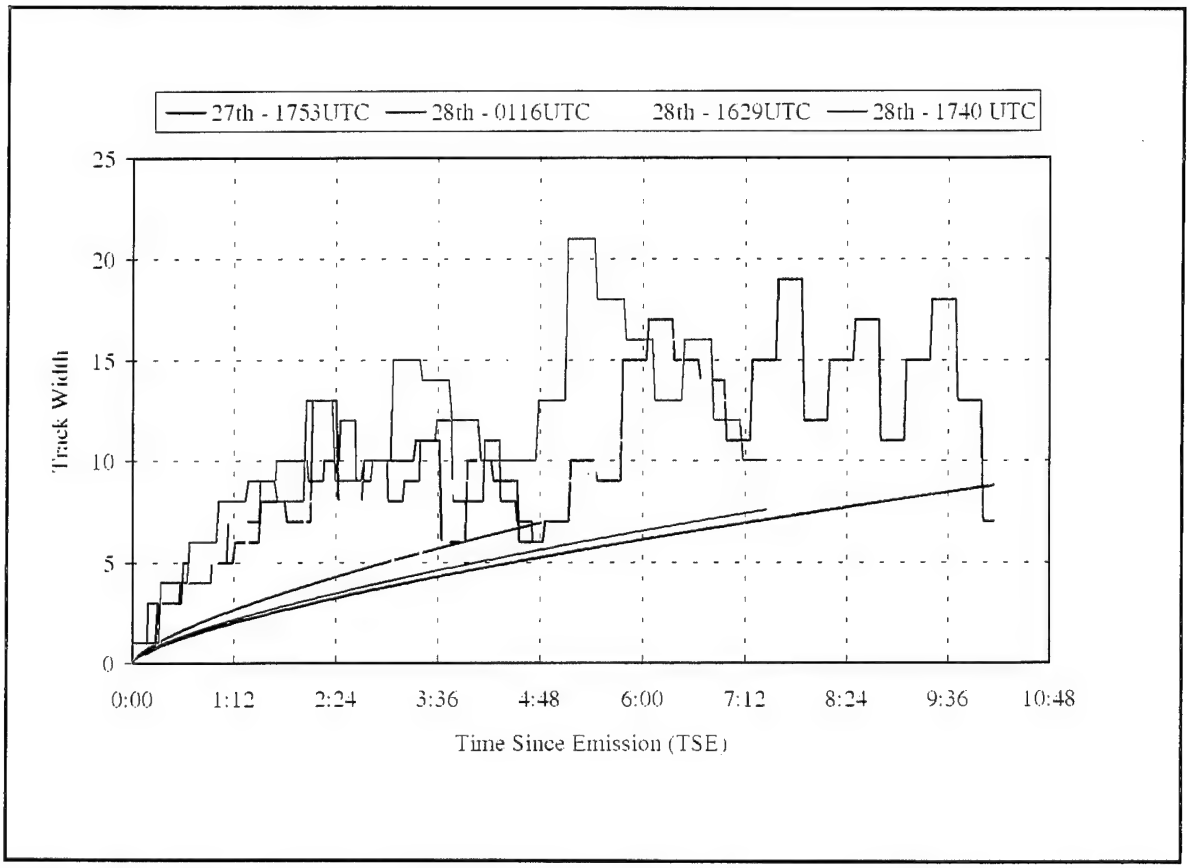

Figure 30. Average Widths for Zim America (4XGR) Shiptracks. Width is averaged over each 10 km segment of shiptrack. Smooth curves represent predicted growth based on twice the standard deviation of the plume concentration.

3. Century Highway (Callsign 8JNP)

Century Highway is an oil burning vehicles carrier 186 meters in length, displacing 46,186 tons. Shiptracks associated with this vessel were first observed on 13 June 1994 at 1653 UTC (0953 local). Figures 31 through 37 show the movement of this shiptrack through six satellite images over a period of 48 hours. Based on the ship's synoptic weather reports Century Highway was on a southeasterly heading at a speed of between 16 and 20 knots. True winds were reported out of the northwest from 10 to 20 knots producing relative winds from the east. All Century Highway shiptracks in these successive images correlated well with the reported conditions. Table 4 lists Century Highway's reported conditions. Note that course and speed are mean values for the coded range reported. Relative wind is based on this mean reported value.

Date/Time YYMMDD HHMM	**Position** LAT/LON	**Course/Speed** DEG/KTS	**True Wind** DEG/KTS	**Rel Wind** DEG/KTS
940613 1653	33.2n/127.9w	135/18	330/16	075/05
940614 0047	31.9n/125.1w	135/18	000/20	060/15
940614 1311	29.2n/121.8w	135/18	000/20	060/15
940614 1720	28.8n/120.4w	135/18	350/14	085/10
940615 0035	27.6n/118.3w	135/18	340/14	085/08
940615 1707	24.3n/113.4w	135/18	200/03	145/19

Table 4. Position and Wind Reports for Century Highway (8JNP).

a. Radiative Characteristics

Analysis of the radiative characteristics reveals subtle differences between this data series and that discussed with Tai He and Zim America. Figure 38 shows that ambient cloud reflectance values show a slight decrease from 8% at 13 1653 UTC to 3% at 14 0047 UTC when the shiptrack advects into a less uniform stratus region. This was seen in the Tai He and Zim America cases as well, however in this instance the

mechanism is not cloud thinning but movement from solid stratus to a broken cloud regime. Reflectance increases again to 18% at 14 1720 UTC then increases significantly to 25% at 15 0035 UTC as the track moves into a dense stratus field. Values then lower again to 15% as the track moves into a more broken cloud regime. Track reflectance (Figure 39) shows the same trend with reflectance values 2% to 5% higher than ambient values. This case clearly shows the dependence of the track radiative characteristics of those of the ambient cloud in which the shiptrack is formed.

DPC3 values (Figure 40) show an increase from approximately 30% at 13 1653 UTC to approximately 50% at 14 0047 UTC then drop again to 30% at 14 1720 UTC and further to approximately 20% at 15 1707 UTC. The satellite imagery reveals that the track is barely discernable from the background cloud--confirmed by DPC3 values which decrease from near 50% at 14 0047 UTC to approximately 20% at 14 1720 UTC. This trend is continued in the 15 0035 UTC image. DPC1 values (Figure41) show a great deal variability throughout the series of tracks, with mean values near zero.

b. Track Width

Track widths for Century Highway all show the same characteristic growth pattern (Figure 42). The predicted pattern matches well with the observed widths. The departure from the Tai He and Zim America cases is in the maximum width attained at distance from the source, where the width range is from 7 to 10 km instead of 10 to 12 km as seen in the previous cases. Note that the slow growth predicted for the 15 1707 UTC track is due to a combination of a low true to relative wind ration(3:20) and a large relative wind speed (20 knots). The observed track for this time follows this trend as well.

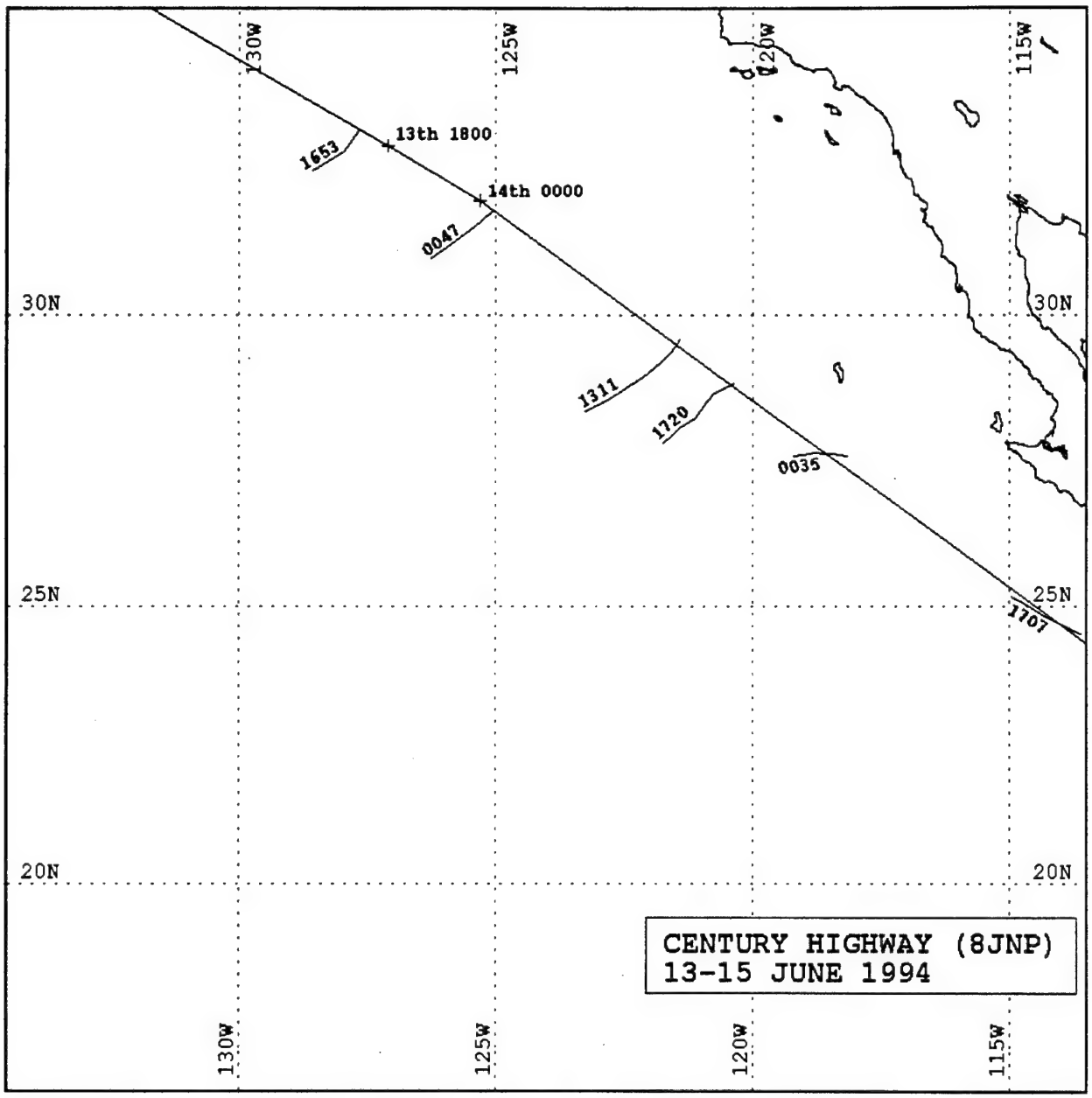

Figure 31. Transit History for Vehicles Carrier Century Highway (8JNP). Ship positions shown with day and time. Associated shiptracks are denoted by curved lines extending from transit path with satellite pass times indicated on individual tracks.

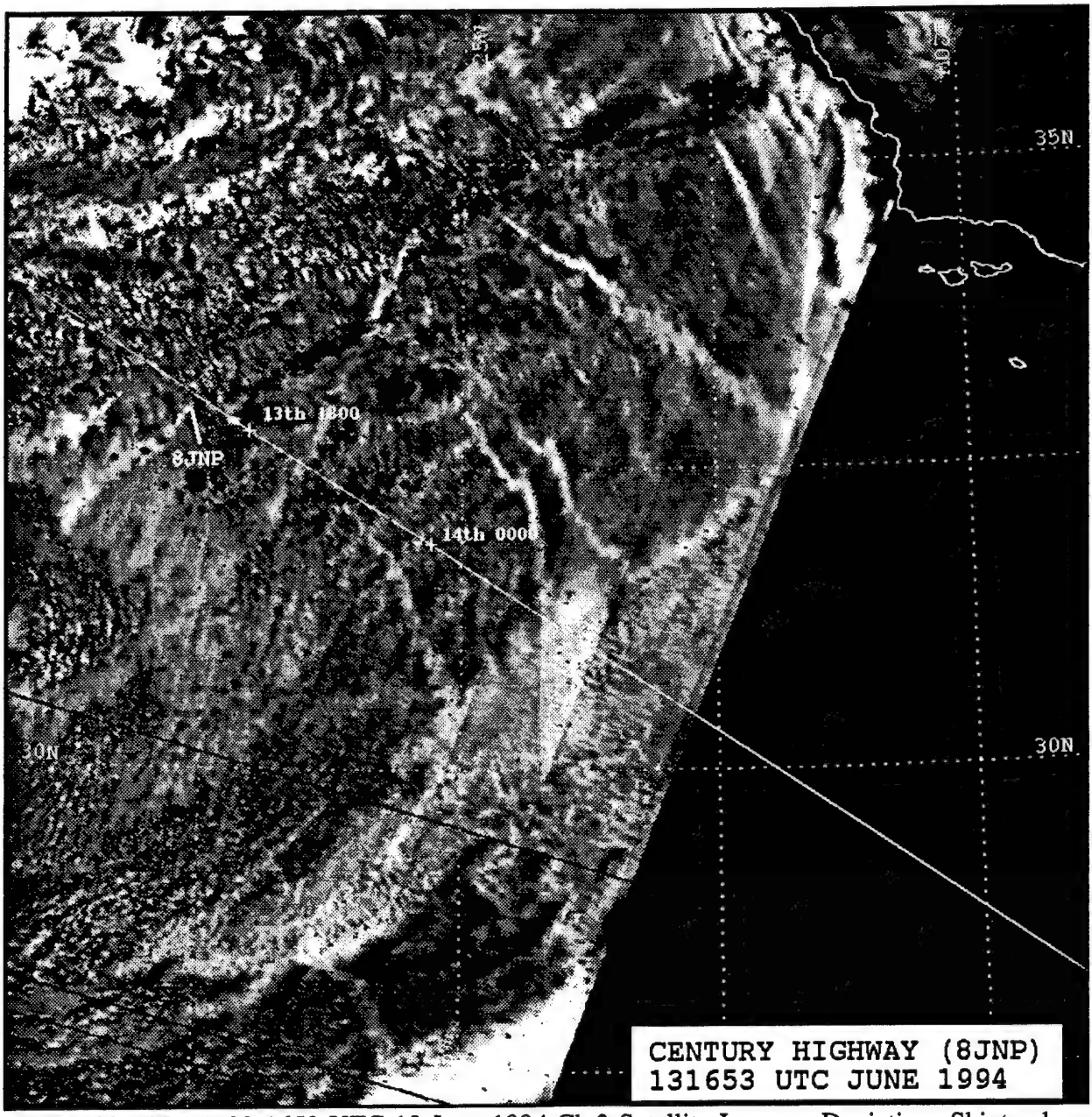

Figure 32. NOAA 09 1653 UTC 13 June 1994 Ch.3 Satellite Imagery Depicting Shiptrack Produced by Vehicles Carrier Century Highway (8JNP). Solid line denotes Century Highway position history based on synoptic weather reports. Shiptrack location indicated by callsign 8JNP.

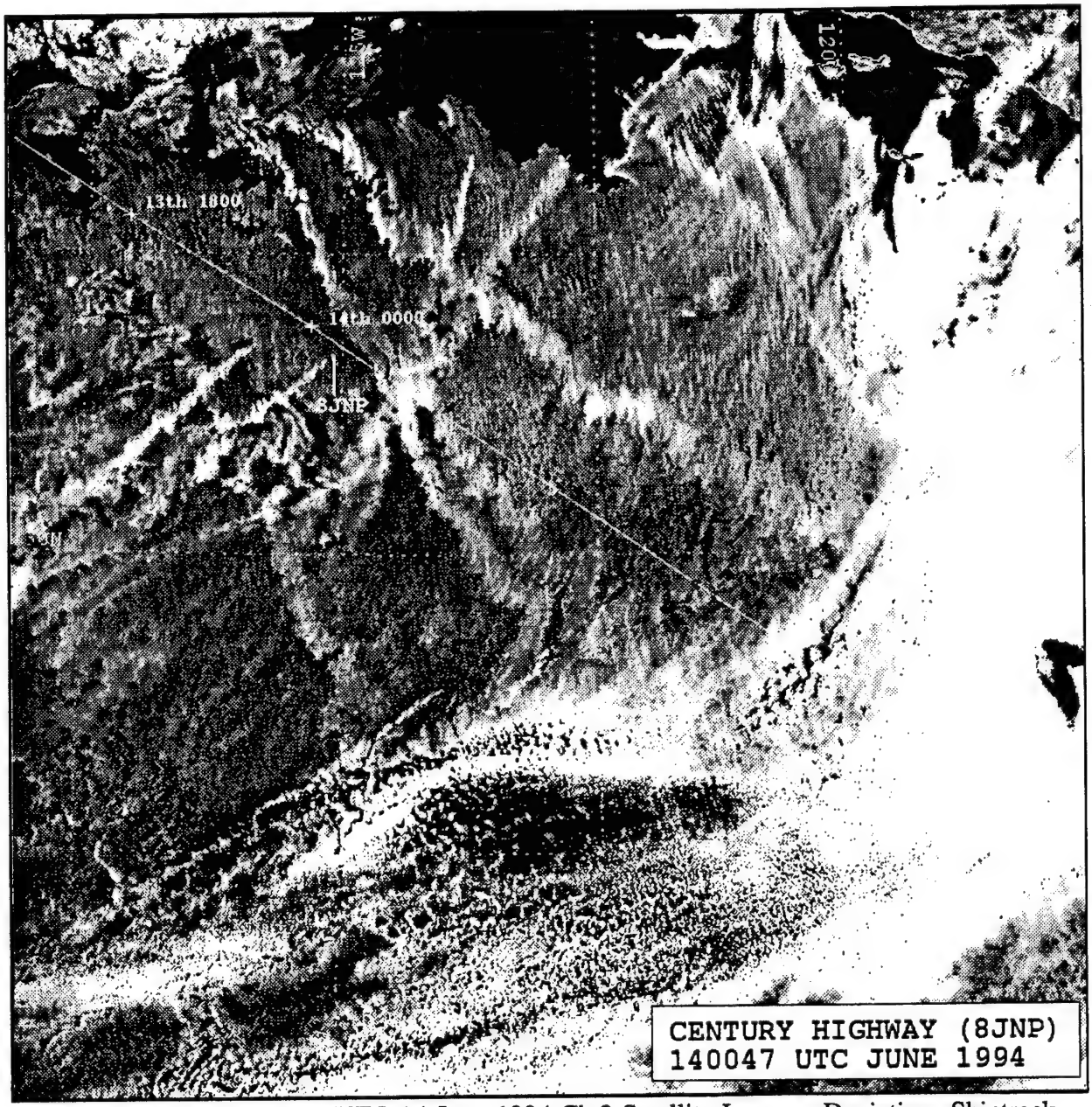

Figure 33. NOAA 11 0047 UTC 14 June 1994 Ch.3 Satellite Imagery Depicting Shiptrack Produced by Vehicles Carrier Century Highway (8JNP). Solid line denotes Century Highway position history based on synoptic weather reports. Shiptrack location indicated by callsign 8JNP.

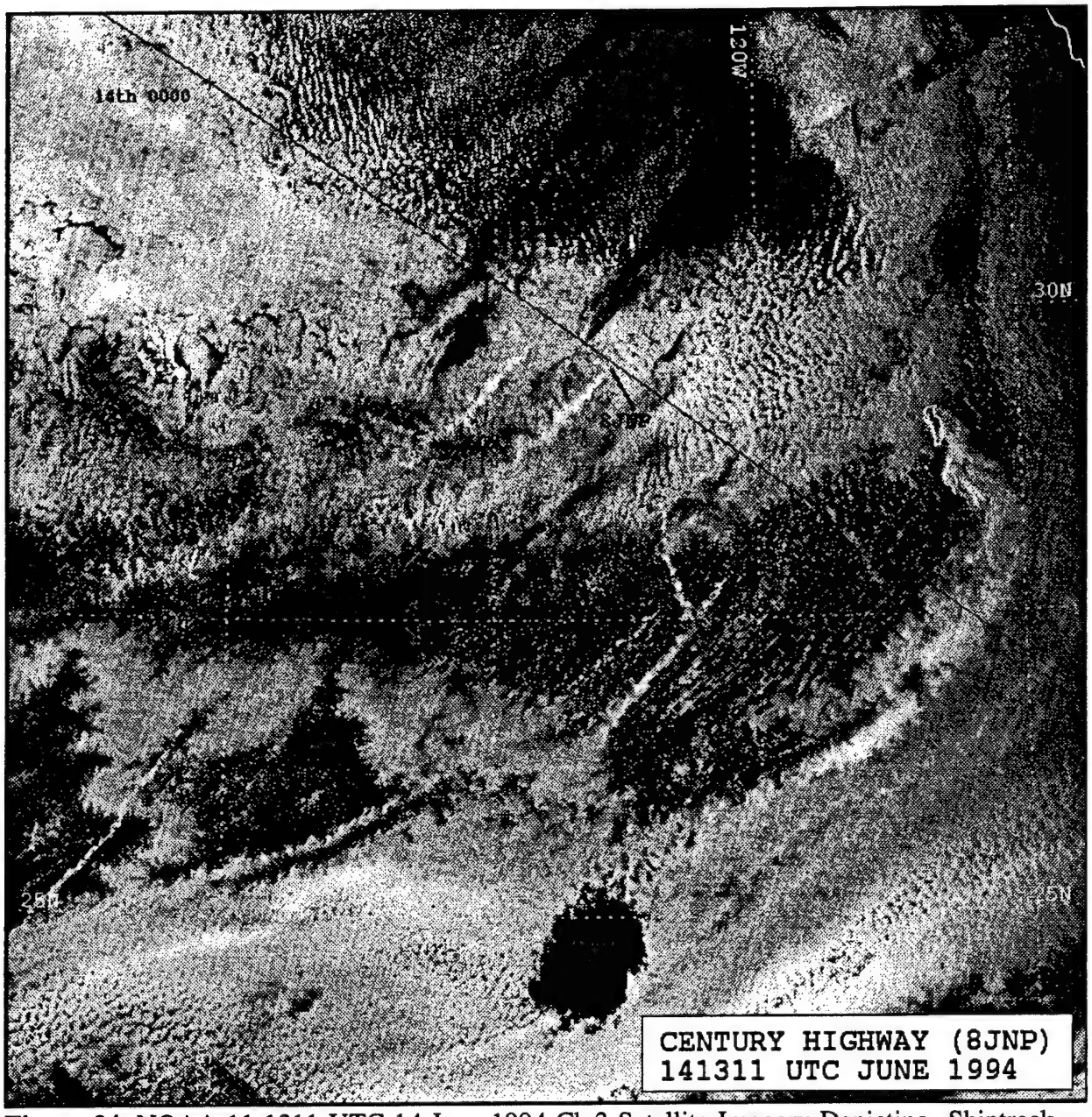

Figure 34. NOAA 11 1311 UTC 14 June 1994 Ch.3 Satellite Imagery Depicting Shiptrack Produced by Vehicles Carrier Century Highway (8JNP). Solid line denotes Century Highway position history based on synoptic weather reports. Shiptrack location indicated by callsign 8JNP.

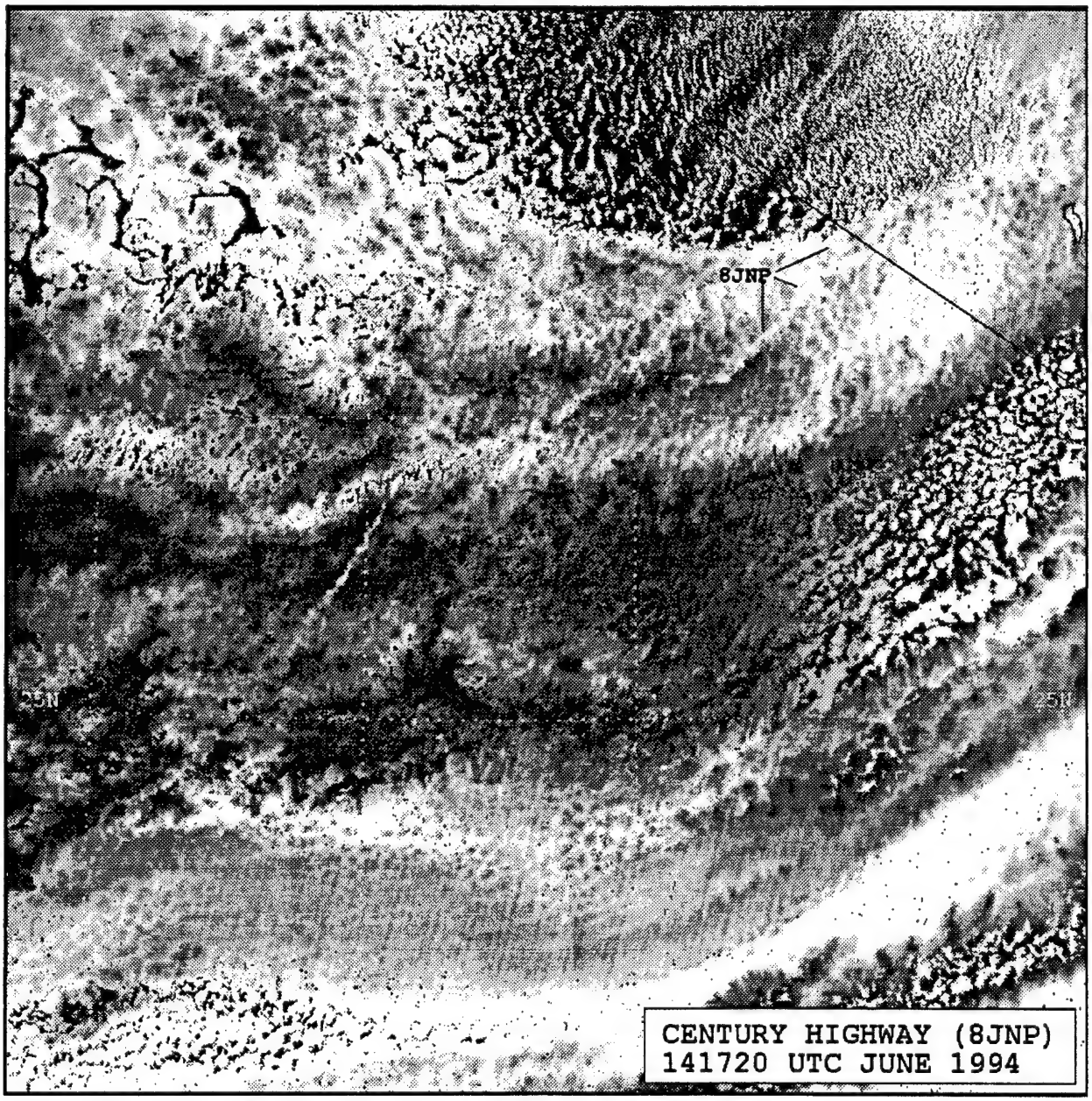

Figure 35. NOAA 09 1720 UTC 14 June 1994 Ch.3 Satellite Imagery Depicting Shiptrack Produced by Vehicles Carrier Century Highway (8JNP). Solid line denotes Century Highway position history based on synoptic weather reports. Shiptrack location indicated by callsign 8JNP.

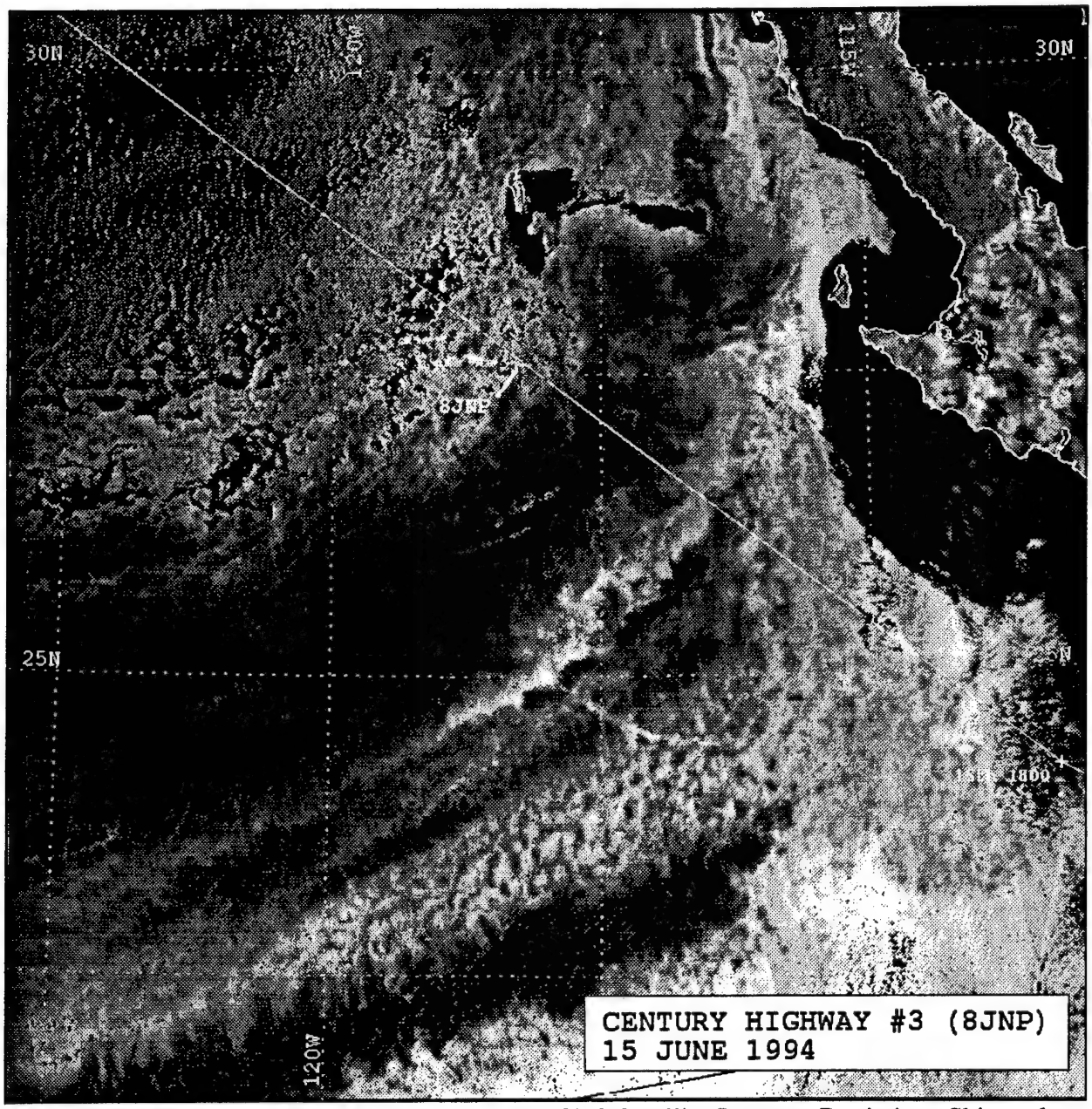

Figure 36. NOAA 11 0035 UTC 15 June 1994 Ch.3 Satellite Imagery Depicting Shiptrack Produced by Vehicles Carrier Century Highway (8JNP). Solid line denotes Century Highway position history based on synoptic weather reports. Shiptrack location indicated by callsign 8JNP.

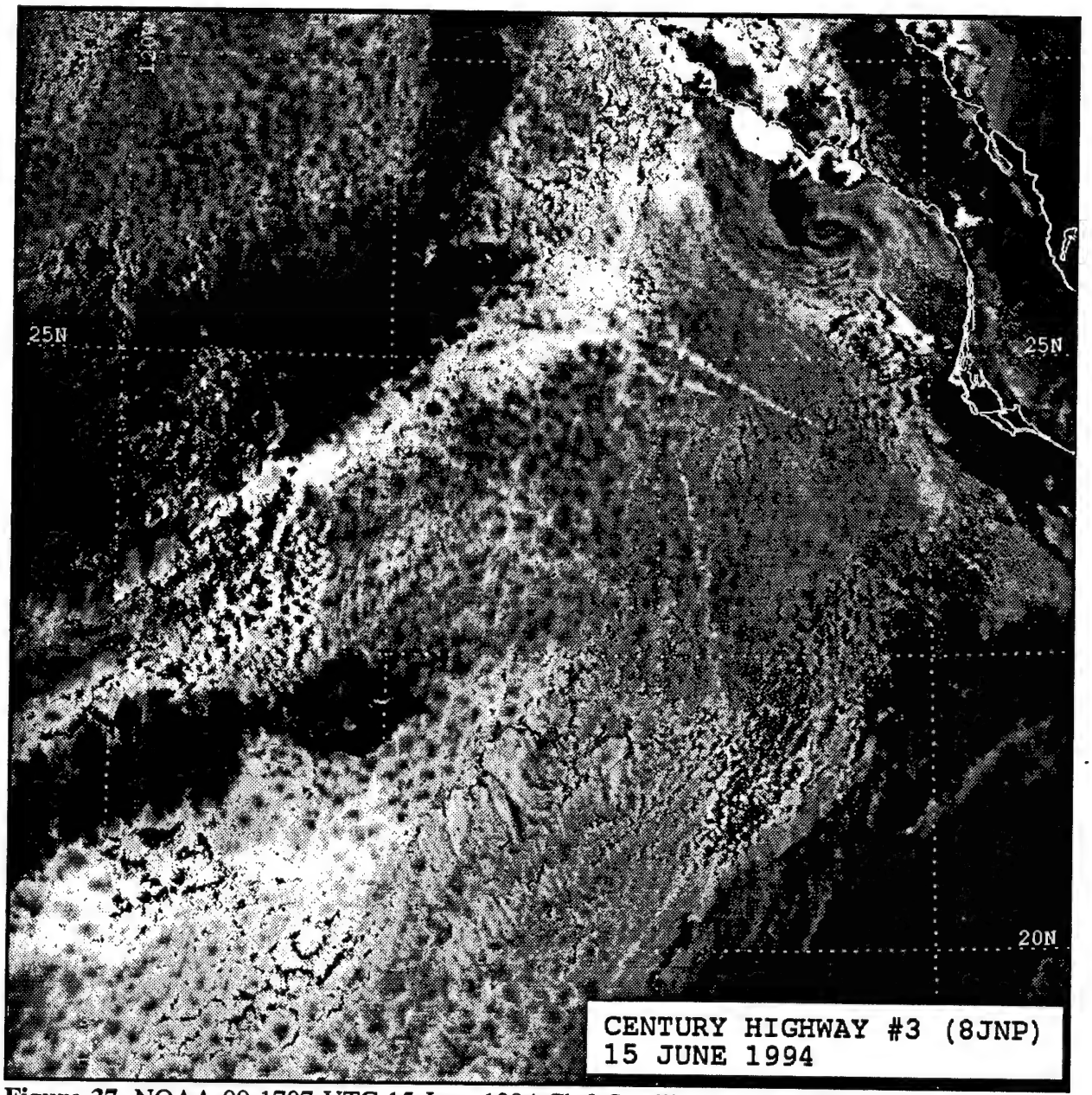

Figure 37. NOAA 09 1707 UTC 15 June 1994 Ch.3 Satellite Imagery Depicting Shiptrack Produced by Vehicles Carrier Century Highway (8JNP). Solid line denotes Century Highway position history based on synoptic weather reports. Shiptrack location indicated by callsign 8JNP.

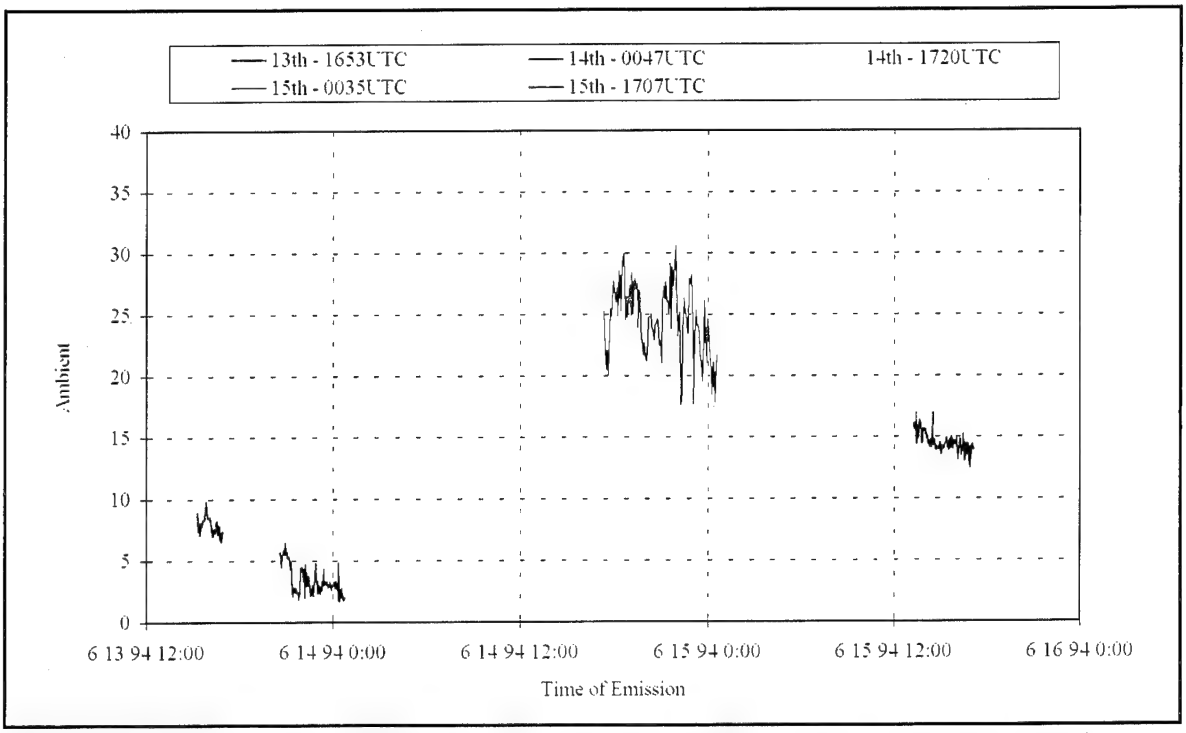

Figure 38. Ch.3 Ambient Reflectance for Vehicles Carrier Century Highway (8JNP).

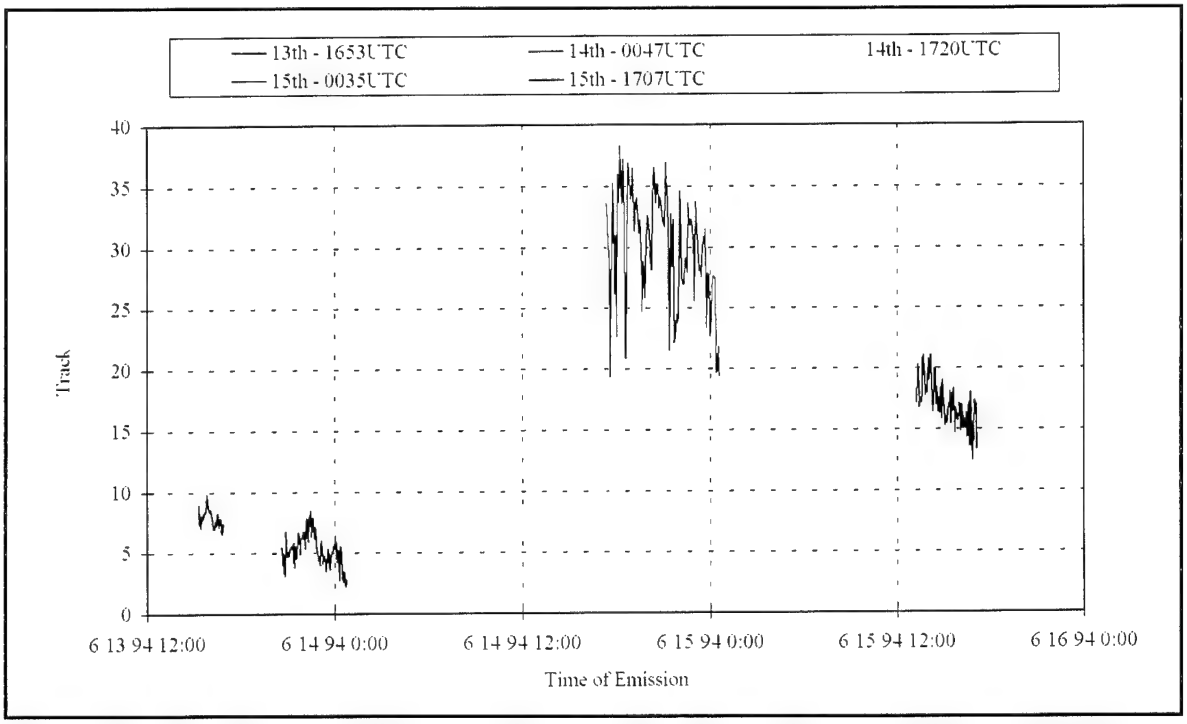

Figure 39. Ch.3 Shiptrack Reflectance for Vehicles Carrier Century Highway (8JNP).

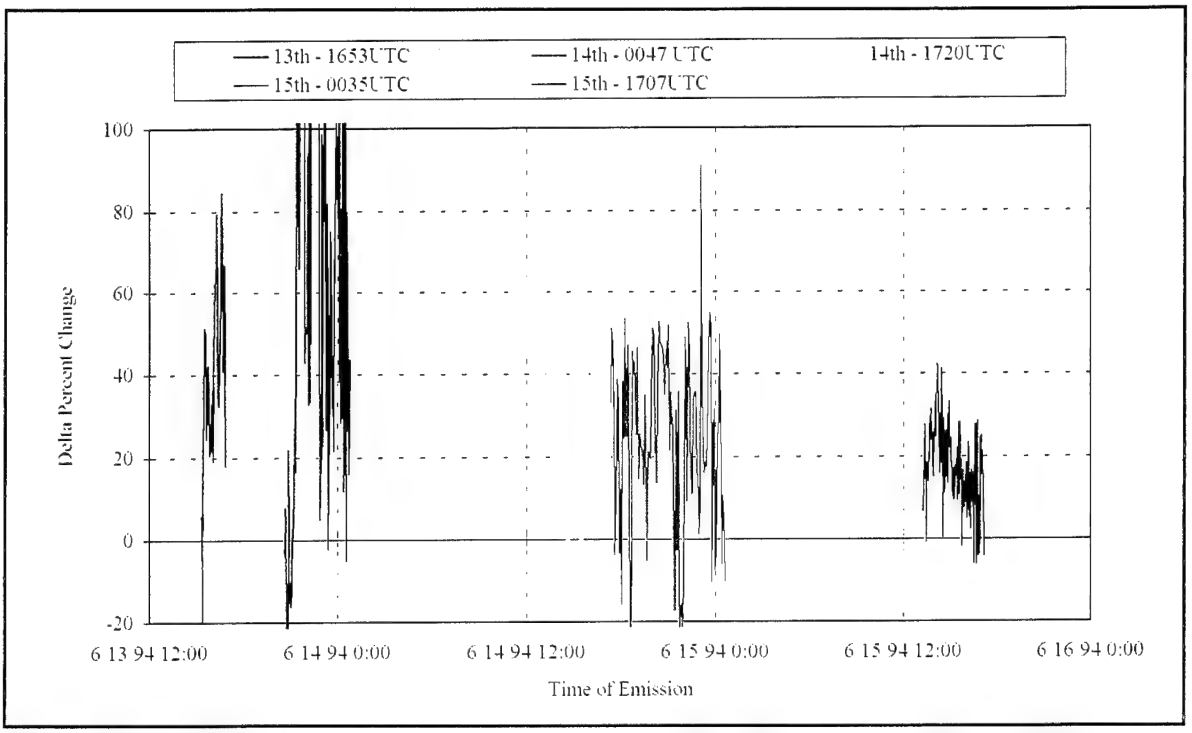

Figure 40. AVHRR Ch.3 Delta Percent Change for Vehicles Carrier Century Highway (8JNP).

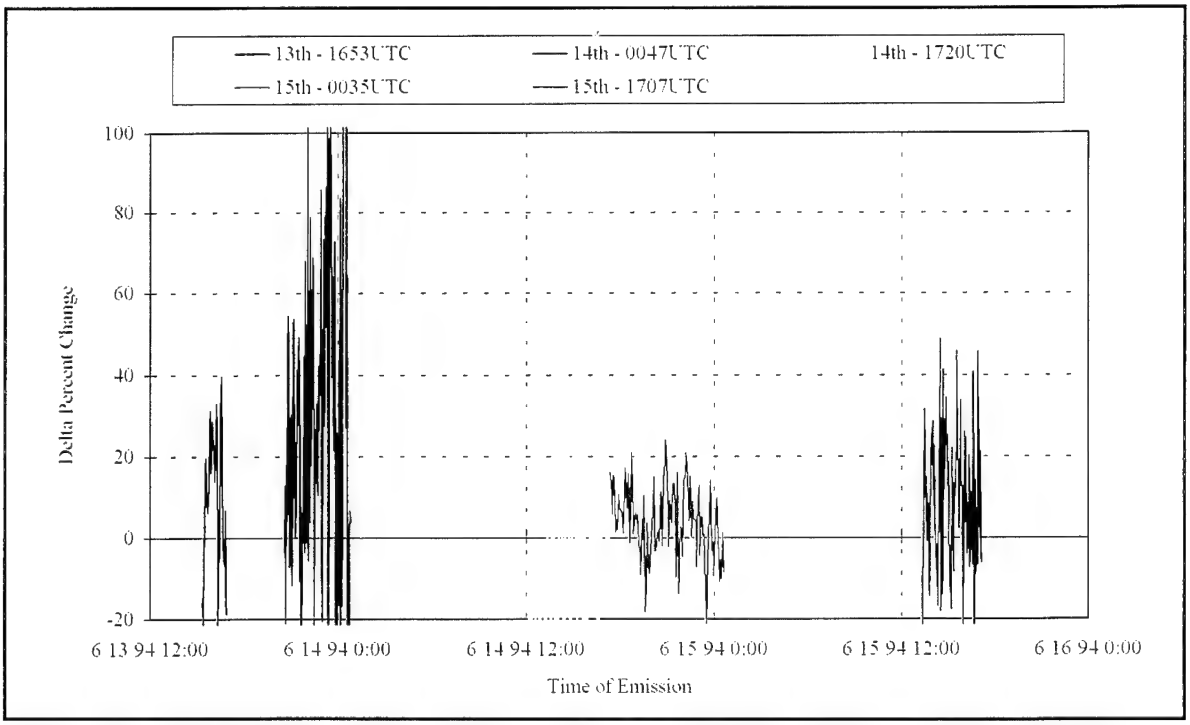

Figure 41. AVHRR Ch.1 Delta Percent Change for Vehicles Carrier Century Highway (8JNP).

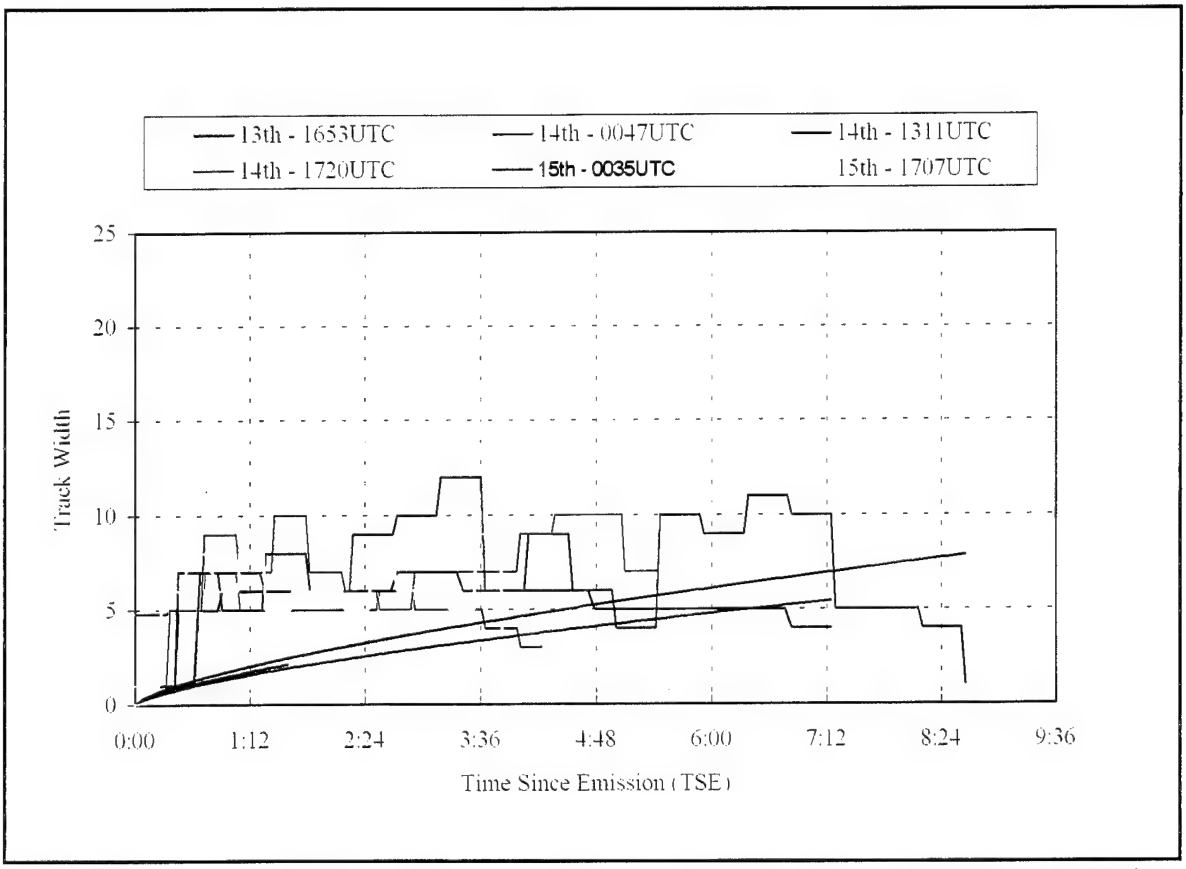

Figure 42. Average Widths for Century Highway (8JNP) Shiptracks. Width is averaged over each 10 km segment of shiptrack. Smooth curves represent predicted growth based on twice the standard deviation of the plume concentration.

4. Hercules Highway (Callsign JKOW)

Hercules Highway is also an oil burning vehicles carrier 179 meters in length, displacing 46,875 tons. Shiptracks associated with this vessel were first observed on 13 June 1994 at 1653 UTC (0953 local). Figures 43 through 49 show the movement of this shiptrack through six satellite images over a period of 48 hours. Based on the ship's synoptic weather reports Hercules Highway was on a southeasterly heading at a speed of between 16 and 20 knots. True winds were reported out of the northwest from 10 to 20 knots producing relative winds from the east. All Century Highway shiptracks in these successive images correlated well with the reported conditions. Table 5 lists Hercules Highway's reported conditions. Note that course and speed are mean values for the coded range reported. Relative wind is based on this mean reported value.

Date/Time YYMMDD HHMM	**Position** LAT/LON	**Course/Speed** DEG/KTS	**True Wind** DEG/KTS	**Rel Wind** DEG/KTS
940613 1653	33.2n/128.8w	135/18	330/15	085/05
940614 0047	31.9n/126.1w	135/18	000/20	060/15
940614 1311	29.8n/122.3w	135/18	350/14	085/10
940614 1720	29.0n/121.0w	135/18	340/14	085/08
940615 0035	27.9n/119.1w	135/18	330/15	085/05
940615 1707	24.6n/114.2w	135/18	350/05	125/14

Table 5. Position and Wind Reports for Hercules Highway (JKOW).

a. Radiative Characteristics

Analysis of radiative characteristics indicates slightly increasing reflectance values similar to those discussed with Century Highway. Figure 50 shows a decrease in ambient reflectance from 8% at 13 653 UTC to 3% at 14 0047 UTC, increasing again to 7% at 14 1720 UTC. The 15 0035 UTC ambient cloud and track values (Figure 51) show a slight increase from the 14 1720 UTC values, from 7%to 8% for ambient cloud and

from 9% to 12% for shiptrack, but not to the extent shown in the Century Highway case which went from 8% to 24% for ambient cloud and from 9% to 28% in track reflectance during the same timeframe. This results from Hercules Highway's track location in the broken cloud region of the larger stratus field that encompasses Century Highway's track. The 15 1707 UTC data are again similar for both ships as their tracks are in a more uniform cloud region. Ambient and track reflectance jump to 15% and 18%, respectively, as the track advects into this brighter region (Century Highway shows the same values).

DPC3 values, Figure 52, are increasing from approximately 40% at 13 1653 UTC to approximately 80% 14 0047 UTC . They then decrease from approximately 35% at 14 1720 UTC, and remain at that level, in the mean, through the remaining images. DPC1 values shown in Figure 53, show much variability, fluctuating about 0% in the mean throughout the series. Decreasing DPC3 values from 14 0047 UTC onward are consistent with the advection of the shiptrack from a region of broken stratocumulus to a band of dense stratus at 14 1740 UTC where the track is barely discernable from the background cloud. Century Highway is showing the same trend with the same absolute reflectance values. The only departure from this is in the variability of DPC1 and DPC3 values for Hercules Highway at 14 1720 UTC and 15 0035 UTC. Hercules Highway is a more broken stratus area in both instances.

b. Track Width

Hercules Highway track width (Figure 54) shows the slow growth pattern with the same maximum width range of 7-10 km as seen with Century Highway. Predicted growth rates match very well in both cases which is indicated by the similarity of true and relative winds reported by both vessels. Spurious values for the 13 1653 UTC track (20 km) may be the result of bright cloud in the area contaminating the track.

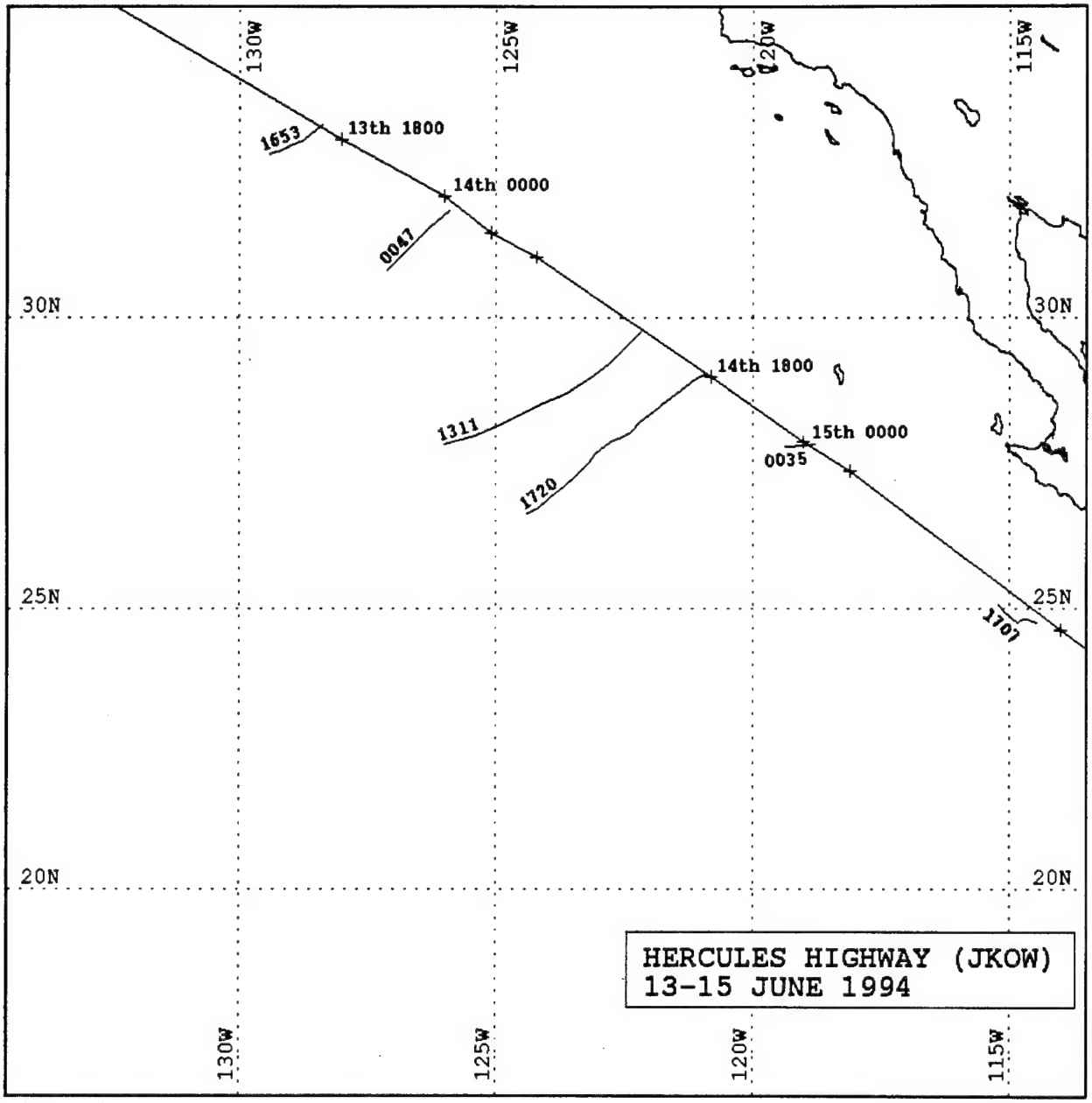

Figure 43. Transit History for Vehicles Carrier Hercules Highway (JKOW). Ship positions shown with day and time. Associated shiptracks are denoted by curved lines extending from transit path with satellite pass times indicated on individual tracks.

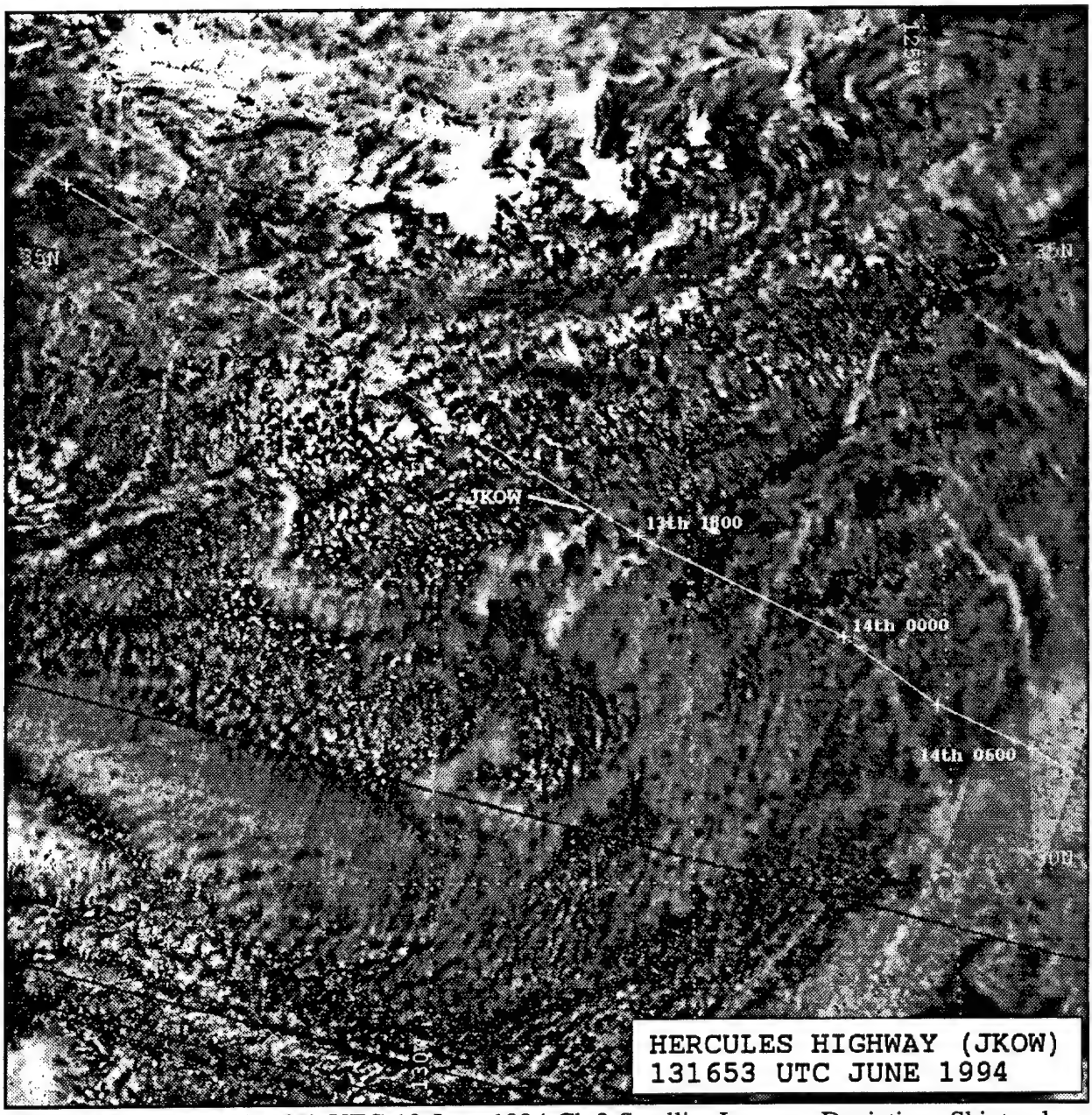

Figure 44. NOAA 09 1653 UTC 13 June 1994 Ch.3 Satellite Imagery Depicting Shiptrack Produced by Vehicles Carrier Hercules Highway (JKOW). Solid line denotes Century Highway position history based on synoptic weather reports. Shiptrack location indicated by callsign JKOW.

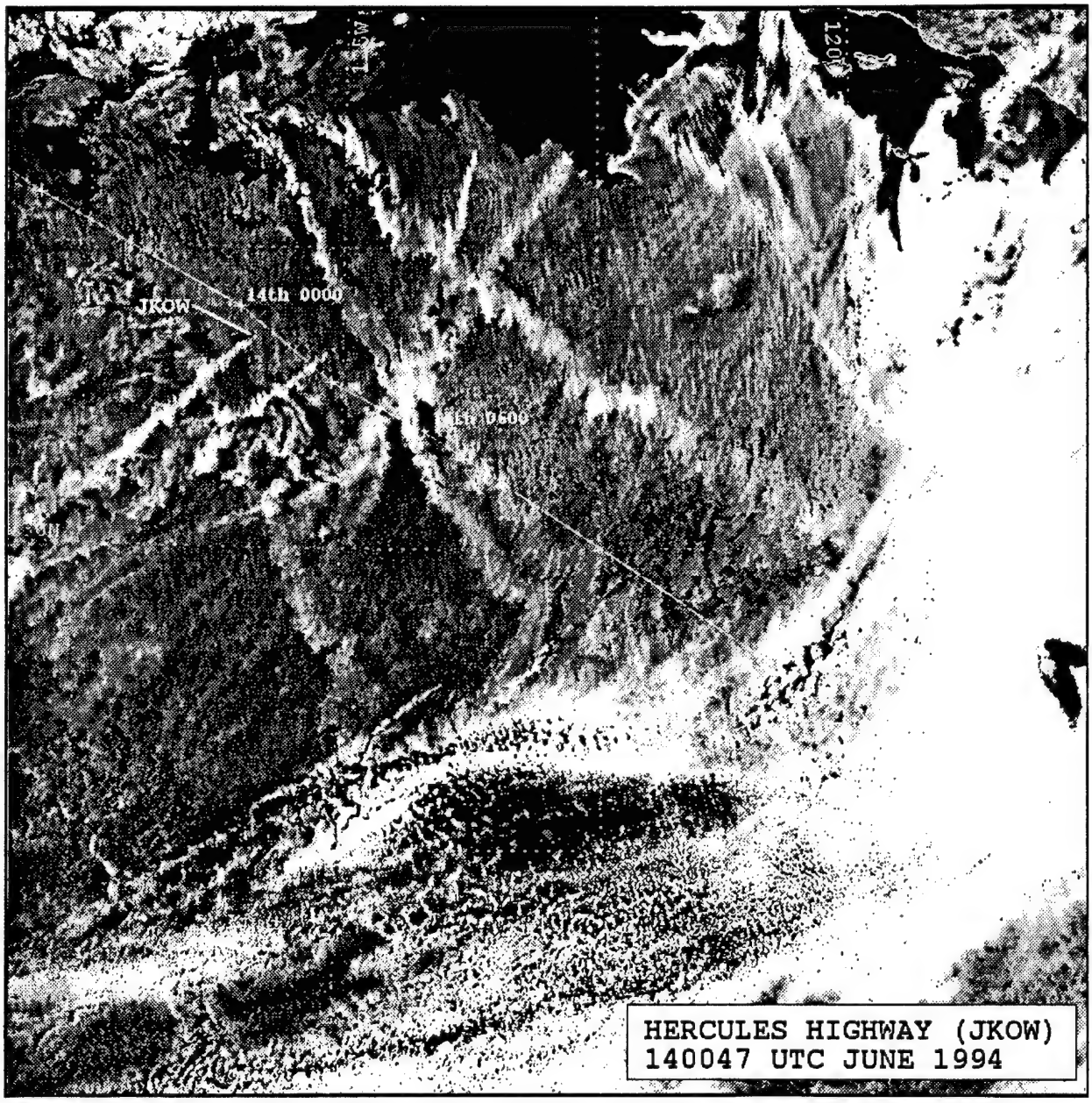

Figure 45. NOAA 11 0047 UTC 14 June 1994 Ch.3 Satellite Imagery Depicting Shiptrack Produced by Vehicles Carrier Hercules Highway (JKOW). Solid line denotes Century Highway position history based on synoptic weather reports. Shiptrack location indicated by callsign JKOW.

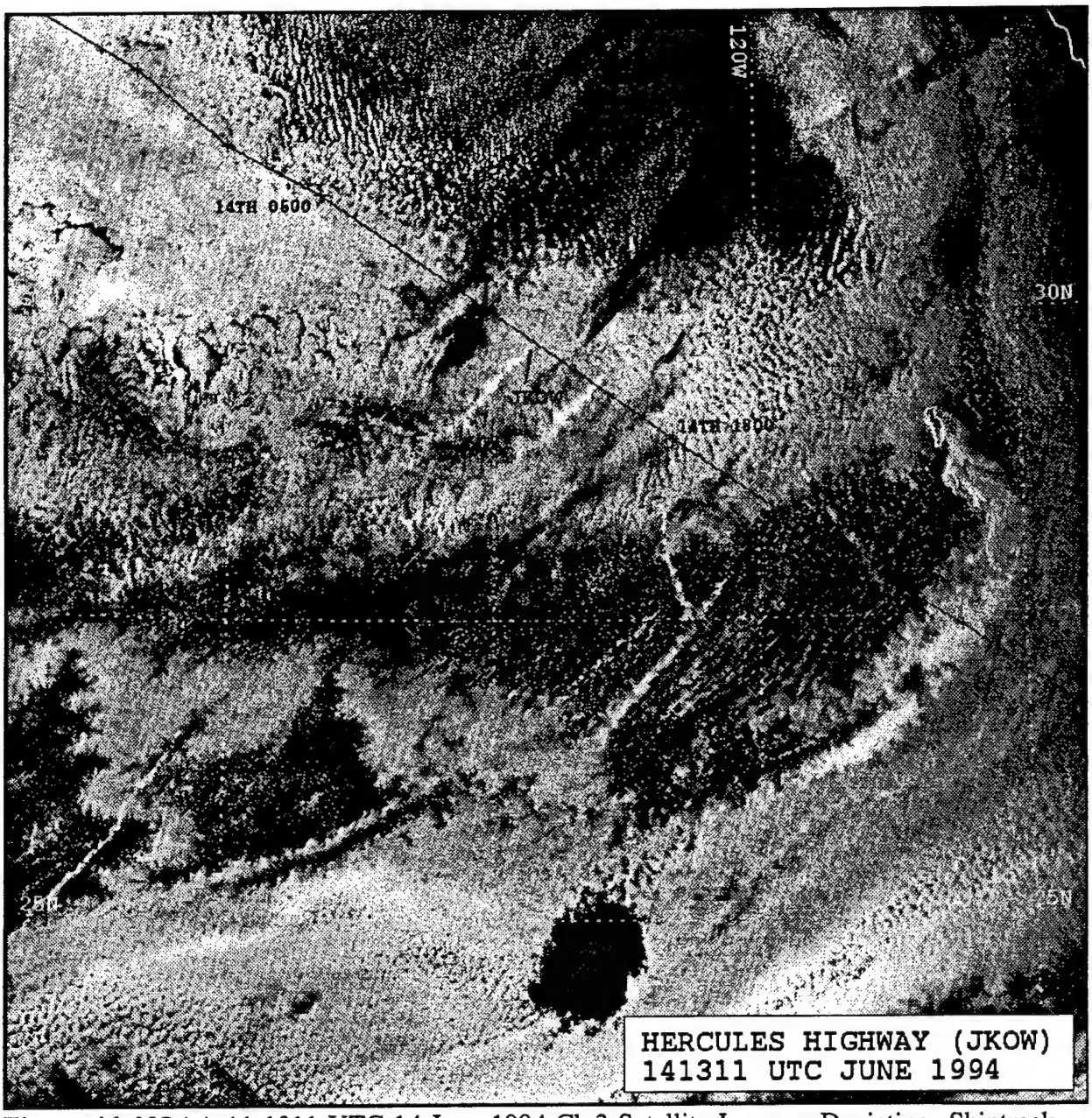

Figure 46. NOAA 11 1311 UTC 14 June 1994 Ch.3 Satellite Imagery Depicting Shiptrack Produced by Vehicles Carrier Hercules Highway (JKOW). Solid line denotes Century Highway position history based on synoptic weather reports. Shiptrack location indicated by callsign JKOW.

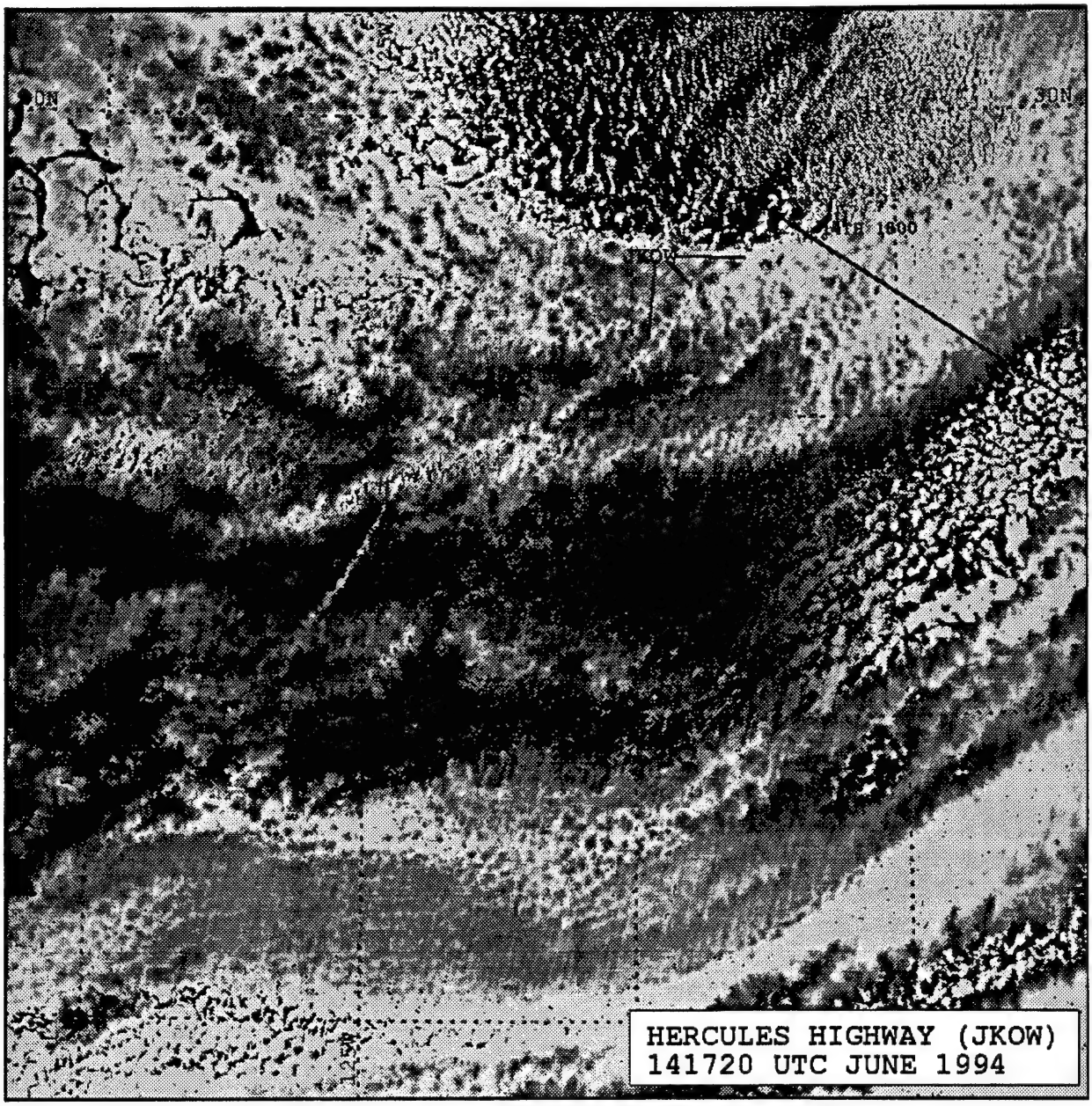

Figure 47. NOAA 09 1720 UTC 14 June 1994 Ch.3 Satellite Imagery Depicting Shiptrack Produced by Vehicles Carrier Hercules Highway (JKOW). Solid line denotes Century Highway position history based on synoptic weather reports. Shiptrack location indicated by callsign JKOW.

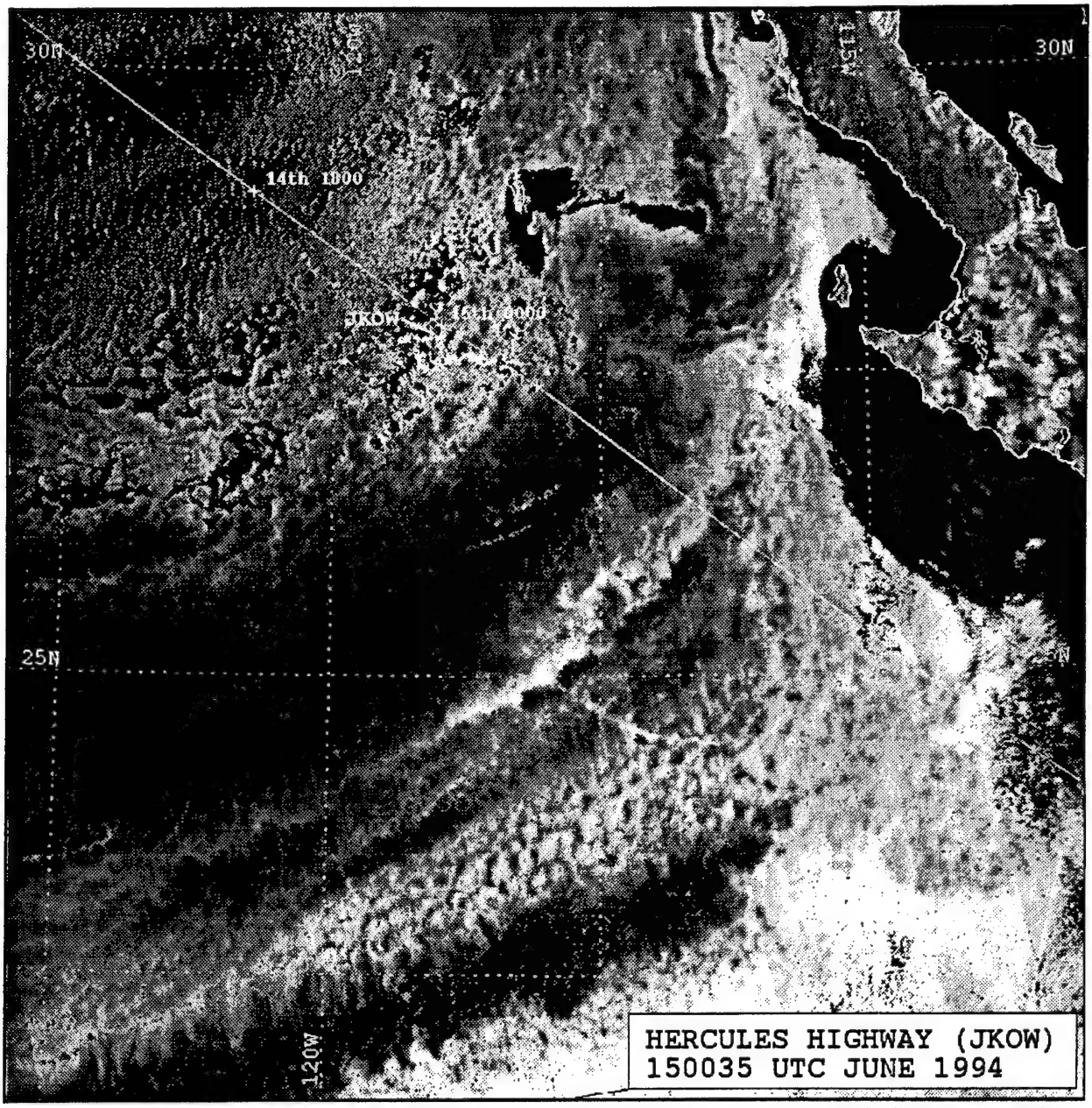

Figure 48. NOAA 11 0035 UTC 15 June 1994 Ch.3 Satellite Imagery Depicting Shiptrack Produced by Vehicles Carrier Hercules Highway (JKOW). Solid line denotes Century Highway position history based on synoptic weather reports. Shiptrack location indicated by callsign JKOW.

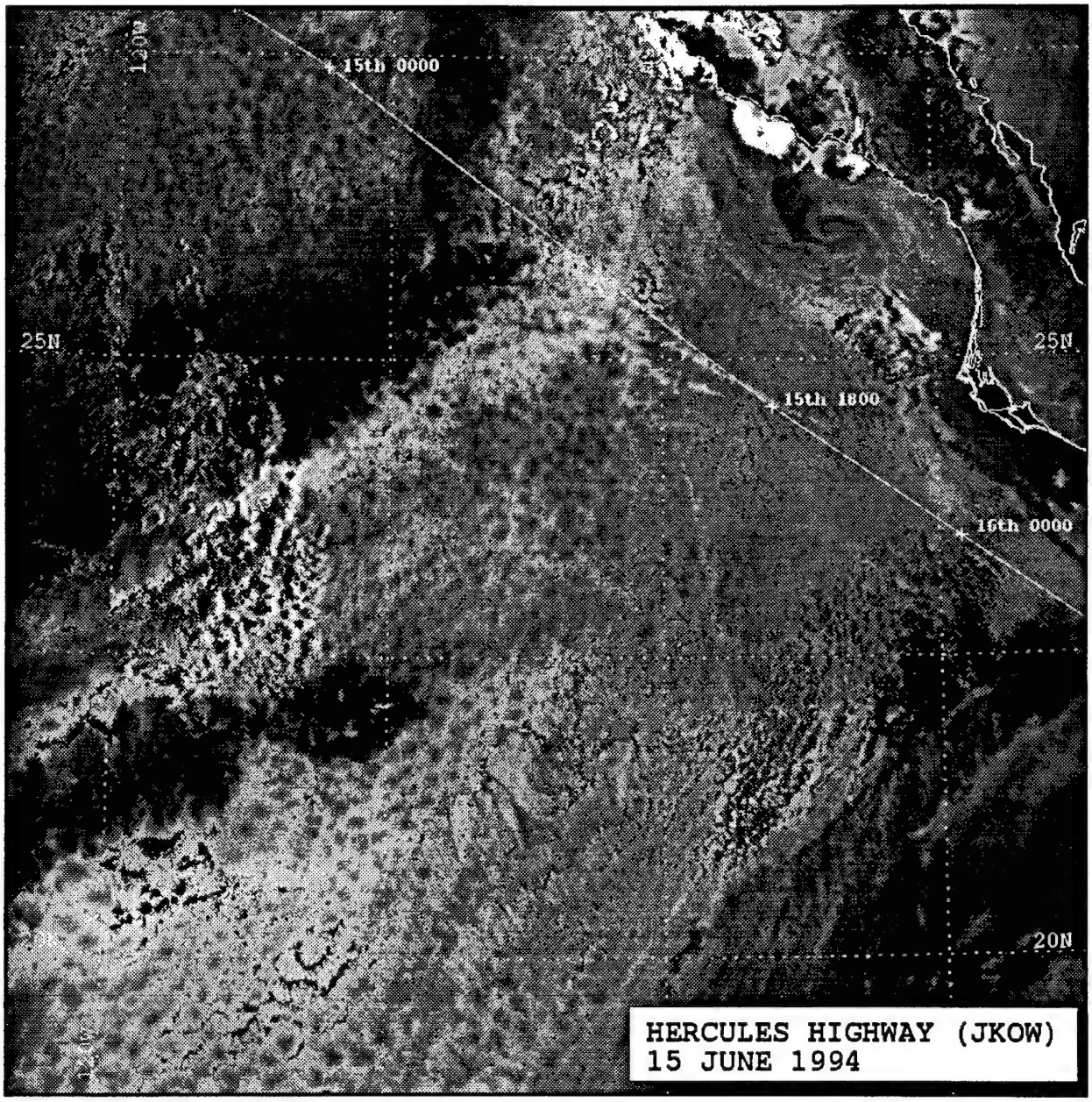

Figure 49. NOAA 09 1707 UTC 15 June 1994 Ch.3 Satellite Imagery Depicting Shiptrack Produced by Vehicles Carrier Hercules Highway (JKOW). Solid line denotes Century Highway position history based on synoptic weather reports. Shiptrack location indicated by callsign JKOW.

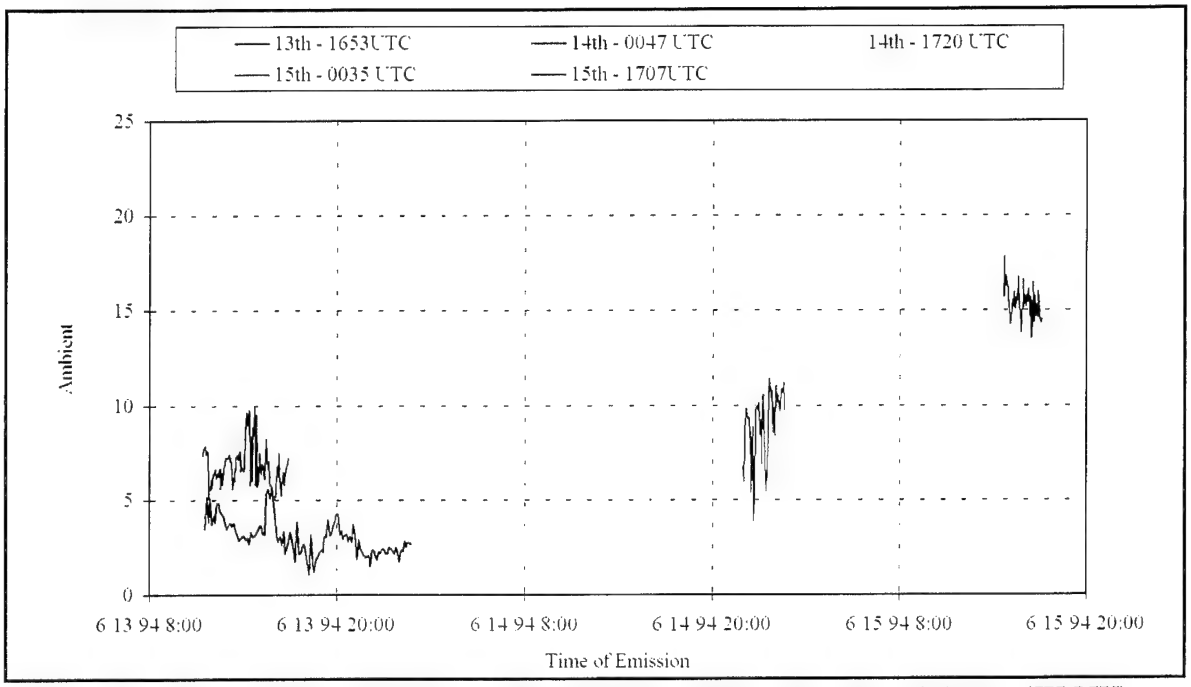

Figure 50. Ch.3 Ambient Reflectance for Vehicles Carrier Hercules Highway (JKOW).

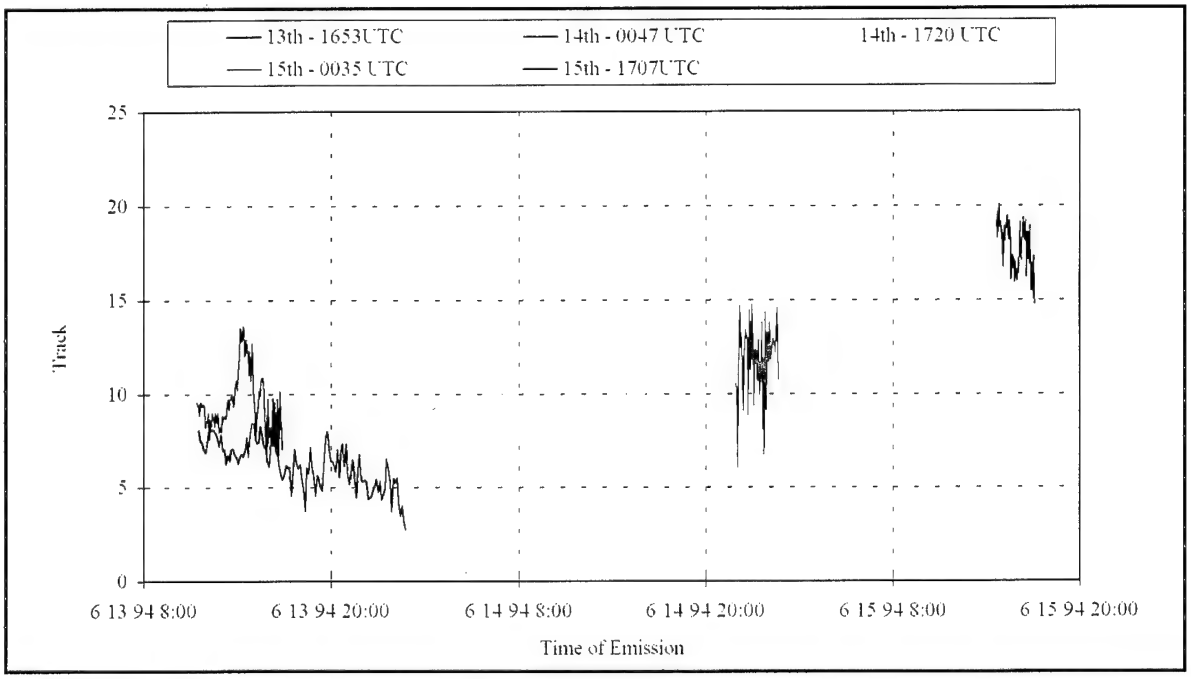

Figure 51. Ch.3 Shiptrack Reflectance for Vehicles Carrier Hercules Highway (JKOW).

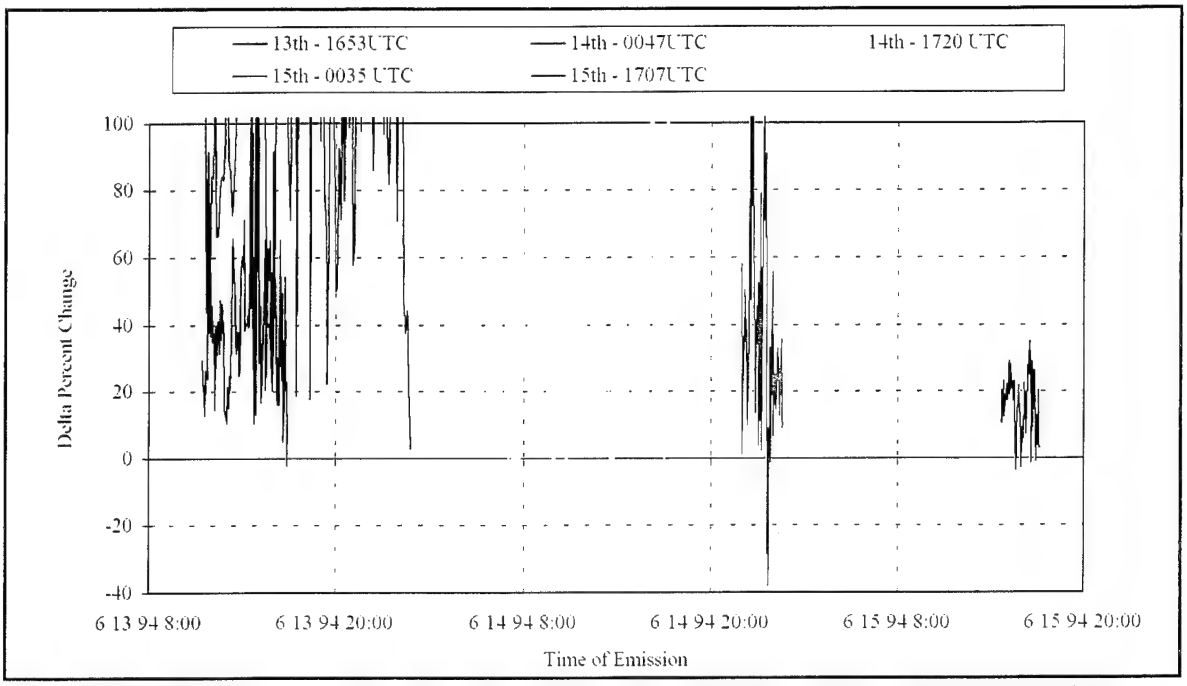

Figure 52. AVHRR Ch.3 Delta Percent Change for Vehicles Carrier Hercules Highway (JKOW).

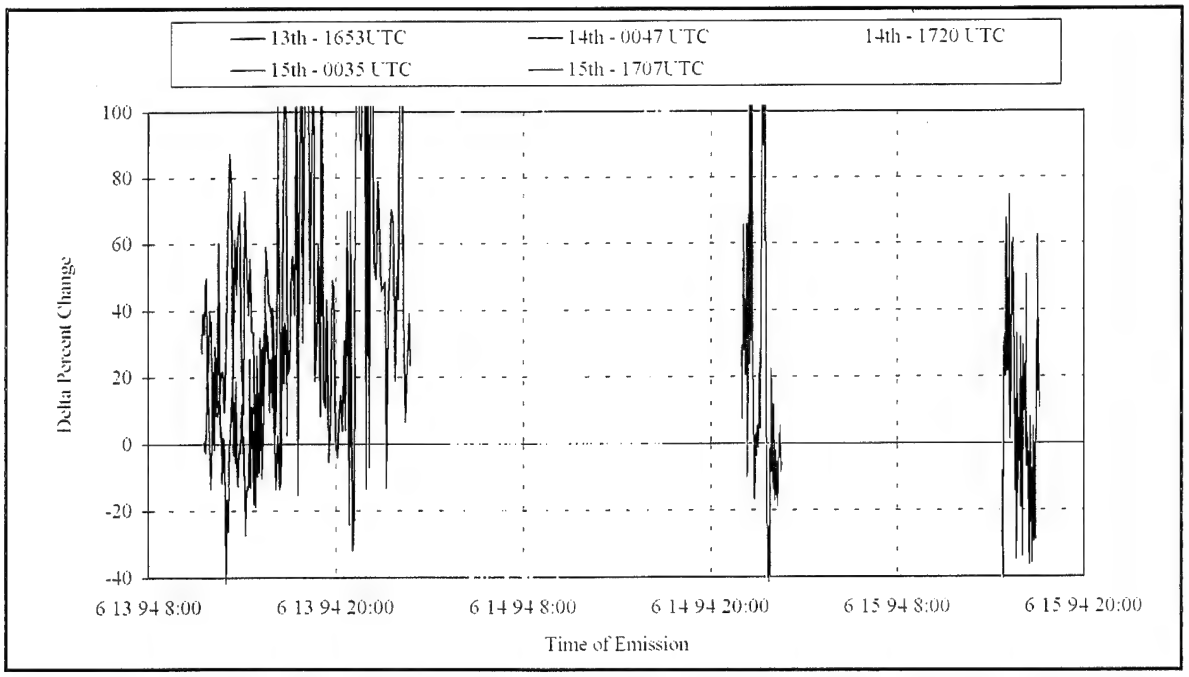

Figure 53. AVHRR Ch.1 Delta Percent Change for Vehicles Carrier Hercules Highway (JKOW).

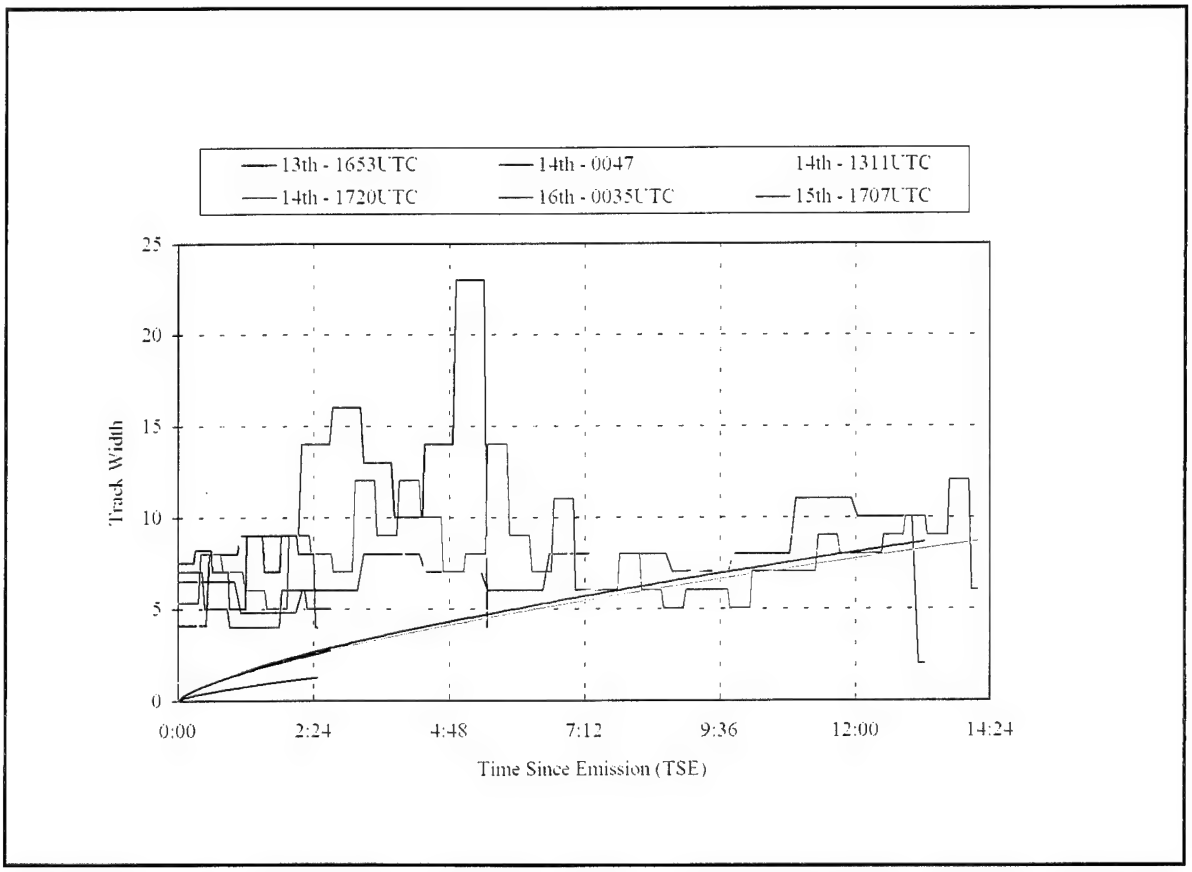

Figure 54. Average Widths for Hercules Highway (JKOW) Shiptracks. Width is averaged over each 10 km segment of shiptrack. Smooth curves represent predicted growth based on twice the standard deviation of the plume concentration.

5. Sea-Land Consumer (Callsign WCHF)

Sea-Land Consumer is a steam driven container ship 219 meters in length, displacing 23,763 tons. Shiptracks associated with this vessel were first observed on 12 June 1994 at 1336 UTC (0636 local). Figures 55 through 59 show the movement of this shiptrack through four satellite images over a period of 12 hours. Based on the ship's synoptic weather reports, Sea-Land Consumer was on a southwesterly heading at a speed of between 21 and 25 knots. True winds were reported out of the north to northeast from 12 to 22 knots producing relative winds from the northwest. All Sea-Land Consumer shiptracks in these successive images correlated well with the reported conditions. Table 6 lists Sea-Land Consumer's reported conditions. Note that course and speed are mean values for the coded range reported. Relative wind is based on this mean reported value.

Date/Time YYMMDD HHMM	**Position** LAT/LON	**Course/Speed** DEG/KTS	**True Wind** DEG/KTS	**Rel Wind** DEG/KTS
940612 1336	31.4n/129.2w	270/23	355/18	305/30
940612 1535	31.1n/130.2w	270/23	350/16	300/30
940612 1745	30.9n/131.6w	270/23	350/15	300/30
940613 0054	30.1n/134.8w	270/23	010/12	300/24

Table 6. Position and Wind Reports for Sea-Land Consumer (WCHF).

a. Radiative Characteristics

Analysis of radiative characteristics shows more classic results than previous cases. Shiptrack and ambient cloud values, Figures 60 and 61, are decreasing as the shiptrack ages. A noteworthy trend in the reflectance values is the decrease from approximately 15% to 7% for ambient cloud and approximately 20% to 10% for track seen from the 12 1535 UTC to the 13 0054 UTC shiptracks. This is opposite to that seen in the Tai He and Zim America cases. There, the ships were approaching the

continent, where in this case, the Sea-Land Consumer is moving away from southern California, out of the influence of continental aerosol contamination.

DPC3 values shown in Figure 62 are consistent between successive tracks with prominent spikes in the 12 1535 UTC and 12 1745 UTC values. Inspection of the images indicates that these peaks are associated with intersection of Sea-Land Consumer's shiptrack with the plume of another ship. The trend in DPC3 values matches well for both shiptracks indicating the relative wind error is small, shown also by the close alignment of the intersection peaks. Figure 63 shows DPC1values with much variability but trending near zero in the mean through the series.

b. Track Width

Track widths again show characteristic growth patterns. A sharp increase over the first two hours of 4-6 km/hr followed by a decrease in growth rate to 2-3 km/hr is consistent with other shiptracks noted above. Maximum width is again at 10 to 12 km which consistent with the widths observed in the Tai He and Zim America cases. These four ships passed through similar environments (in opposite directions) and all are similar in dimension and propulsion. Peaks in width between 16 and 20 km associated with the 12 1745 UTC and 13 0054 UTC tracks are associated with intersections of Sea-Land Consumer's track with other shiptracks in the area. The predicted growth curves correlate well with the slopes of the observed width plots (Figure 64).

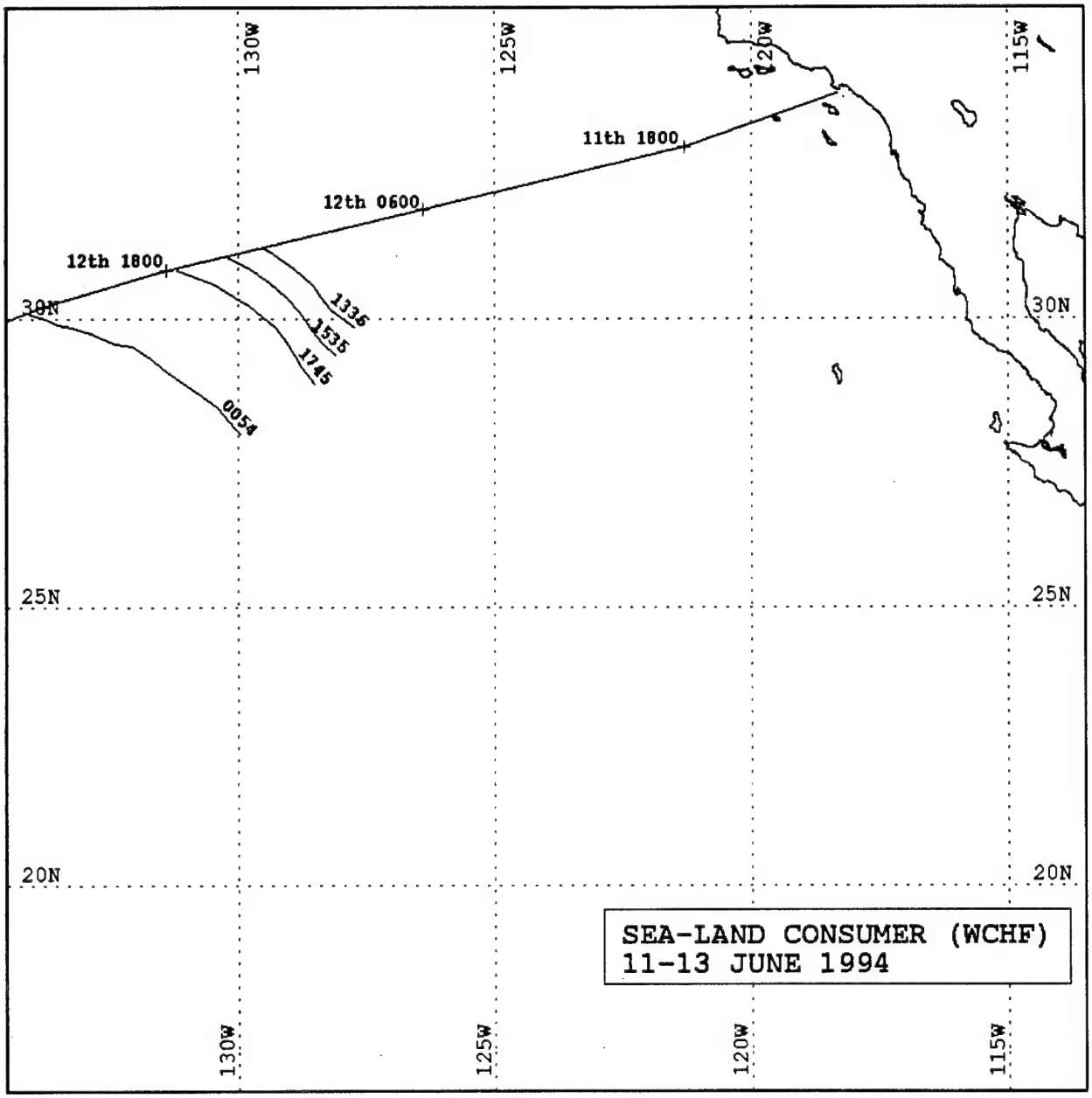

Figure 55. Transit History for Container Ship Sea-Land Consumer (WCHF). Ship positions shown with day and time. Associated shiptracks are denoted by curved lines extending from transit path with satellite pass times indicated on individual tracks.

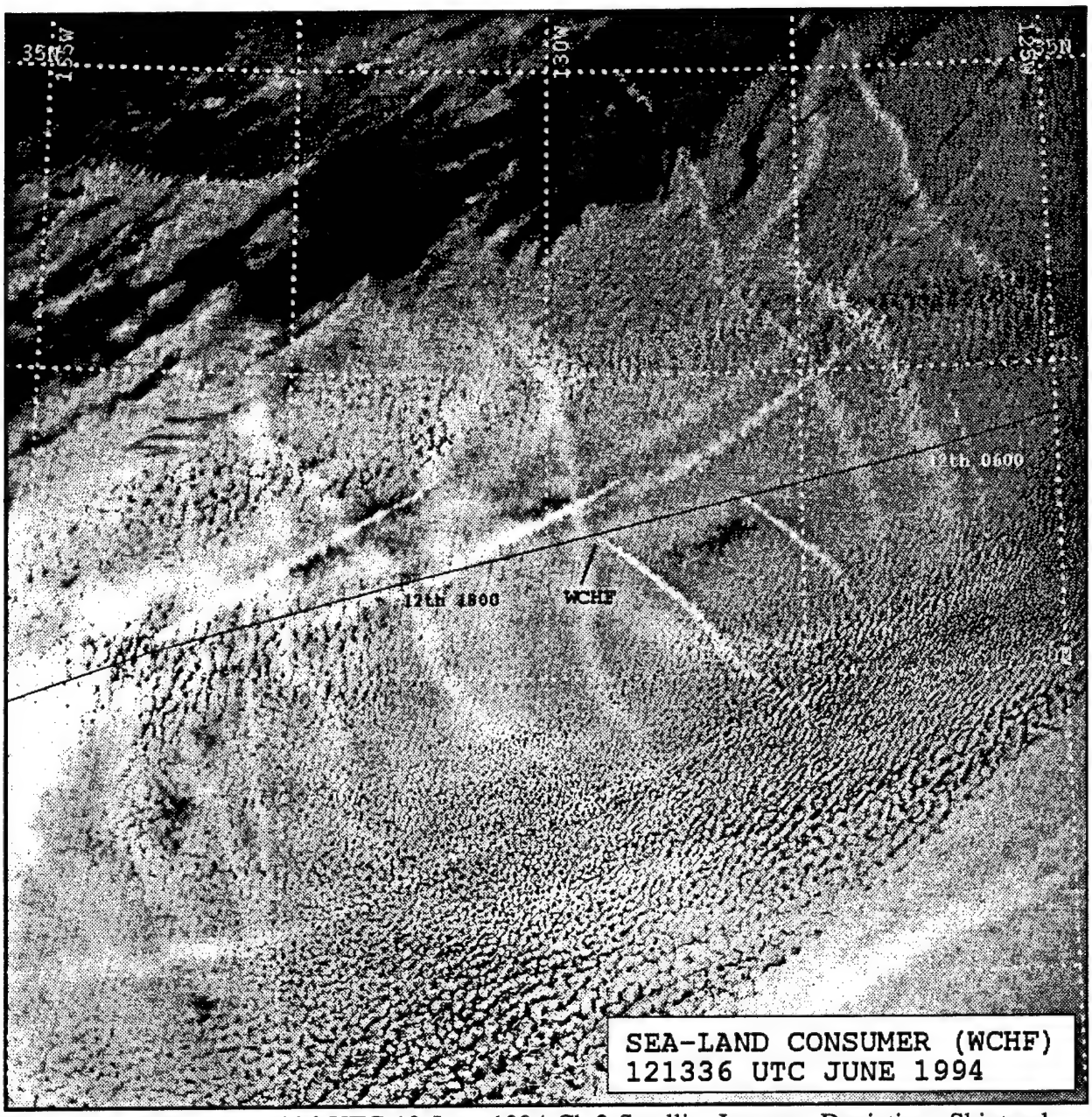

Figure 56. NOAA 11 1336 UTC 12 June 1994 Ch.3 Satellite Imagery Depicting Shiptrack Produced by Container Ship Sea-Land Consumer (WCHF). Solid line denotes Tai He position history based on synoptic weather reports. Shiptrack location indicated by callsign WCHF.

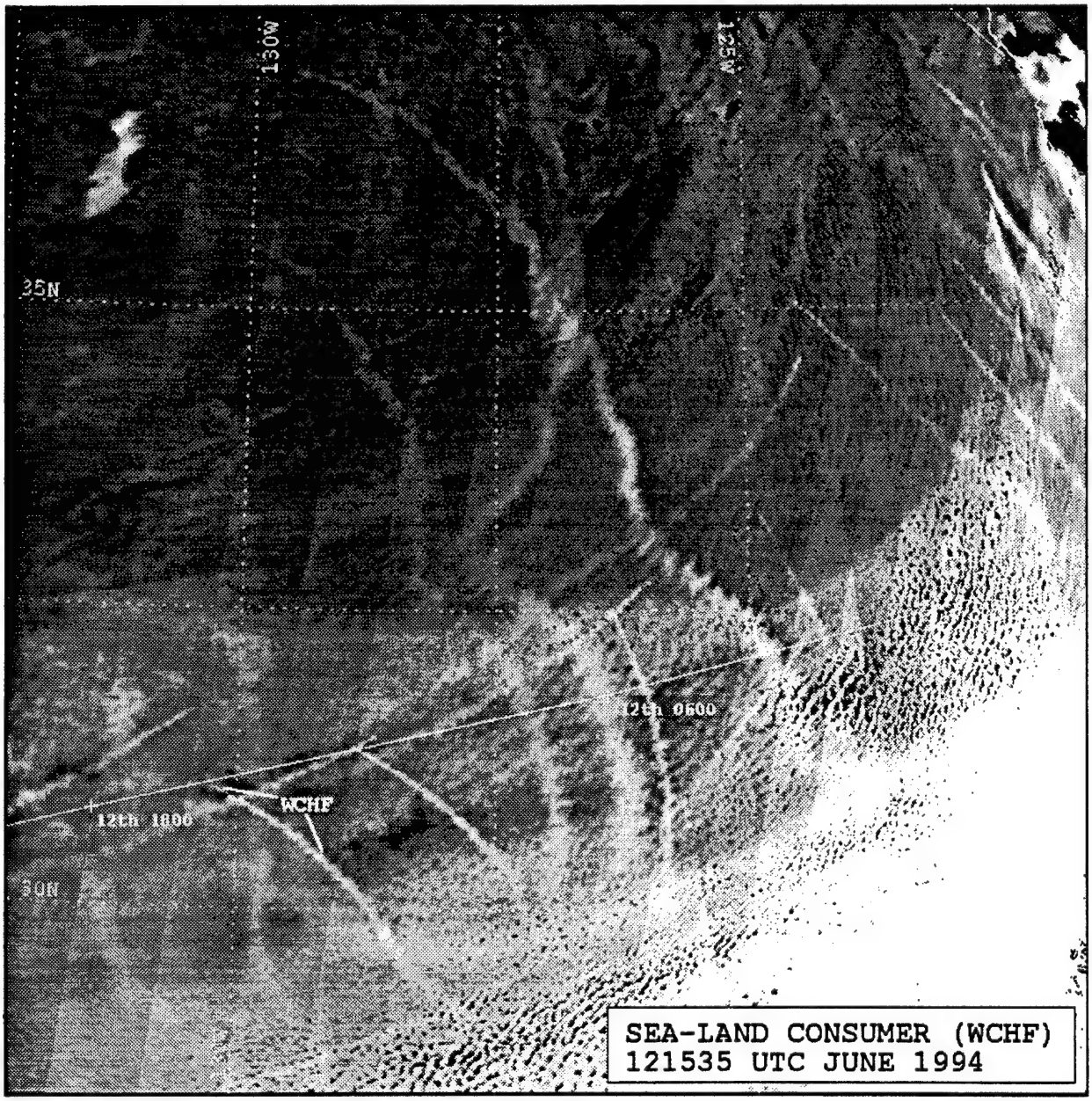

Figure 57. NOAA 12 1535 UTC 12 June 1994 Ch.3 Satellite Imagery Depicting Shiptrack Produced by Container Ship Sea-Land Consumer (WCHF). Solid line denotes Tai He position history based on synoptic weather reports. Shiptrack location indicated by callsign WCHF.

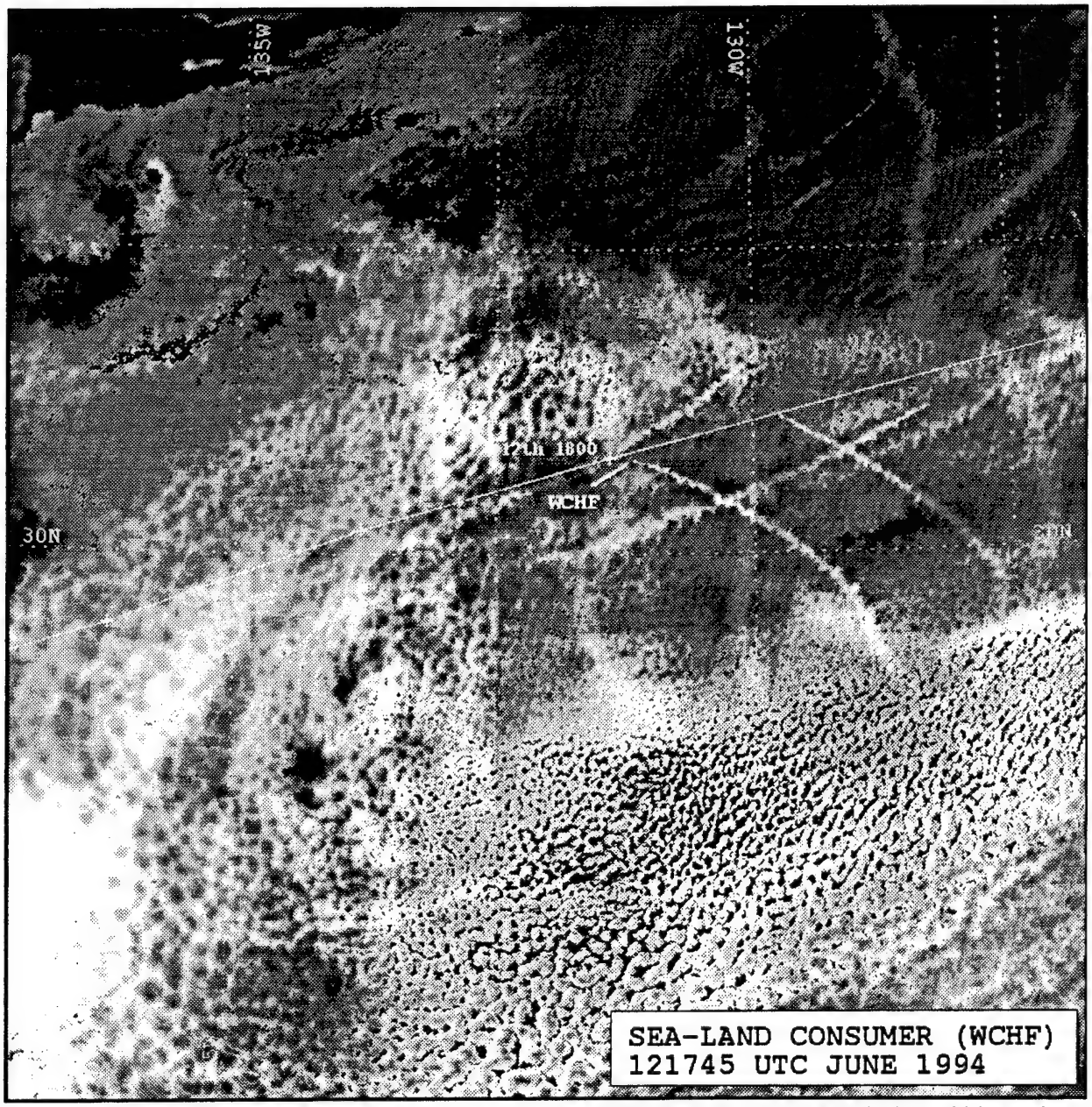

Figure 58. NOAA 09 1745 UTC 12 June 1994 Ch.3 Satellite Imagery Depicting Shiptrack Produced by Container Ship Sea-Land Consumer (WCHF). Solid line denotes Tai He position history based on synoptic weather reports. Shiptrack location indicated by callsign WCHF.

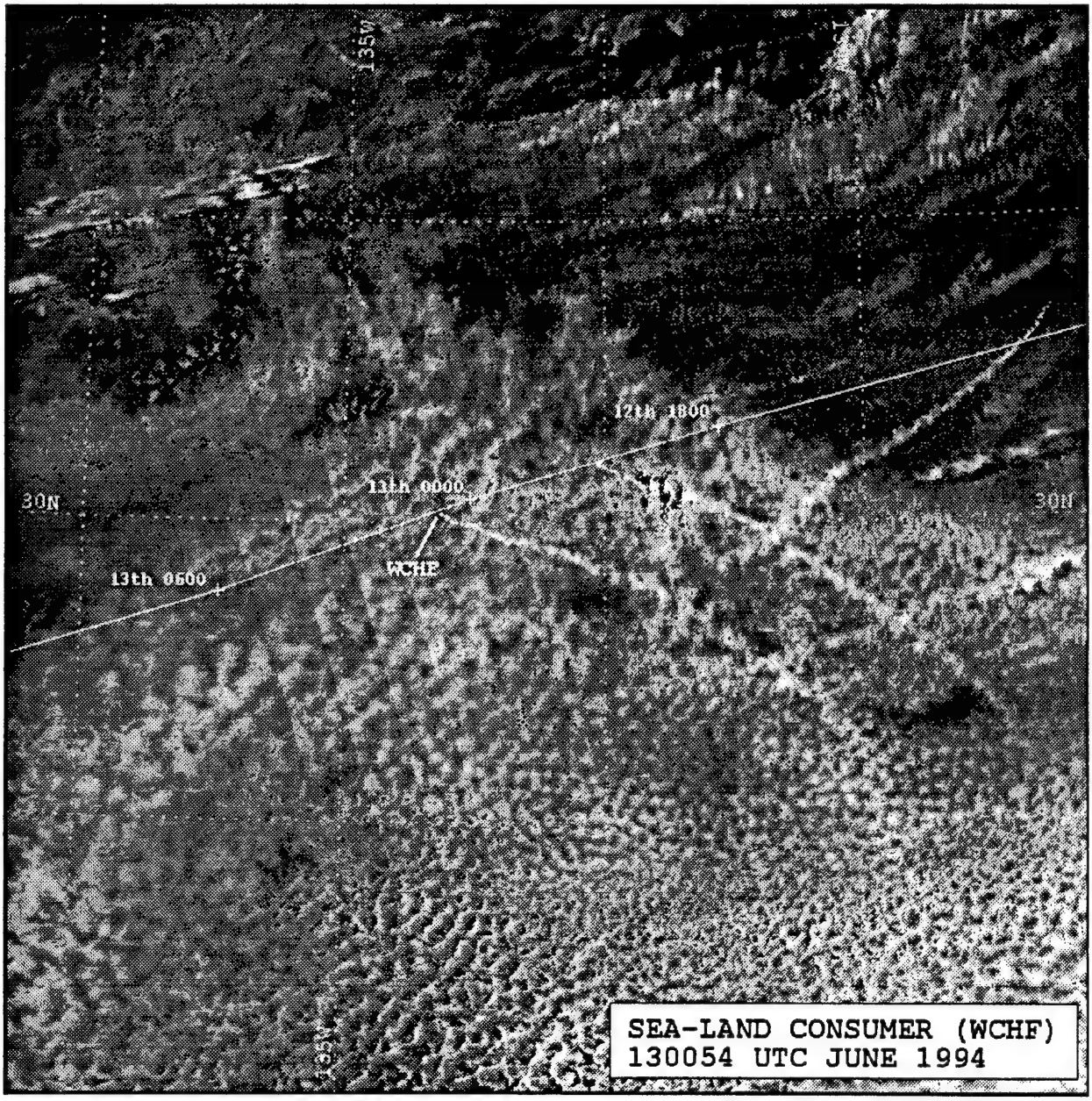

Figure 59. NOAA 11 0054 UTC 13 June 1994 Ch.3 Satellite Imagery Depicting Shiptrack Produced by Container Ship Sea-Land Consumer (WCHF). Solid line denotes Tai He position history based on synoptic weather reports. Shiptrack location indicated by callsign WCHF.

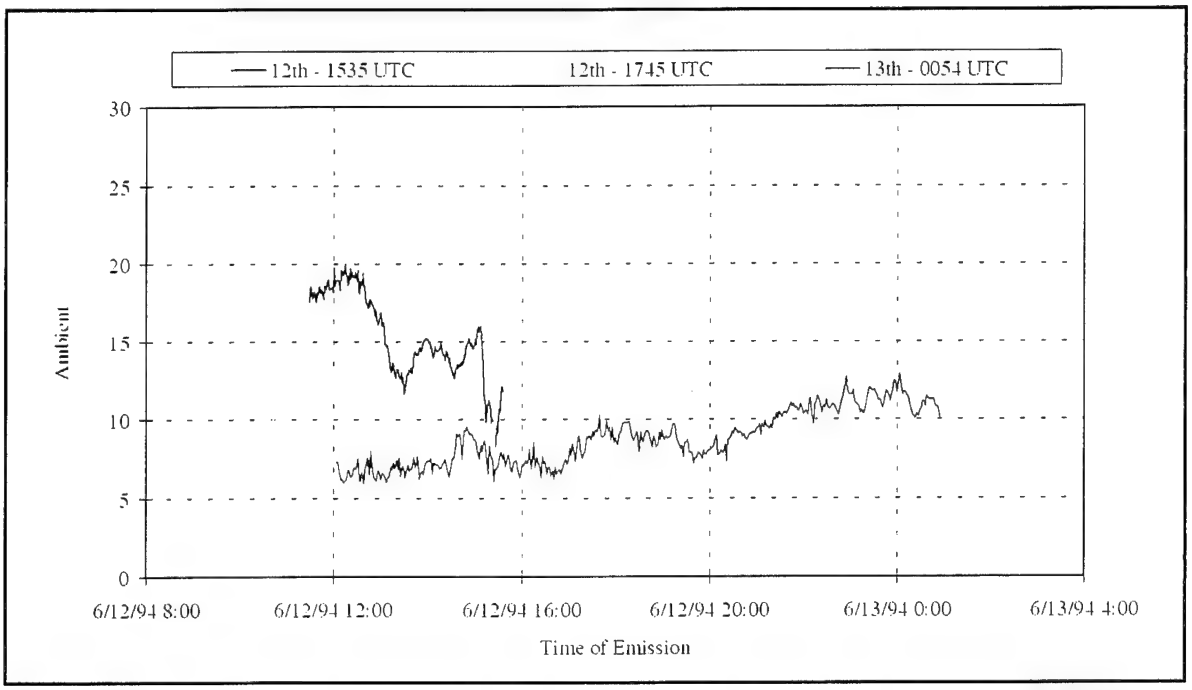

Figure 60. Ch.3 Ambient Reflectance for Container Ship Sea-Land Consumer (WCHF).

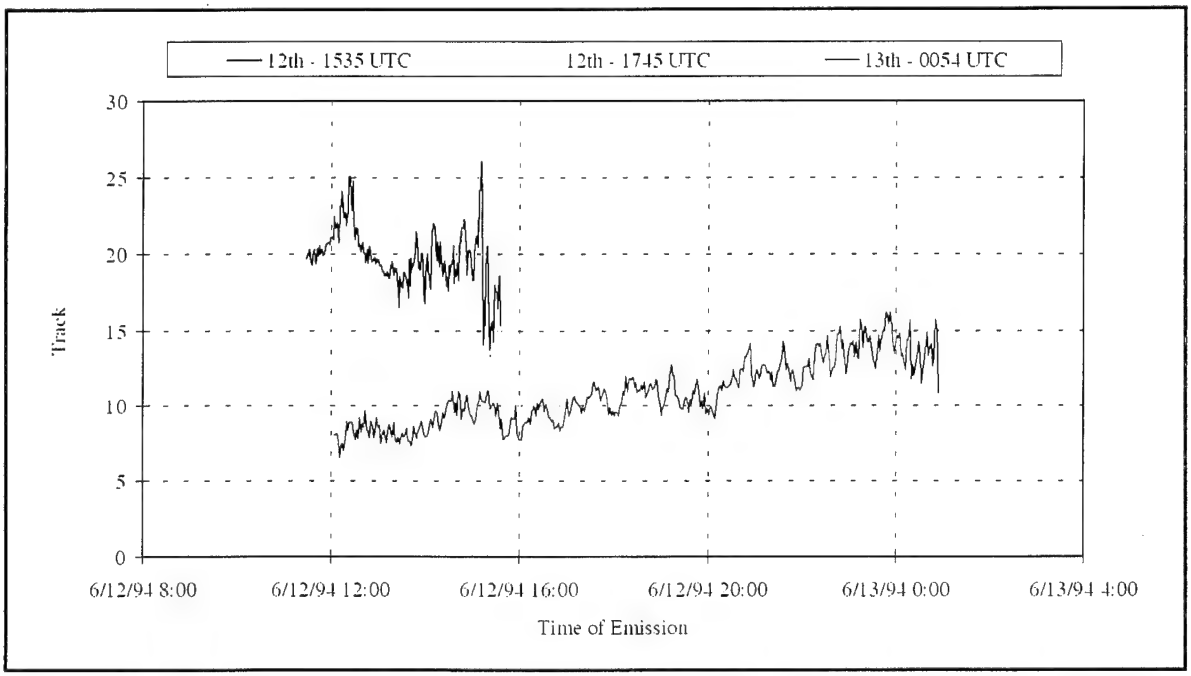

Figure 61. Ch.3 Shiptrack Reflectance for Container Ship Sea-Land Consumer (WCHF).

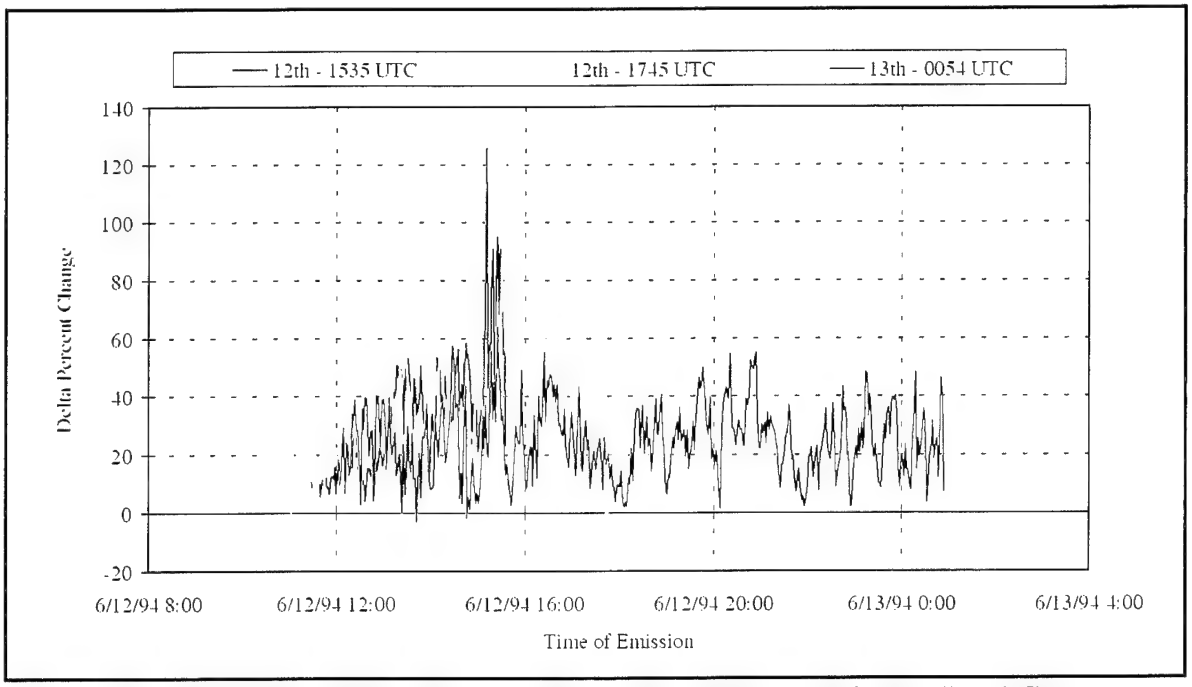

Figure 62. AVHRR Ch.3 Delta Percent Change for Container Ship Sea-Land Consumer (WCHF).

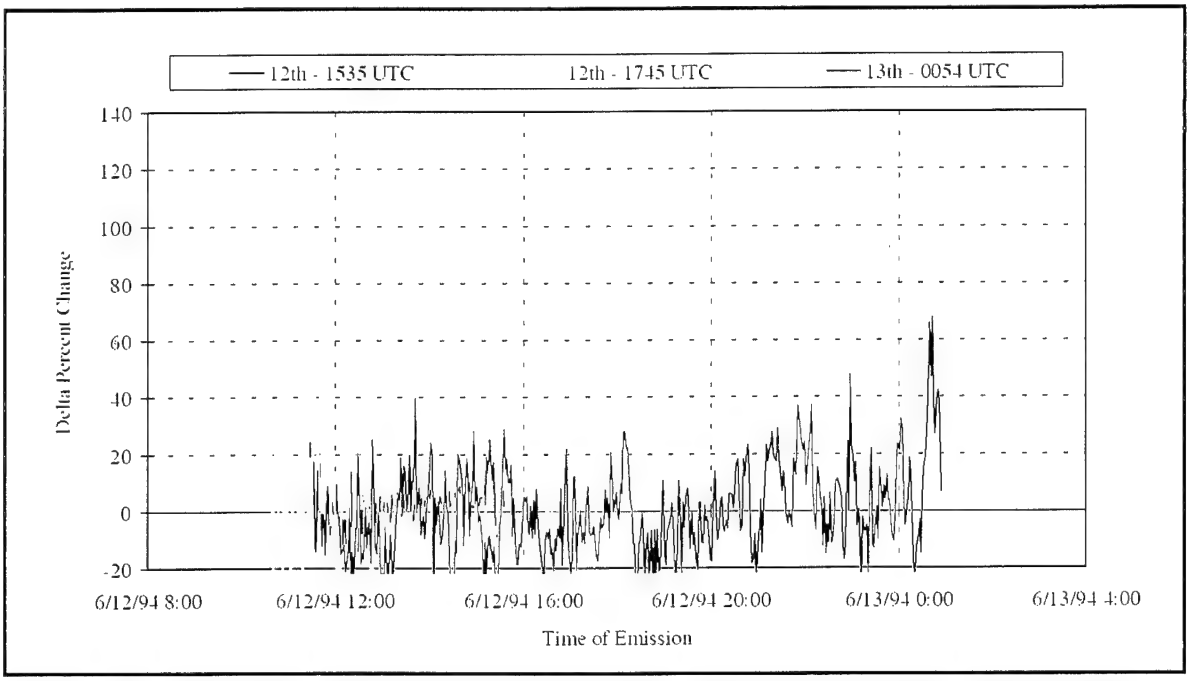

Figure 63. AVHRR Ch.1 Delta Percent Change for Container Ship Sea-Land Consumer (WCHF).

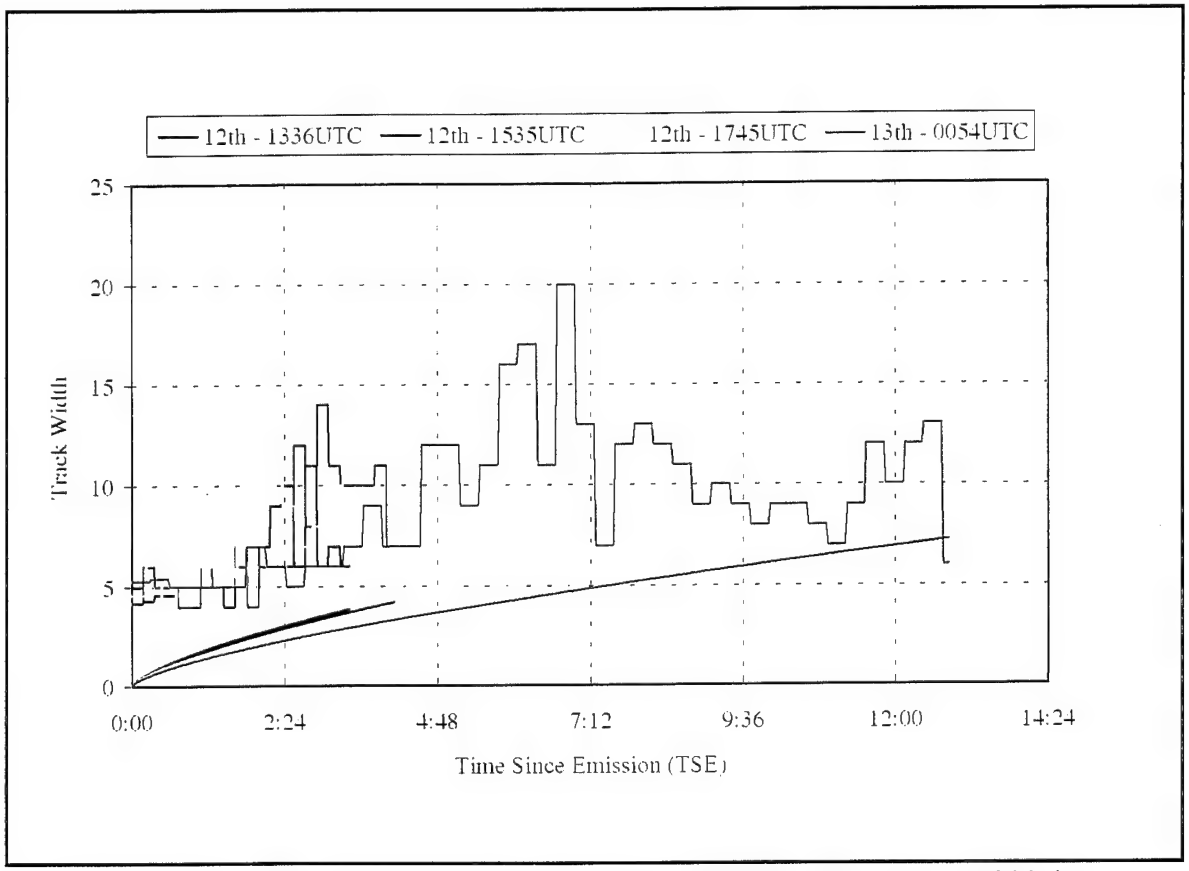

Figure 64. Average Widths for Sea-Land Consumer (WCHF) Shiptracks. Width is averaged over each 10 km segment of shiptrack. Smooth curves represent predicted growth based on twice the standard deviation of the plume concentration.

6. Manulani (Callsign KNIJ)

Manulani is also a steam driven container ship 219 meters in length, displacing 23,785 tons. Shiptracks associated with this vessel were first observed on 12 June 1994 at 1336 UTC (0636 local). Figures 65 through 69 show the movement of this shiptrack through four satellite images over a period of 12 hours. Based on the ship's synoptic weather and position reports, Manulani was on a parallel course with Sea-Land Consumer, southwesterly at a speed of between 21 and 25 knots. True winds were reported out of the north to northeast from 12 to 22 knots producing relative winds from the northwest. All Manulani shiptracks in these successive images correlated well with the reported conditions. Table 7 lists Sea-Land Consumer's reported conditions. Note that course and speed are mean values for the coded range reported. Relative wind is based on this mean reported value.

Date/Time YYMMDD HHMM	**Position** LAT/LON	**Course/Speed** DEG/KTS	**True Wind** DEG/KTS	**Rel Wind** DEG/KTS
940612 1336	31.8n/128.4w	270/23	350/18	305/32
940612 1535	31.6n/129.2w	270/23	350/16	300/30
940612 1745	31.4n/129.5w	270/23	030/16	310/20
940613 0054	30.6n/132.8w	270/23	000/09	290/25

Table 7. Position and Wind Reports for Manulani (KNIJ).

a. Radiative Characteristics

Analysis of radiative characteristics reveals similar results to that of Sea-Land Consumer. Ambient cloud and shiptrack reflectance values (Figures 70 and 71) show lower values for both sets of tracks as the ships progress further from the continent. Ambient values decrease from approximately 14% at 12 1535 UTC to near 7% at 12 1745 UTC. Reflectances remain relatively stable at approximately 7% until near the head of the

Track reflectance follows this trend, decreasing from approximately 18% at 12 1535 UTC to approximately 9% at 12 1745 UTC. The expected decrease in track reflectance with age is evident in the 13 0054 UTC track with ambient reflectance values decreasing from 8% near the head of the track to 5% near the end of the track. Shiptrack reflectance decreases in a similar manner from 10% to 6%. Sea-Land Consumer shows exactly the same trend with reflectance values within 1% of Manulani's.

DPC3 values (Figure 72) show consistent track-to-track values of approximately 25% with peaks associated with bright intersection areas. DPC1 values, shown in Figure 73, reveal values near 0% for the series, with steady fluctuations becoming much more variable in the 12 1745 UTC and 13 0054 UTC tracks as the ship moves from a uniform stratus region to a more broken cloud regime. Sea-Land Consumer shows slightly less variability in these later tracks indicating that Manulani is in area with greater breaks in the clouds.

b. Track Width

The track width composite plot (Figure 74) shows growth patterns consistent with Sea-Land Consumer's. Initial growth rates here are also 4-6 km/hr with maximum width between 9 and 11 km. The peak width of 16 km in the 12 1745 UTC track is associated with an intersection of Manulani's track with another shiptrack in the area. The low rate of growth predicted for the 15 0054 UTC track results from a low true to relative wind ratio (9:25) and high relative wind (25 knots).

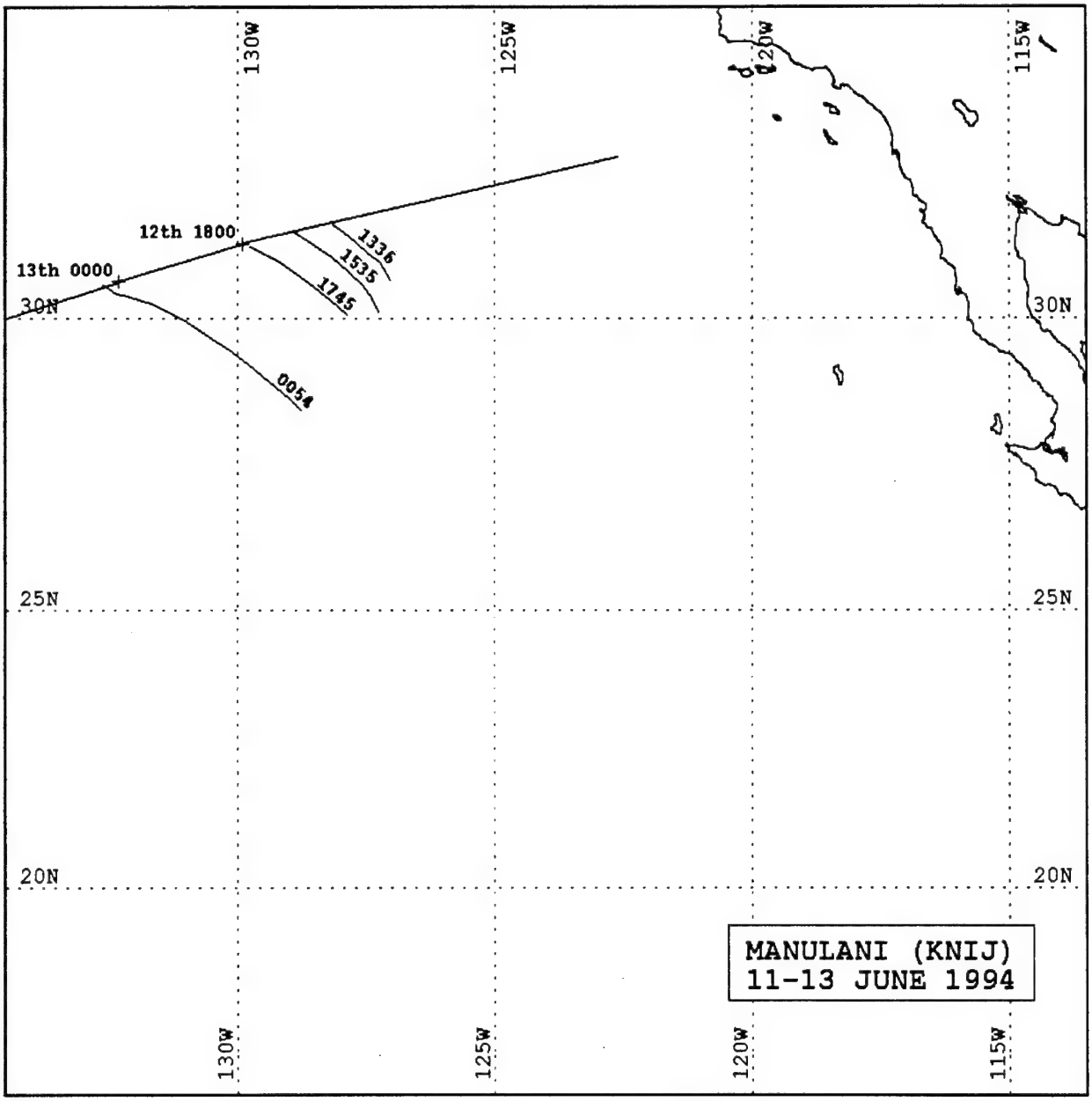

Figure 65. Transit History for Container Ship Manulani (KNIJ). Ship positions shown with day and time. Associated shiptracks are denoted by curved lines extending from transit path with satellite pass times indicated on individual tracks.

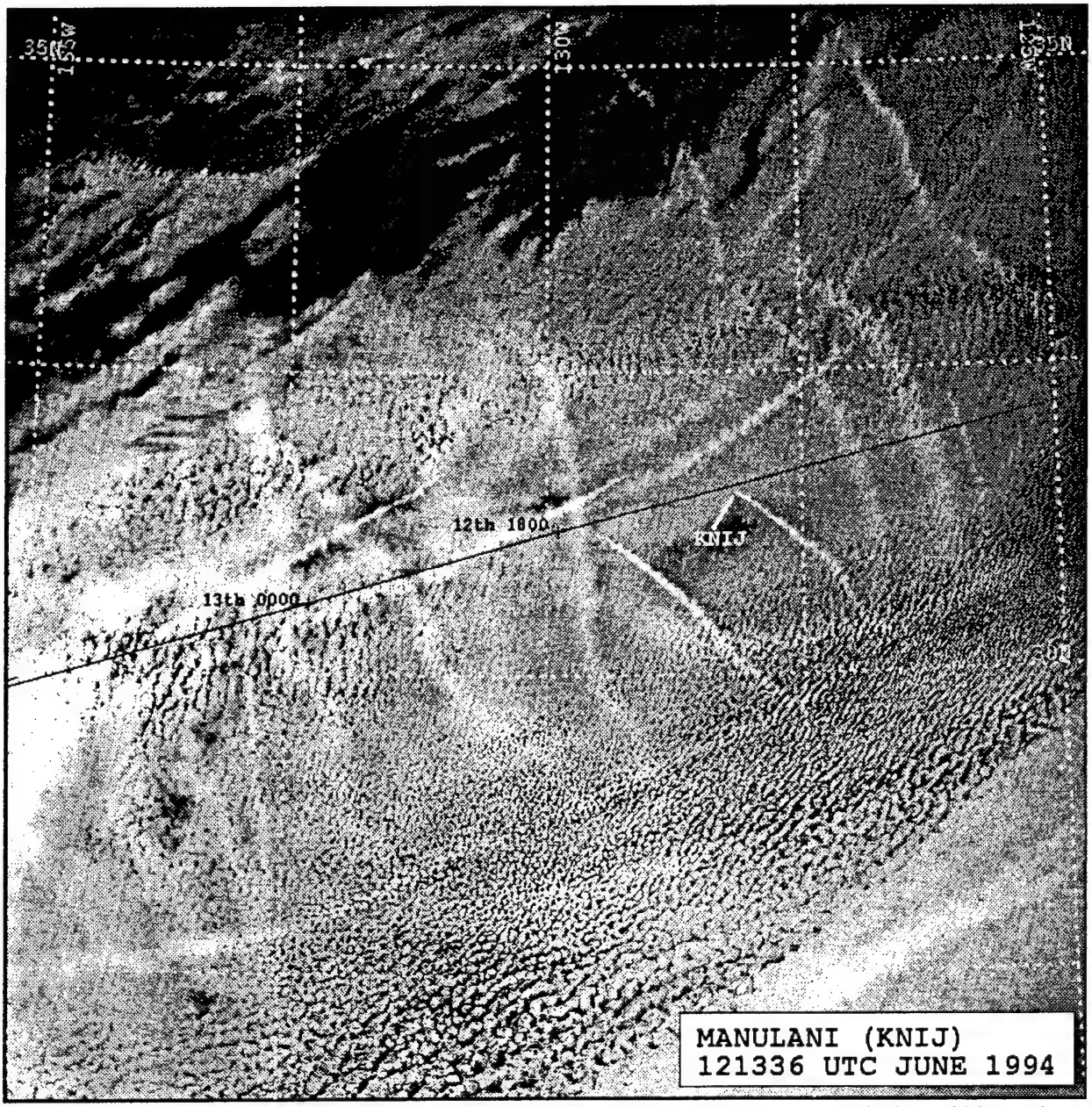

Figure 66. NOAA 11 1336 UTC 12 June 1994 Ch.3 Satellite Imagery Depicting Shiptrack Produced by Container Ship Manulani (KNIJ). Solid line denotes Manulani position history based on synoptic weather reports. Shiptrack location indicated by callsign WCHF.

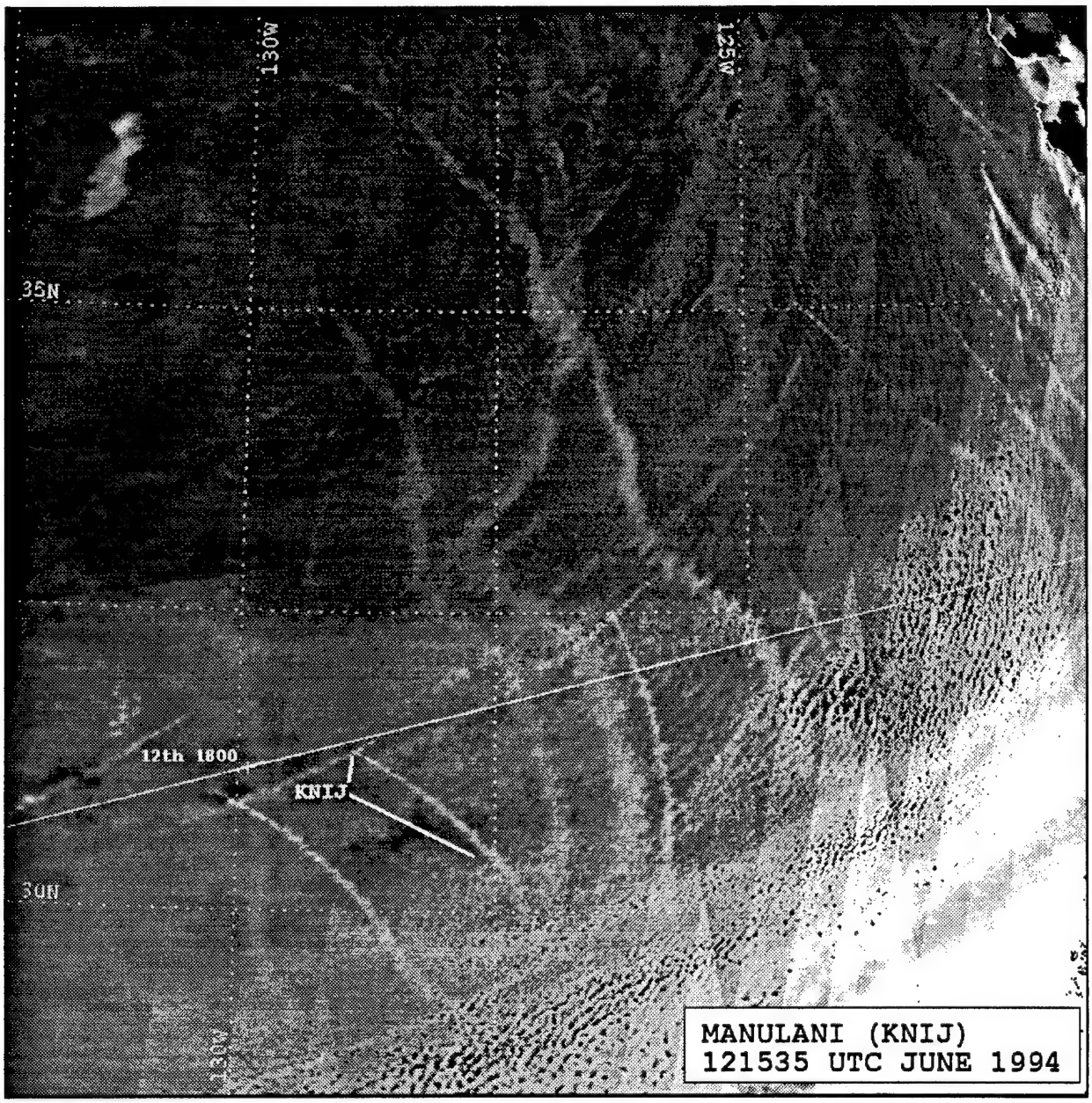

Figure 67. NOAA 12 1535 UTC 12 June 1994 Ch.3 Satellite Imagery Depicting Shiptrack Produced by Container Ship Manulani (KNIJ). Solid line denotes Manulani position history based on synoptic weather reports. Shiptrack location indicated by callsign WCHF.

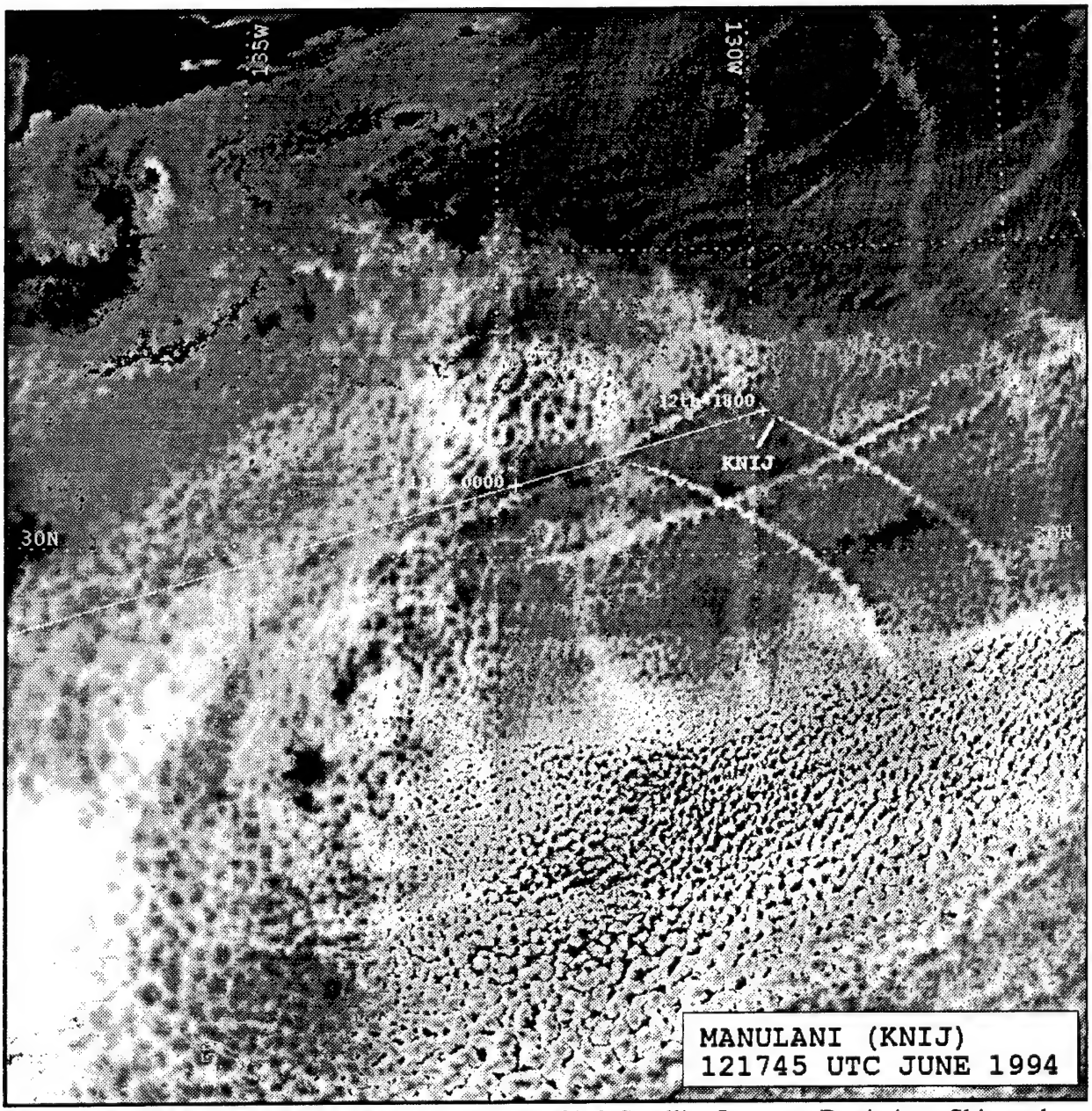

Figure 68. NOAA 09 1745 UTC 12 June 1994 Ch.3 Satellite Imagery Depicting Shiptrack Produced by Container Ship Manulani (KNIJ). Solid line denotes Manulani position history based on synoptic weather reports. Shiptrack location indicated by callsign WCHF.

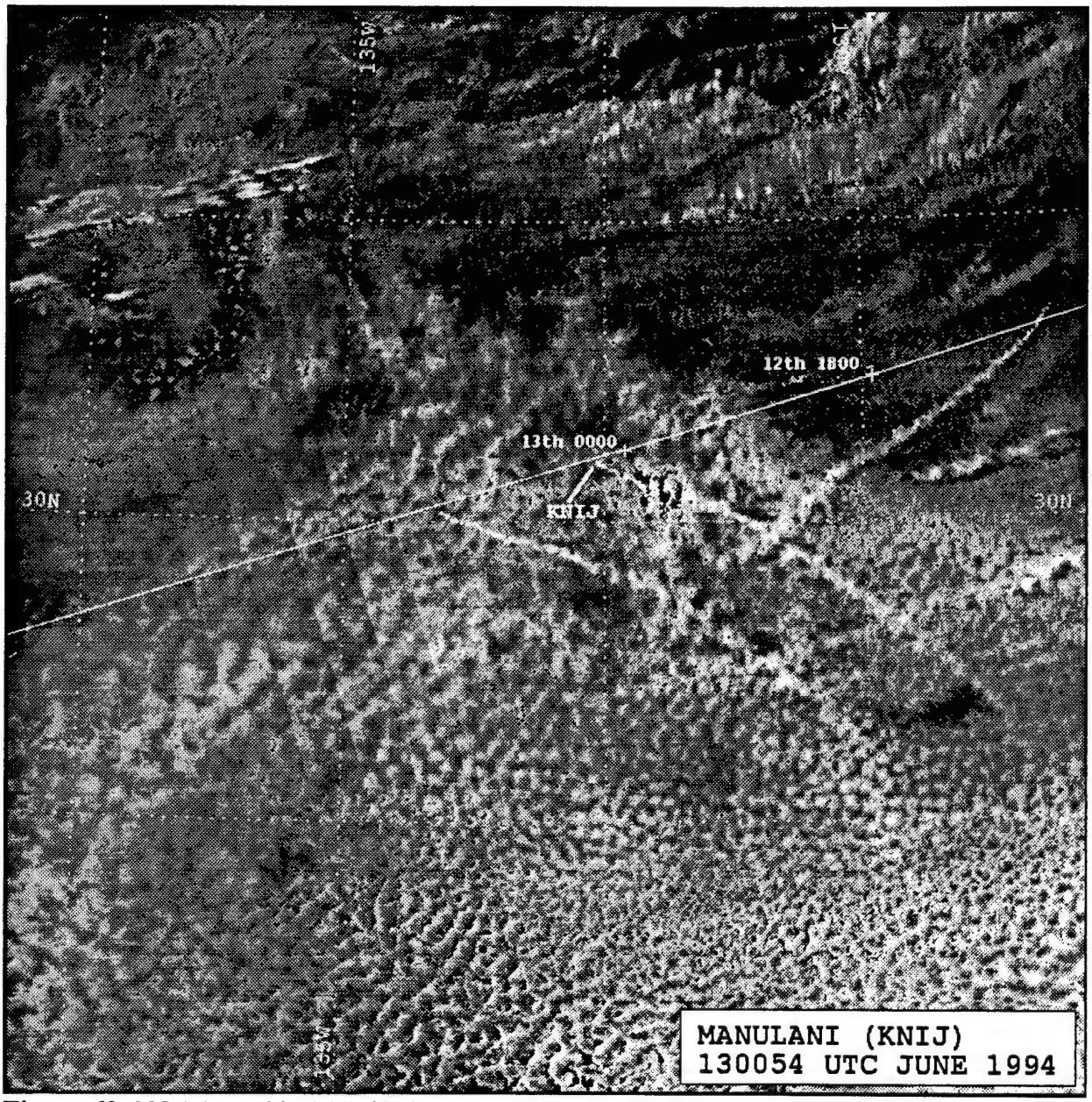

Figure 69. NOAA 11 0054 UTC 13 June 1994 Ch.3 Satellite Imagery Depicting Shiptrack Produced by Container Ship Manulani (KNIJ). Solid line denotes Manulani position history based on synoptic weather reports. Shiptrack location indicated by callsign WCHF.

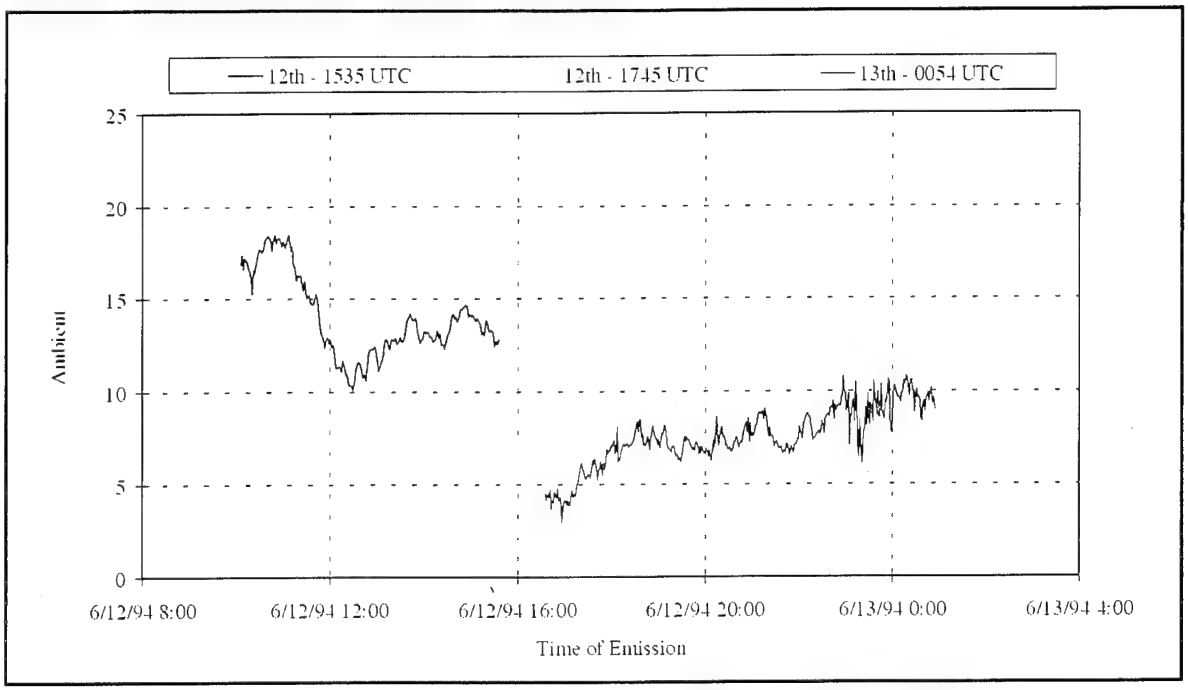

Figure 70. Ch.3 Ambient Reflectance for Container Ship Manulani (KNIJ).

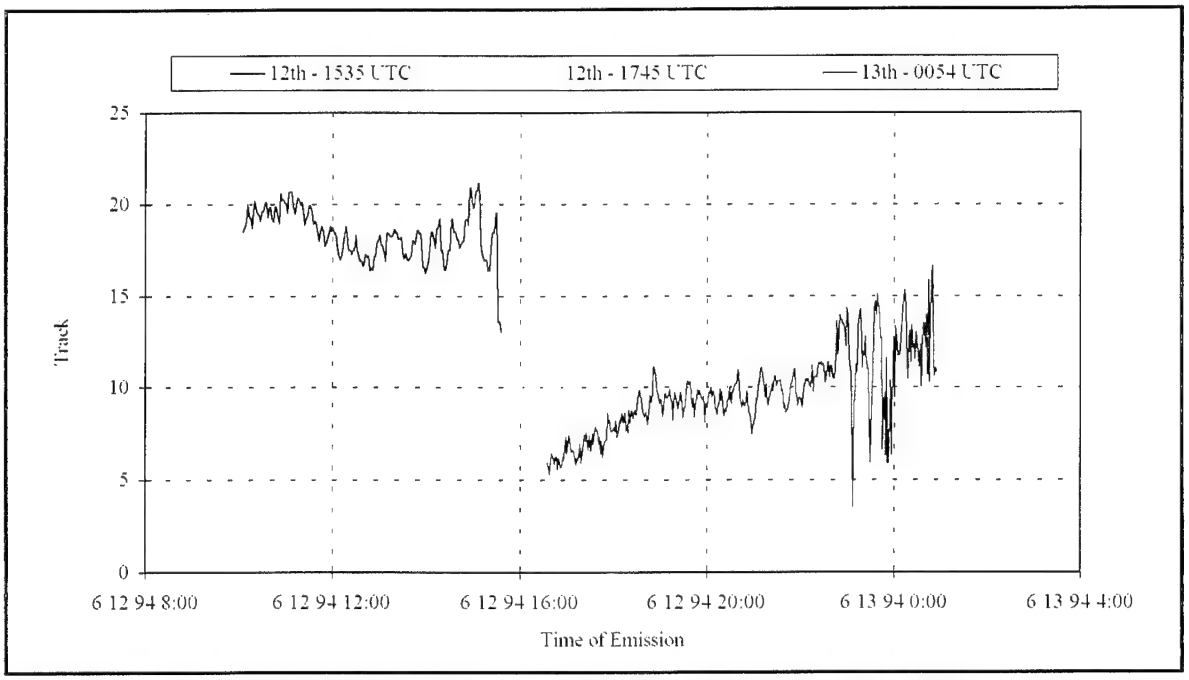

Figure 71. Ch.3 Shiptrack Reflectance for Container Ship Manulani (KNIJ).

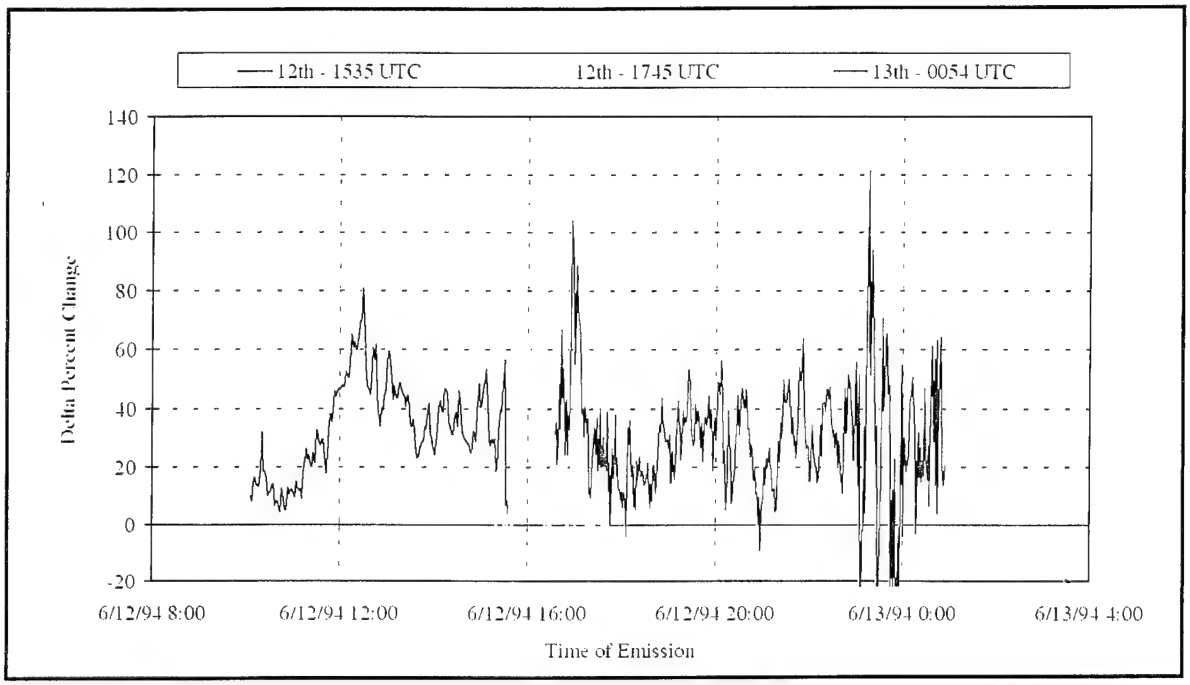

Figure 72. AVHRR Ch.3 Delta Percent Change for Container Ship Manulani (KNIJ).

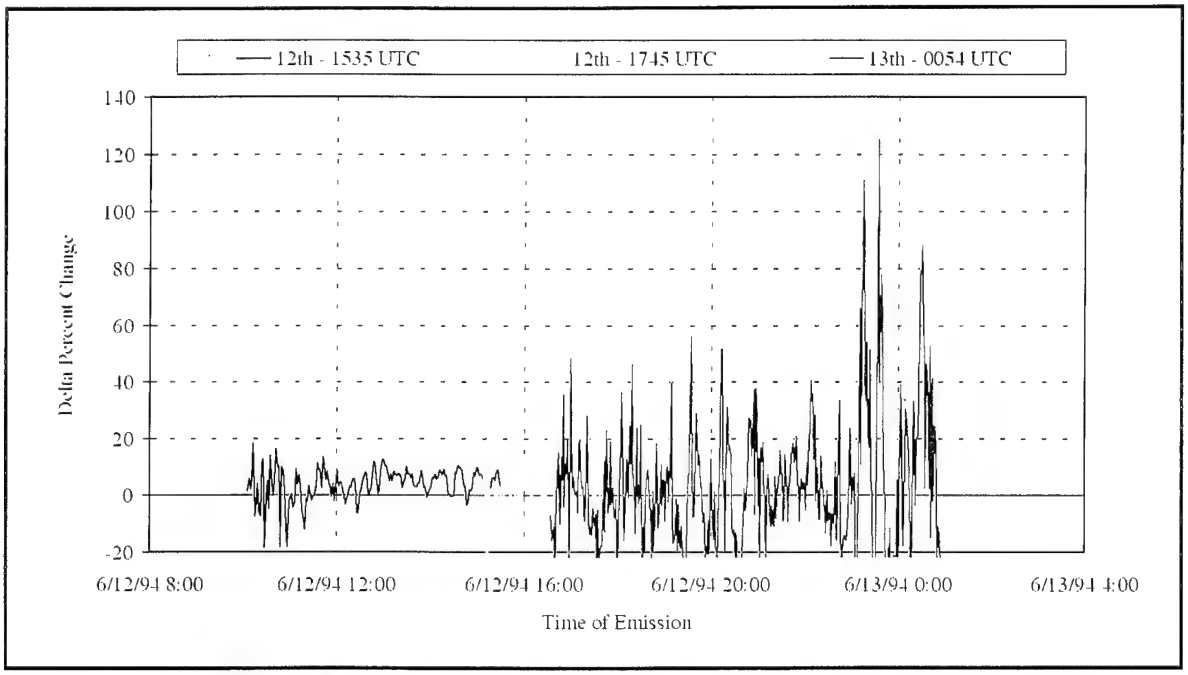

Figure 73. AVHRR Ch.1 Delta Percent Change for Container Ship Manulani (KNIJ).

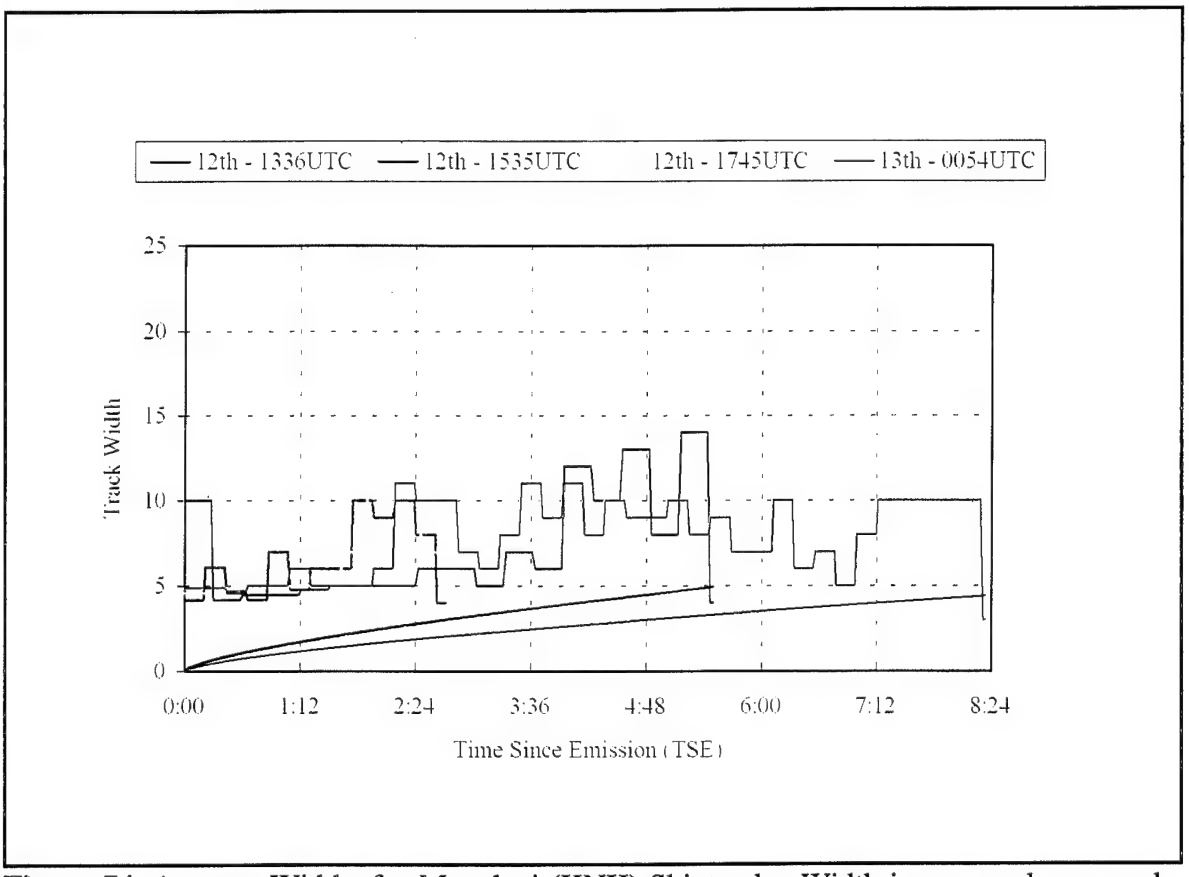

Figure 74. Average Widths for Manulani (KNIJ) Shiptracks. Width is averaged over each 10 km segment of shiptrack. Smooth curves represent predicted growth based on twice the standard deviation of the plume concentration.

IV. CONCLUSIONS AND RECOMMENDATIONS

A. CONCLUSIONS

The purpose of this thesis was to observe and describe the evolution of physical and optical properties of shiptracks over time. To that end a detailed analysis was conducted on multiple shiptracks from six individual ships transiting the eastern north Pacific in June 1994.

The results indicate that in most cases the radiative characteristics of shiptracks follow the same trends as those associated with the ambient cloud in which they form. Aerosol introduced into marine stratus by a passing ship modifies the radiative characteristics of the cloud. This modification of pre-existing cloud results in a unique radiative signature which is evident in enhanced reflectance at the 3.7μm wavelength (channel 3 in AVHRR). The results are summarized as follows:

1. Average Channel 3 Reflectance Values

Reflectance values for shiptrack and ambient cloud increased when moving from open ocean toward the continent (i.e., from "clean" to "dirty" stratus areas) and showed the opposite trend when moving away from the continent. Tai He and Zim America showed increases of approximately 15% (from 5% to 20%) as they approached the coast. Century Highway and Hercules Highway showed increases of approximately 10% (from 8% to 18%) as transited from off the southern California and Baja California coast. Sea-Land Consumer and Manulani showed decreases of approximately 8% (from 20% to 12%) as they transited westward away from the continent.

Under the special circumstance where stratus was undergoing thinning due to dry air entrainment, ambient and shiptrack reflectances exhibited opposing trends. The absolute reflectance of the ambient cloud decreased while the shiptrack reflectance increased. Tai He showed a 3% increase in track reflectance values from 0951 local time to 1053 local time on 27 June. Ambient cloud reflectance decreased by 2% over the same interval.

2. Delta Percent Change (DPC)

DPC between ambient cloud and shiptrack in channel 3 showed average values in the 20% to 30% range. The values were much more variable in broken stratus regions and open ocean areas away from contamination by continental aerosol. Major peaks in DPC3 values were associated with points of intersection with other shiptracks.

DPC between ambient cloud and shiptrack in channel 1 showed average values near zero. This is expected since reflectance is not only dependent on droplet size but also on cloud thickness and liquid water content. Values also exhibited greater variability in broken stratus, open ocean areas.

The important point to note is that in continental CCN affected clouds ("dirty" stratus), the impact of shiptracks on cloud reflectance is minimal. Hence, DPC3 values are low. This was demonstrated by all three pairs of ships. Tai He and Zim America as they transited toward the continent exhibited decreasing DPC3 values from roughly 40% to between 20% and 30%. Sea-Land Consumer and Manulani experienced the same trend but in the reverse direction as they moved away from the continent. DPC3 values increased from 10% to between 20% and 30%. Century Highway and Hercules Highway showed consistent DPC3 values with only a slight decrease from 25% to 18% as they transited from off the coast of southern California toward Baja California.

3. Track Width

The overall trend in track width for all six case studies was similar. Specifically:

-- The rate of width increase was rapid within the first two hours (between 5 and 8 km/hr) decreasing thereafter.

-- Associated with the decrease in rate of growth, the track reached its greatest width, usually between 10 and 12 km.

-- The rate of growth appears to be tied to wind considerations. In observed cases, the largest true wind appeared to create larger rates of growth. For predicted values, the

ratio of true to relative wind determined the growth trend. The larger the ratio, the larger the growth.

-- The predicted width (the standard deviation of the plume concentration) was consistent with observed patterns.

B. RECOMMENDATIONS

This thesis represents the first attempt to study multiple shiptracks associated with a particular ship over successive satellite passes. It has demonstrated the utility of observing two ships in tandem, transiting through similar environments. A useful future study would be to focus on ships in close proximity on similar courses and speeds with different fuel/propulsion types. This would provide a detailed analysis of the effect each ship's effluent had on the overlying cloud.

The phenomenon of ambient cloud thinning with an accompanying increase in shiptrack brightness needs further study. Observing additional shiptracks from multiple ships would give insight into the frequency of occurrence of this interesting phenomenon.

The effects of dispersion on track width needs further investigation. This study did not consider the effects of absolute mass concentration on track dispersive characteristics. Additional data from aircraft measurements will give insight into this problem.

APPENDIX. SHIPTRACK SCATTERPLOTS

Scatterplots of individual shiptracks are located in this Appendix. They appear in the order in which they occurred in the text and are keyed to the following figures:

Figures	Ship
A.1.a. - A.1.g.	Tai He (BOAB)
A.2.a - A.2.d.	Zim America (4XGR)
A.3.a. - A.3.e.	Century Highway (8JNP)
A.4.a. - A.4.e.	Hercules Highway (JKOW)
A.5.a. - A.6.c.	Sea-Land Consumer (WCHF)
A.6.a. - A.6.c.	Manulani (KNIJ)

Each figure is displayed as a panel of six plots which are sequenced as follows:

Location	Description
Upper left	Ch.1, Ch.3 ambient cloud reflectance
Upper right	Ch.1, Ch.3 shiptrack reflectance
Center left	Ch.4 temperatures for ambient cloud and shiptrack
Center right	Ch.1, Ch.3, and Ch.4 differences (delta) between shiptrack and ambient cloud
Lower left	Ch1., Ch.3 delta percent change
Lower right	Track width (Width I - pixel values Width II - average of every 10 pixels over entire length of shiptrack)

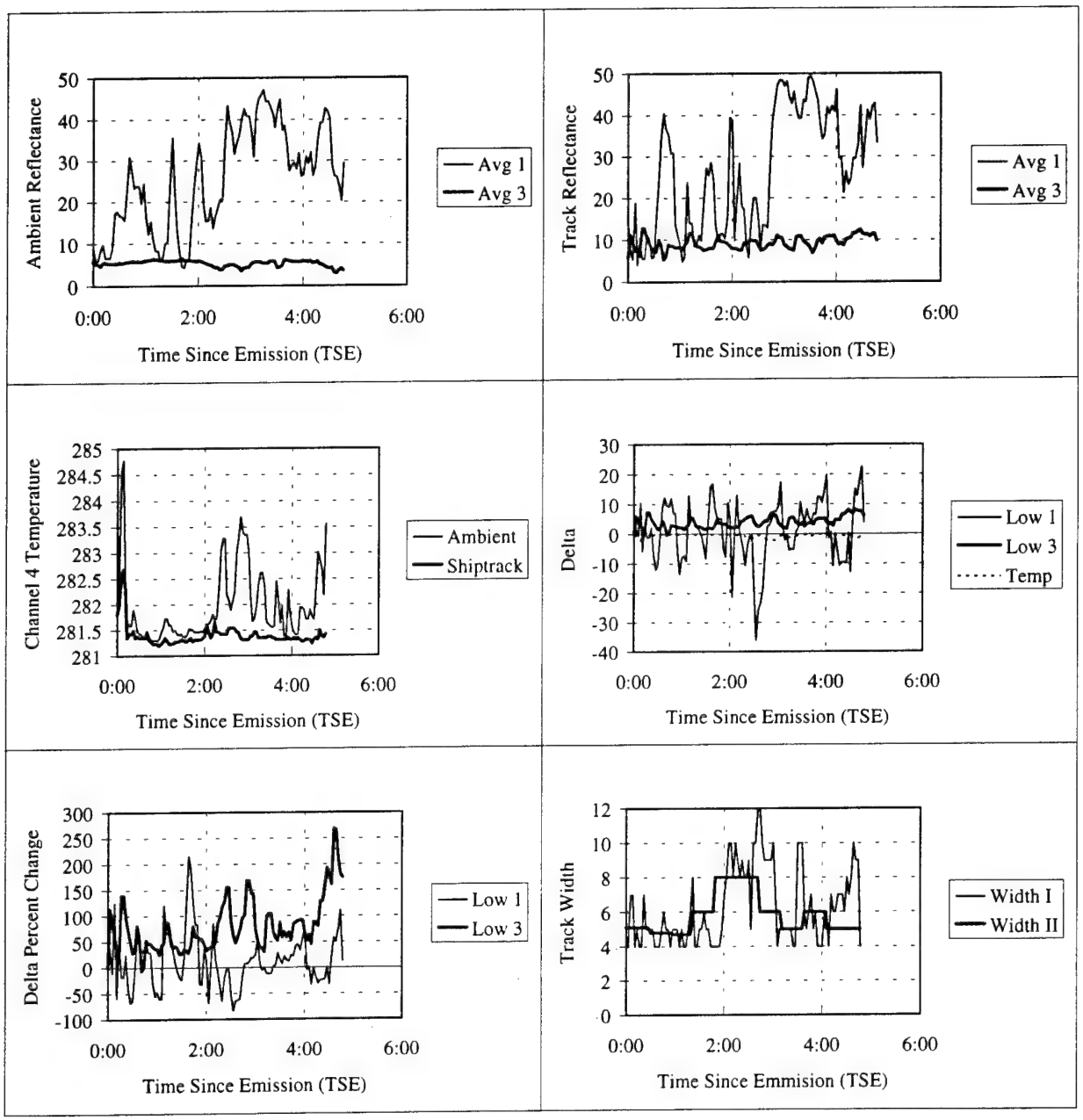

Figure A.1.a. TSE for Tai He (BOAB) 26 June 1994 1800 UTC

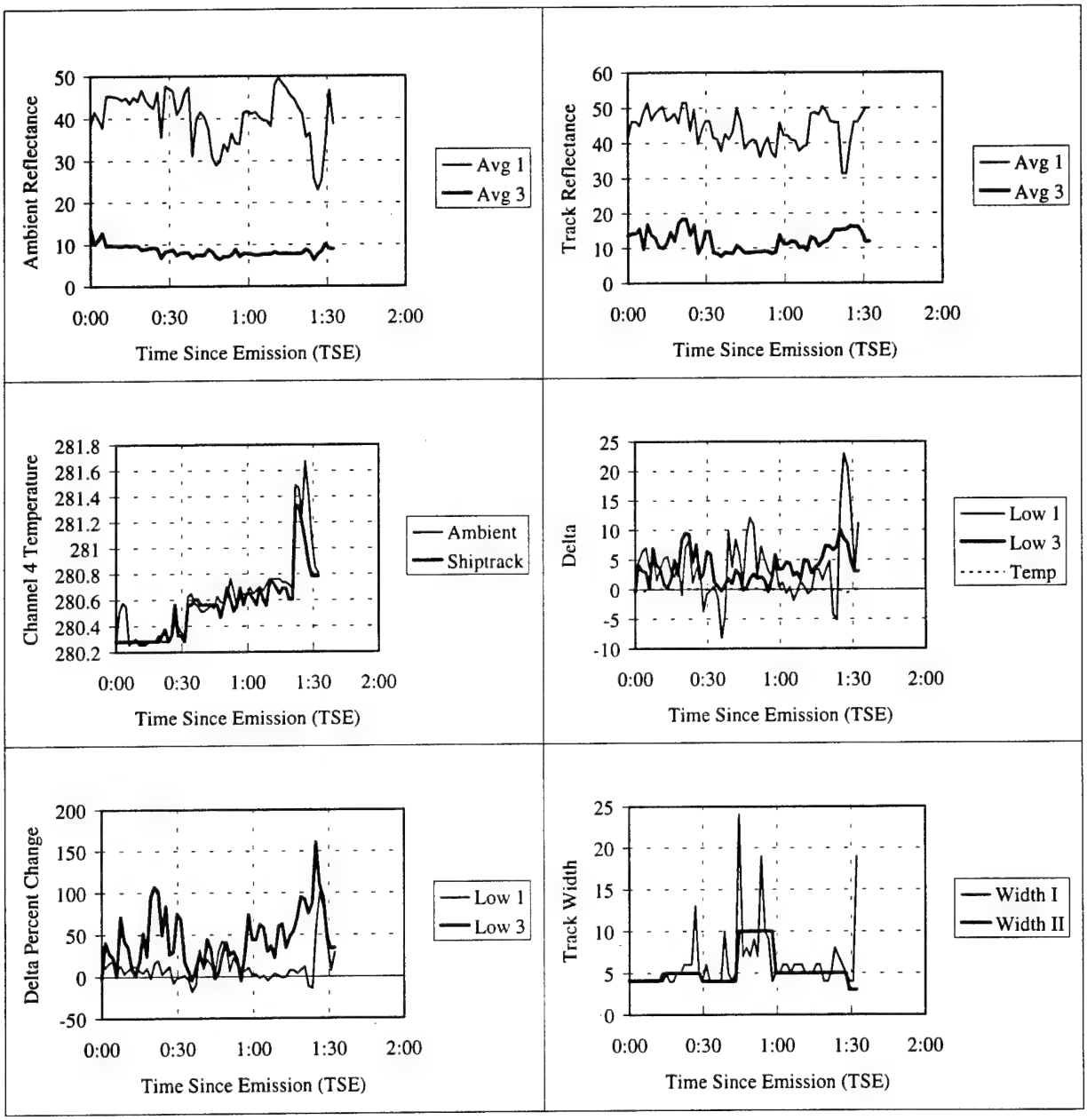

Figure A.1.b. TSE for Tai He (BOAB) 27 June 1994 0124 UTC

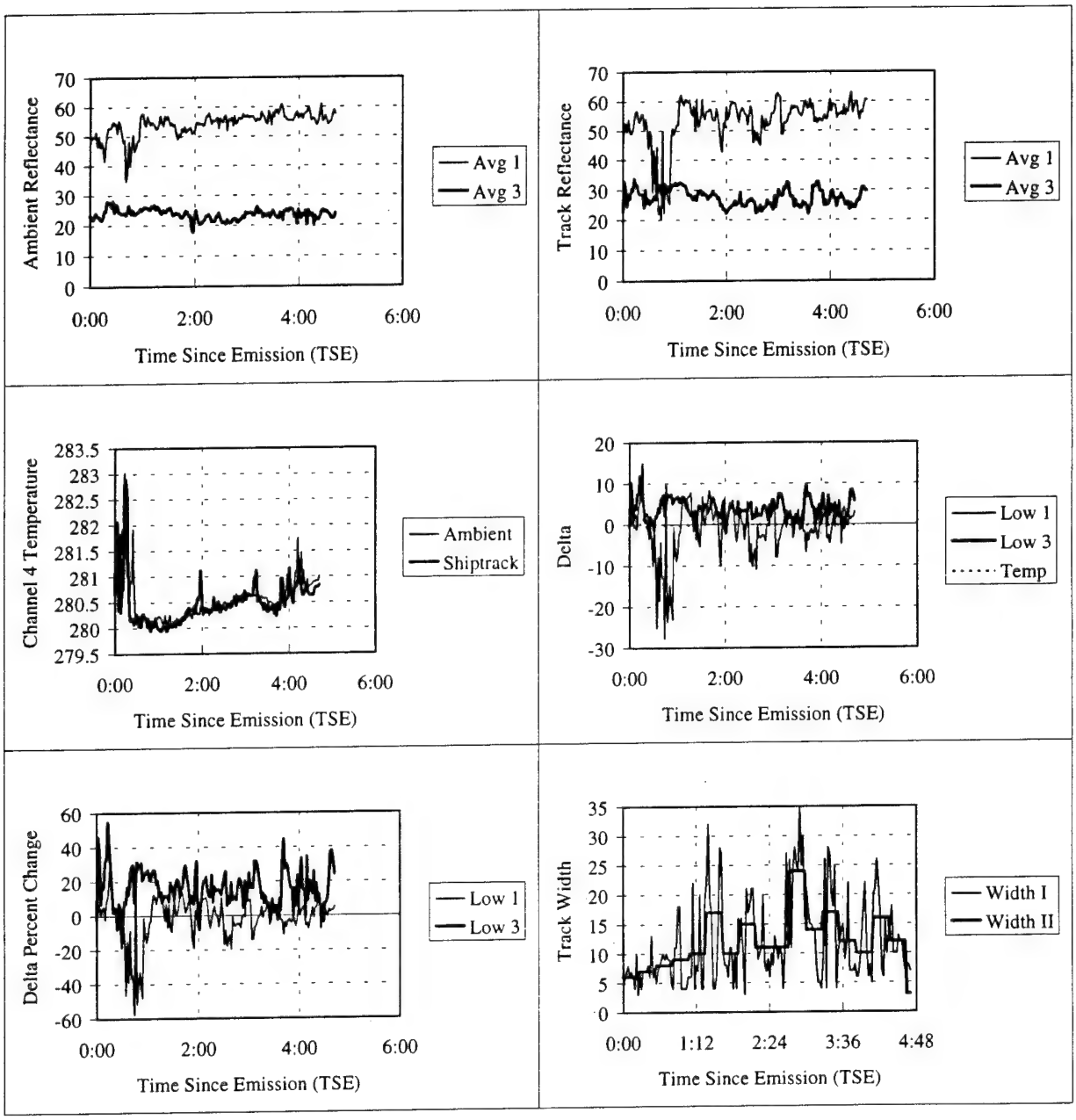

Figure A.1.c. TSE for Tai He (BOAB) 27 June 1994 0246 UTC

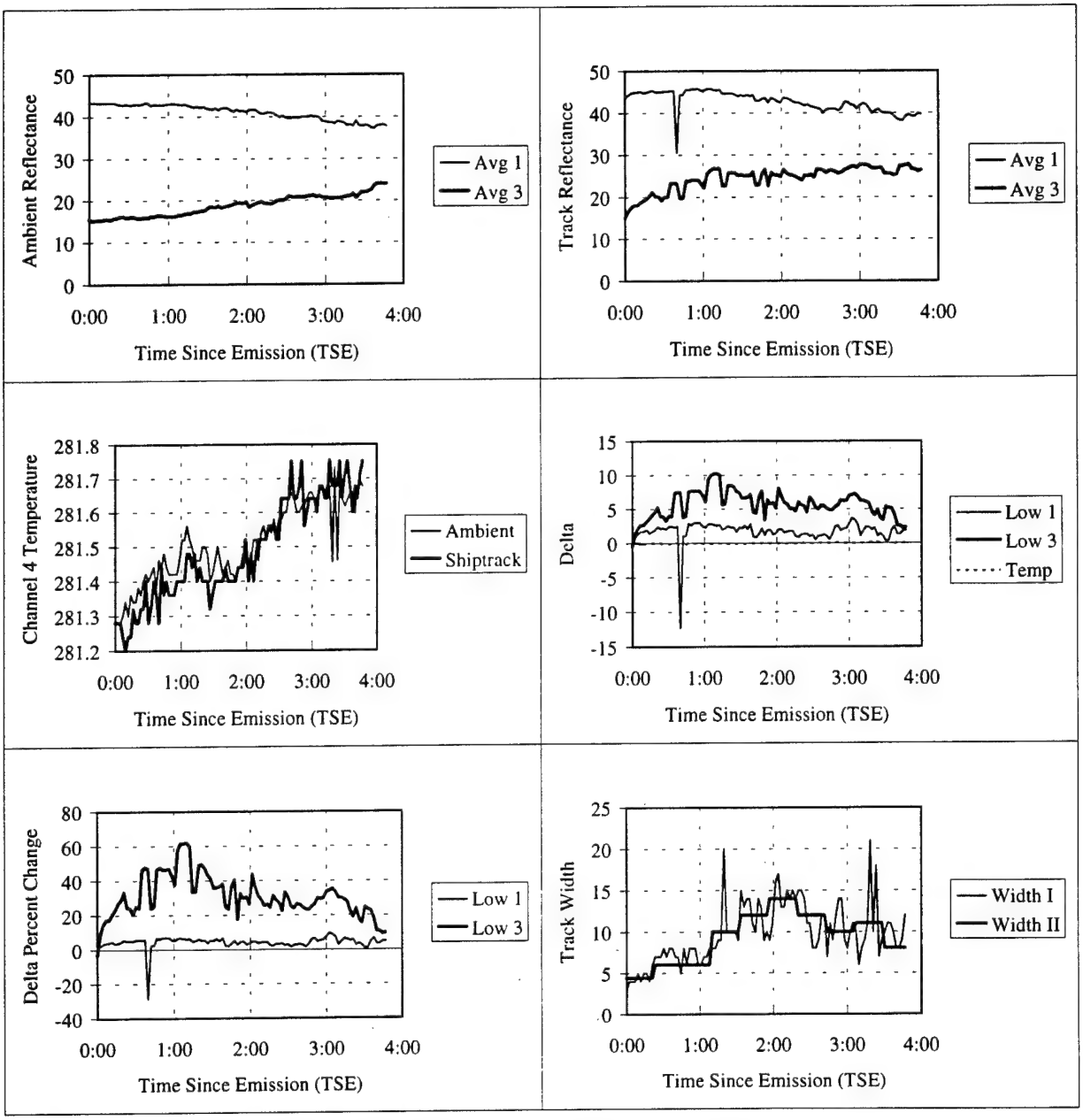

Figure A.1.d. TSE for Tai He (BOAB) 27 June 1994 1511 UTC

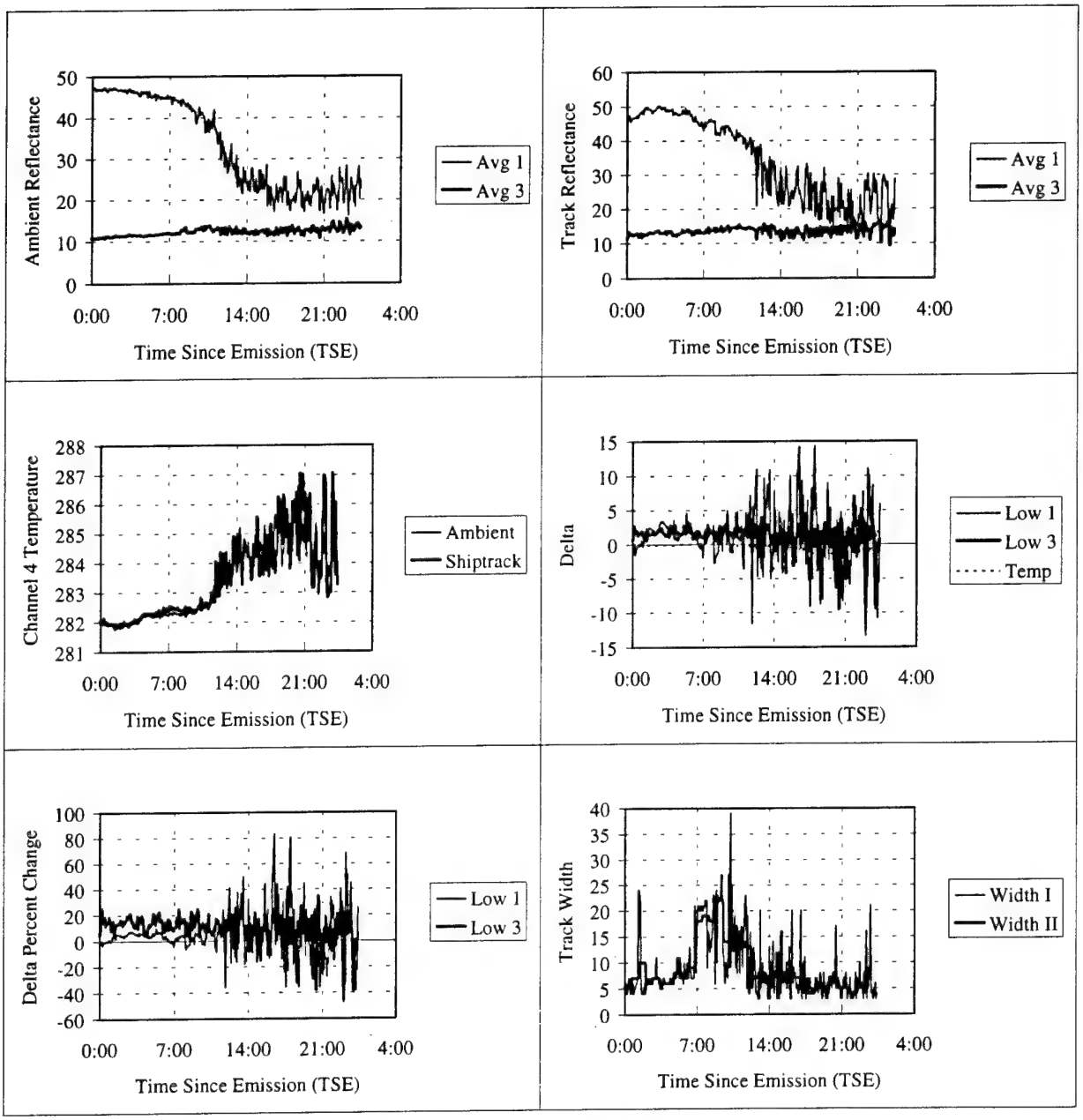

Figure A.1.e. TSE for Tai He (BOAB) 27 June 1994 1651 UTC

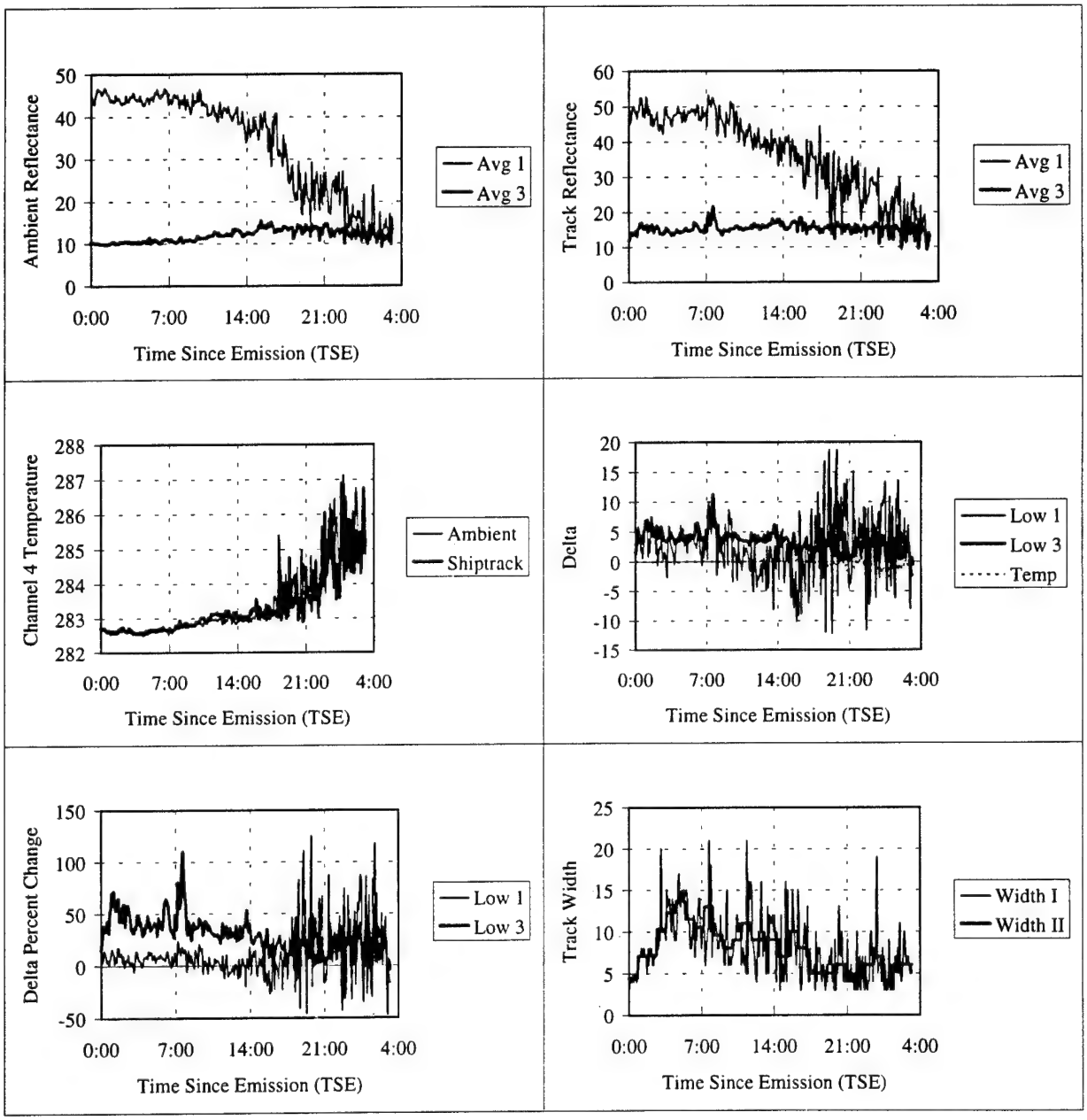

Figure A.1.f. TSE for Tai He (BOAB) 27 June 1994 1753 UTC

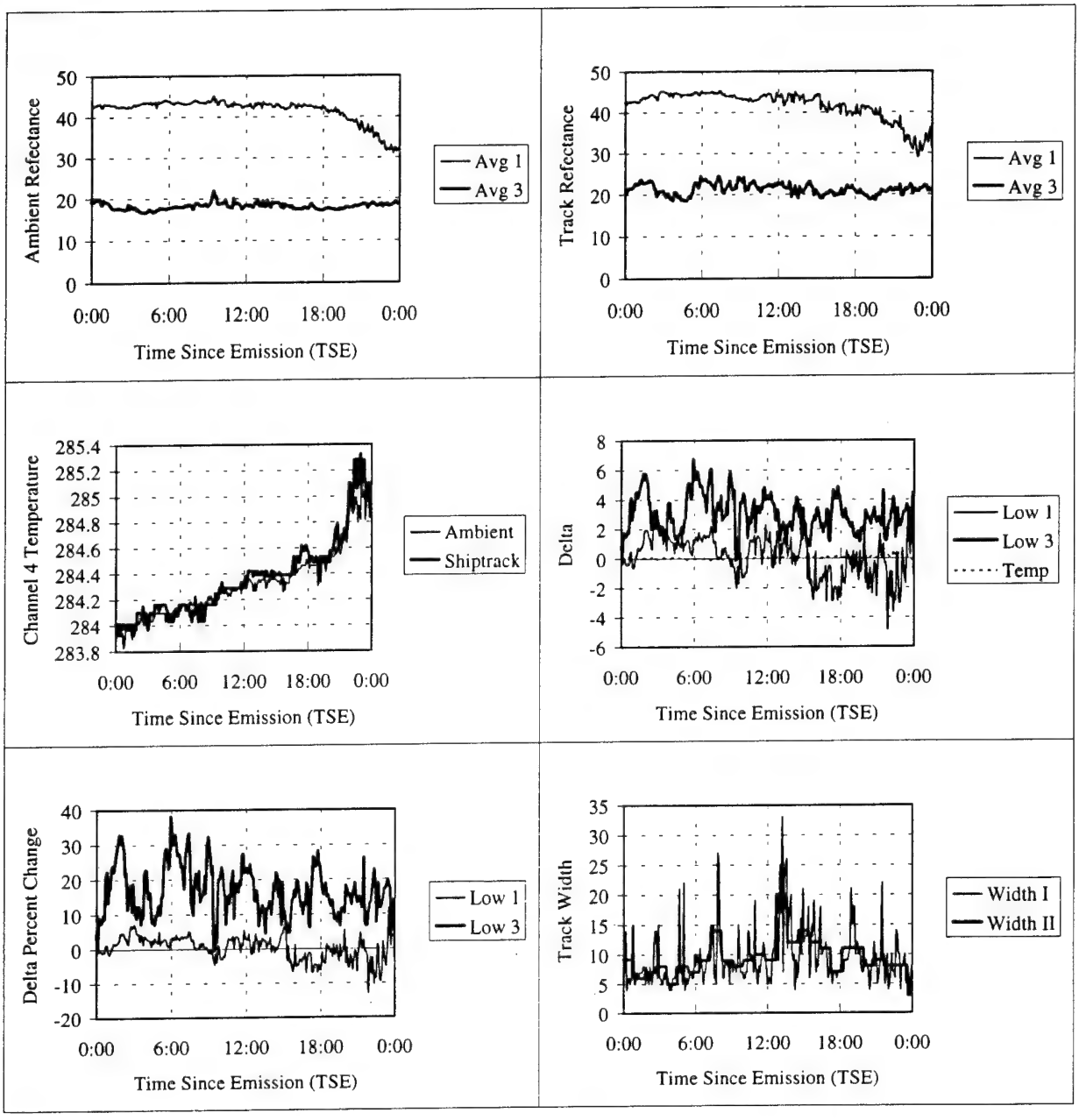

Figure A.1.g. TSE for Tai He (BOAB) 28 June 1994 0116 UTC

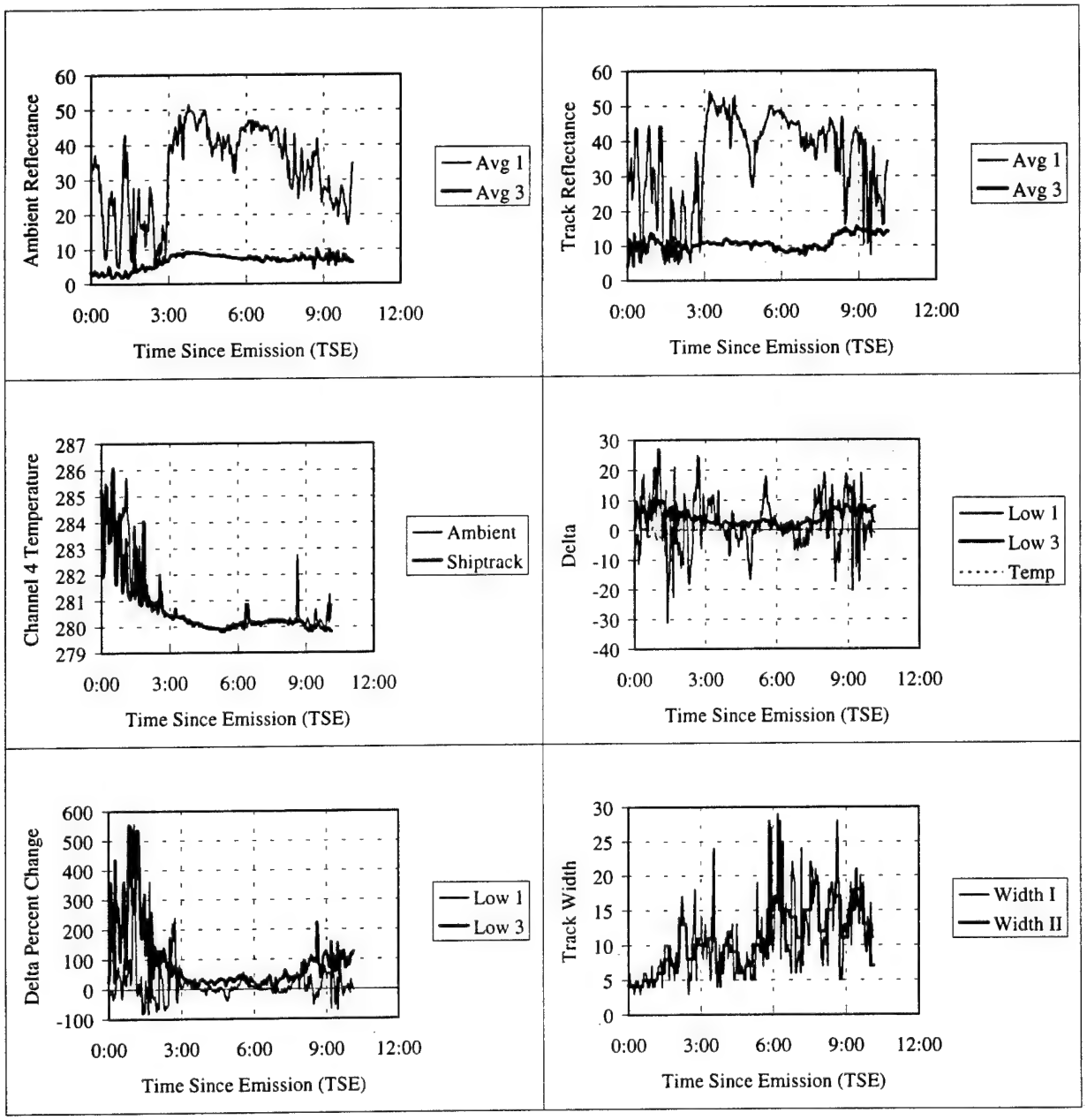

Figure A.2.a. TSE for Zim America (4XGR) 27 June 1994 1753 UTC

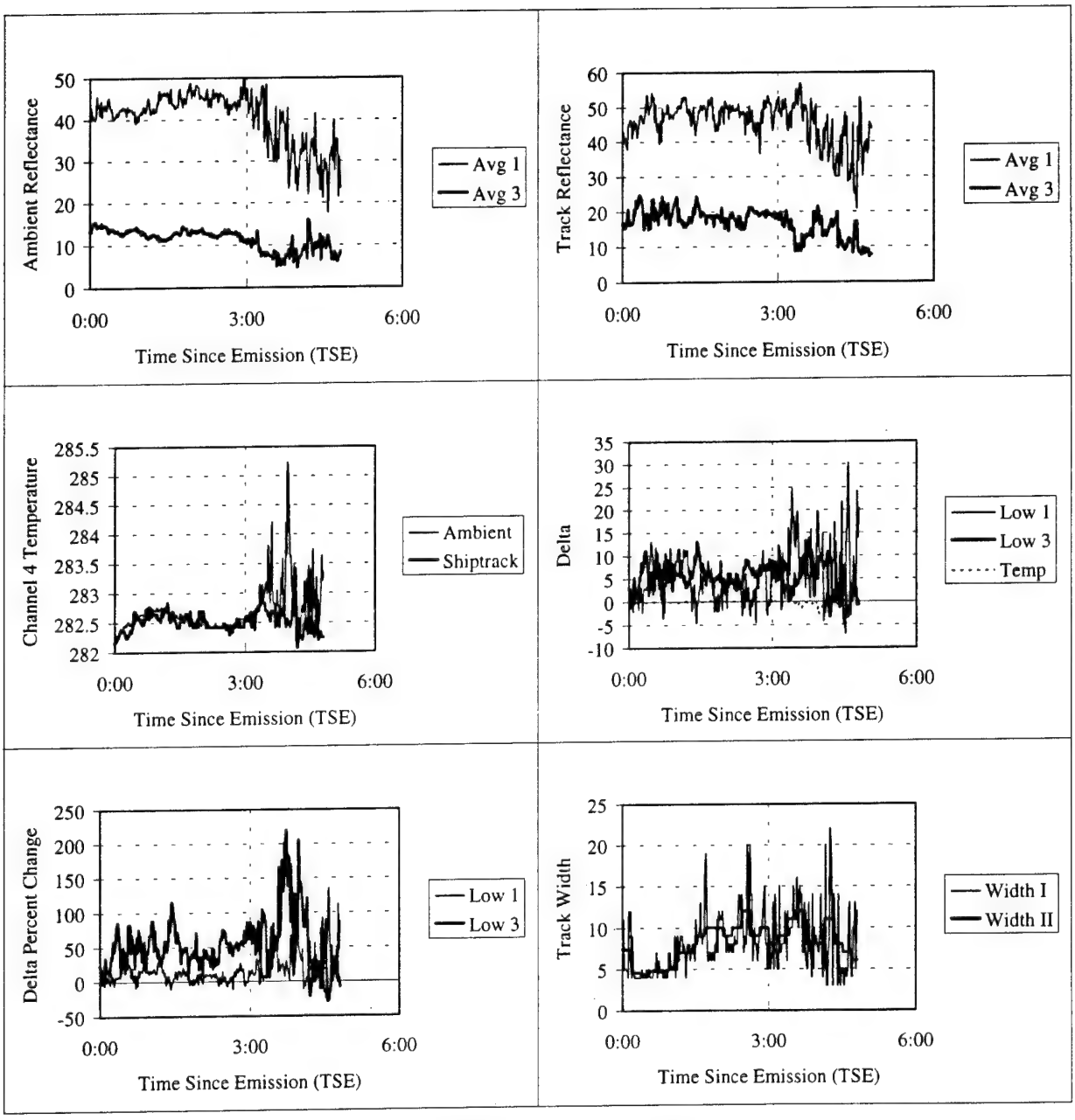

Figure A.2.b. TSE for Zim America (4XGR) 28 June 1994 0116 UTC

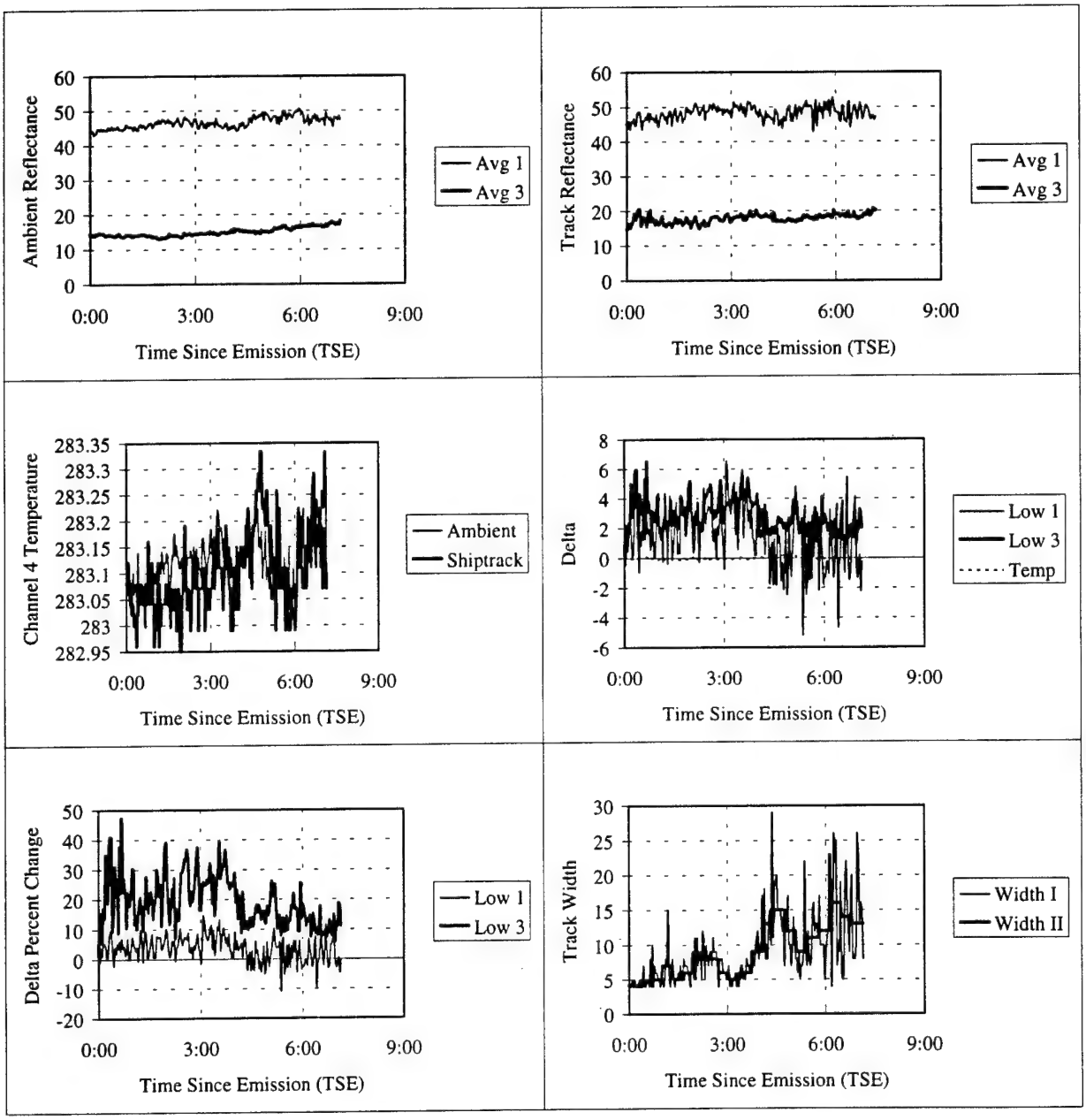

Figure A.2.c. TSE for Zim America (4XGR) 28 June 1994 1629 UTC

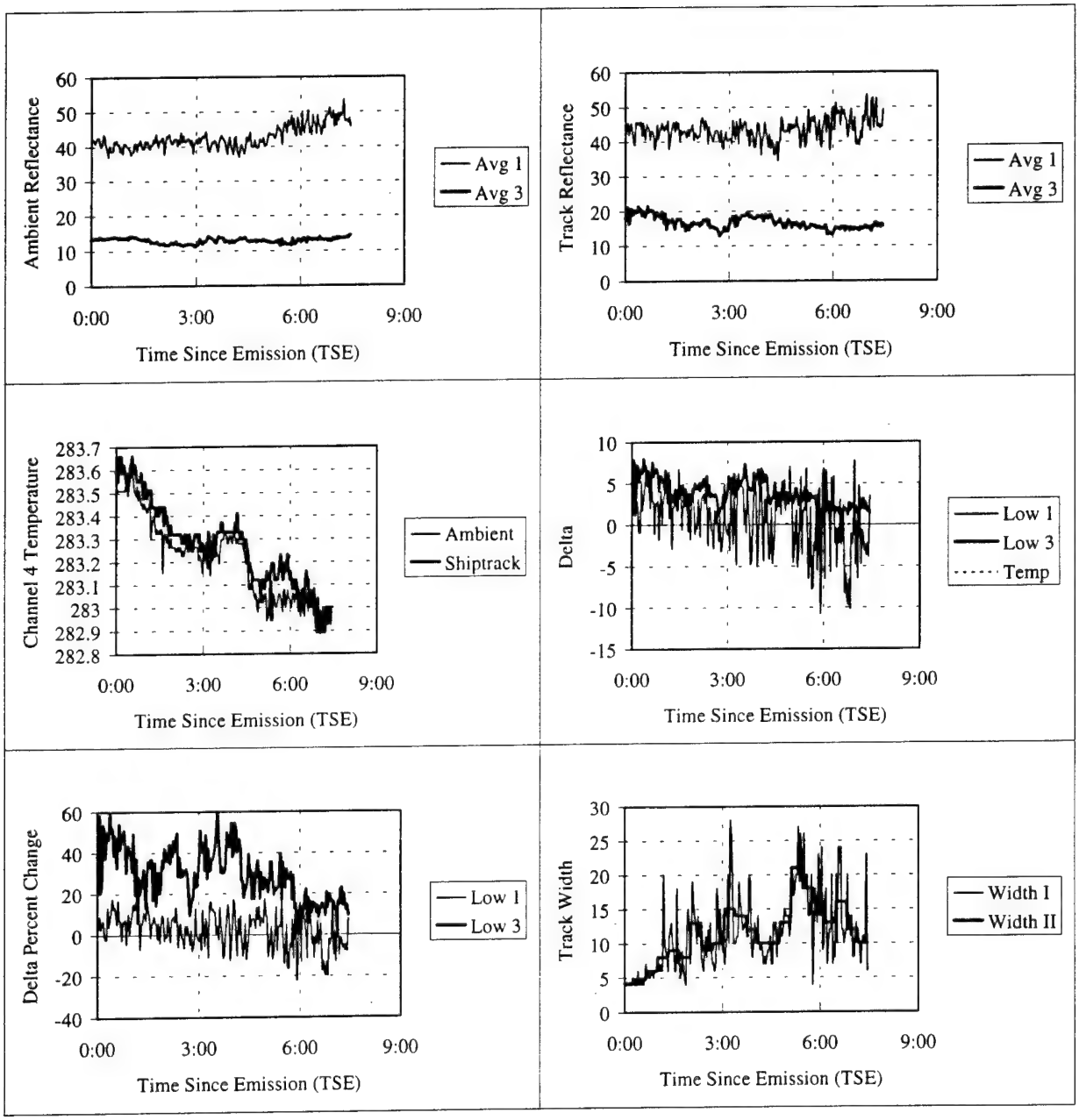

Figure A.2.d. TSE for Zim America (4XGR) 28 June 1994 1740 UTC

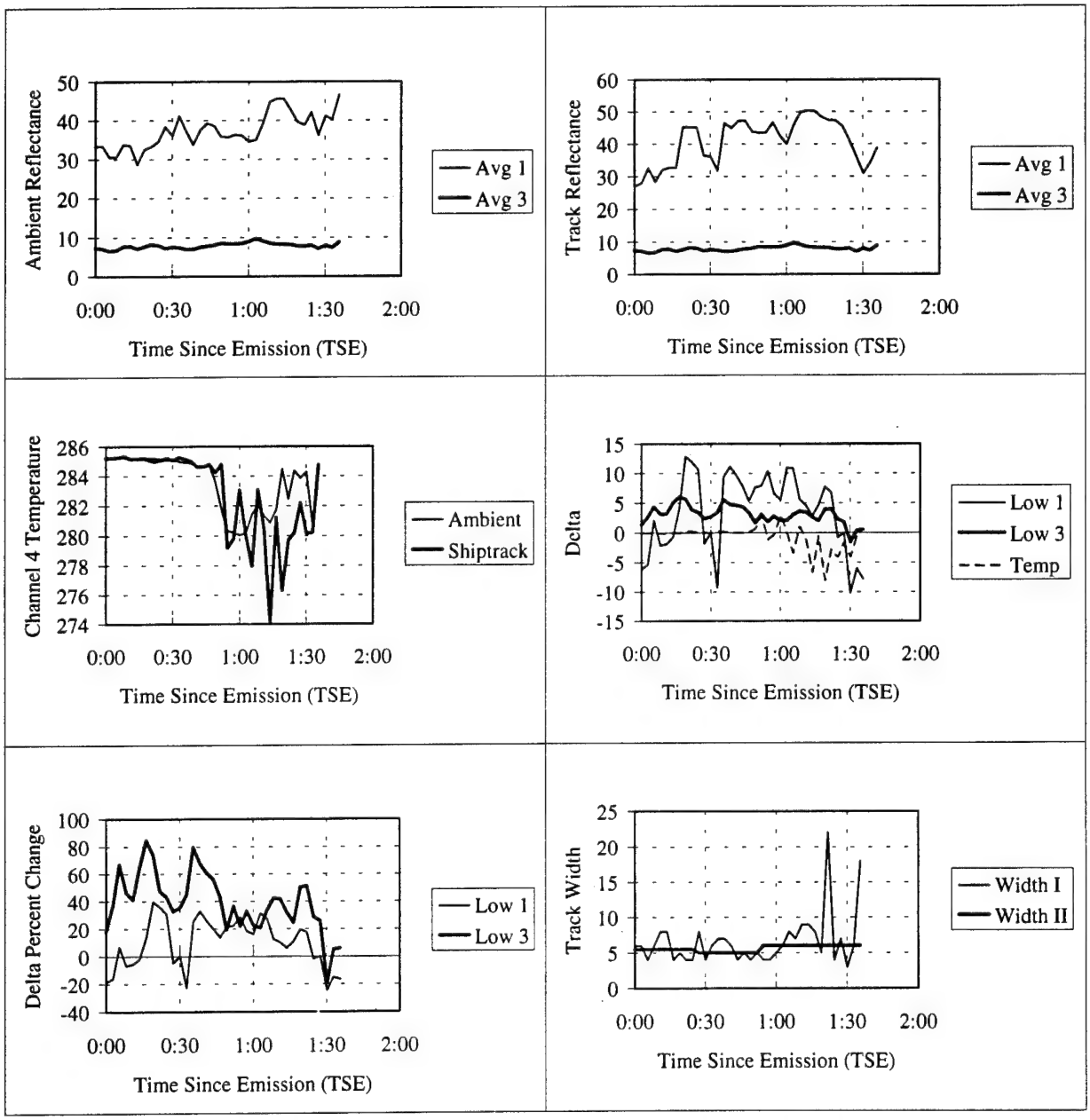

Figure A.3.a. TSE for Century Highway (8JNP) 13 June 1994 1653 UTC

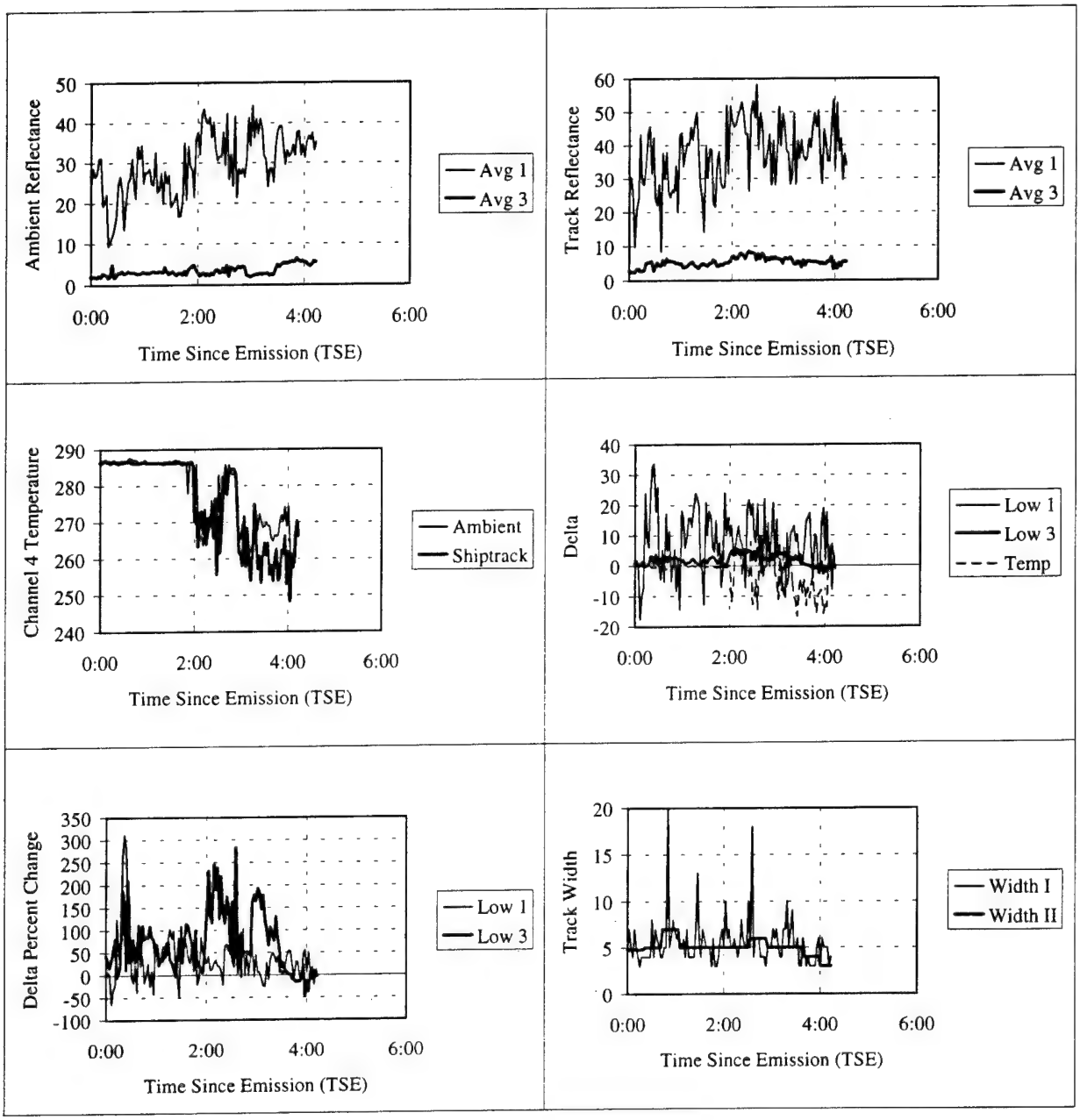

Figure A.3.b. TSE for Century Highway (8JNP) 14 June 0047 UTC

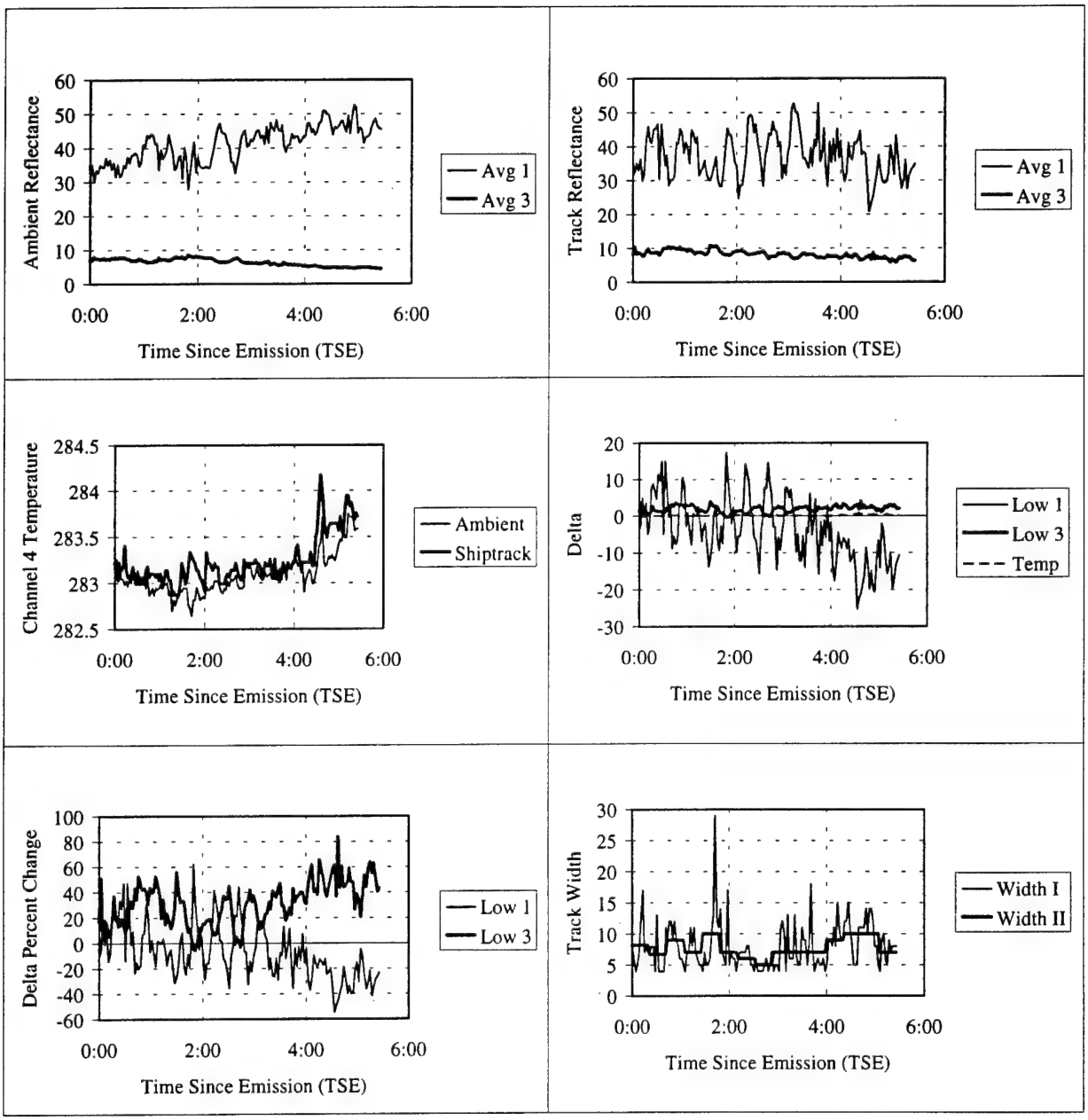

Figure A.3.c. TSE for Century Highway (8JNP) 14 June 1720 UTC

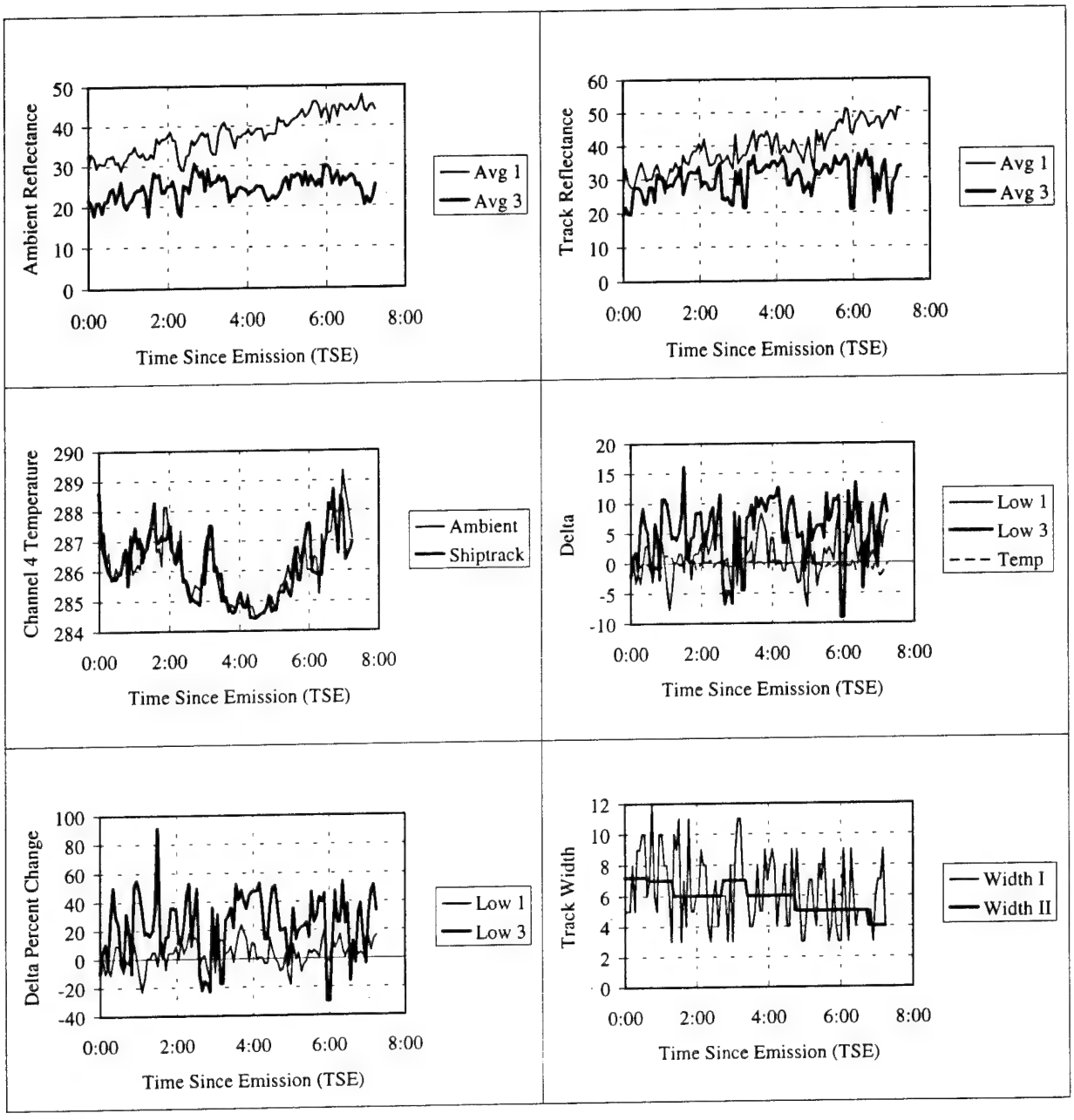

Figure A.3.d. TSE for Century Highway (8JNP) 15 June 0035 UTC

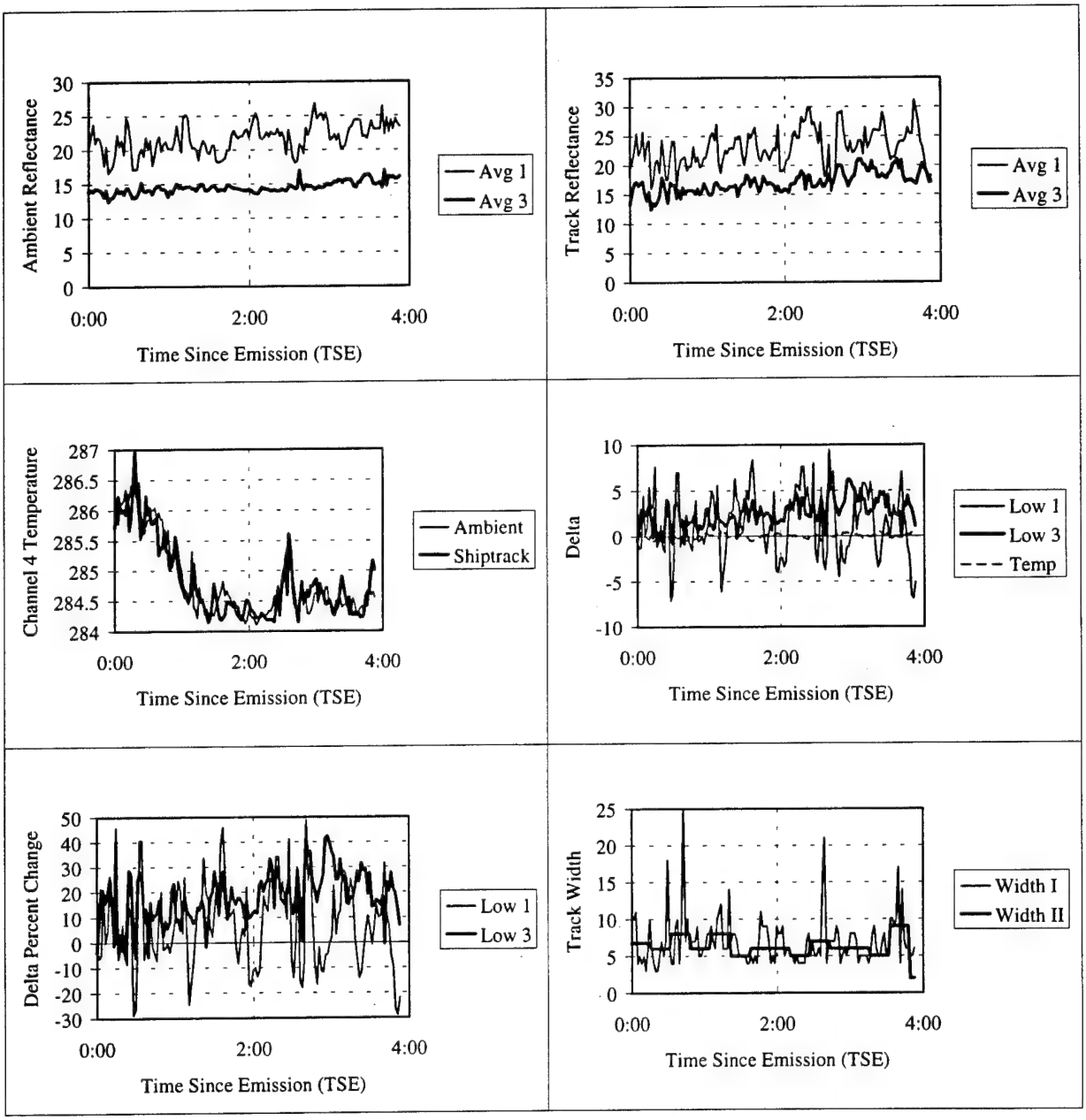

Figure A.3.e. TSE for Century Highway (8JNP) 15 June 1994 1707 UTC

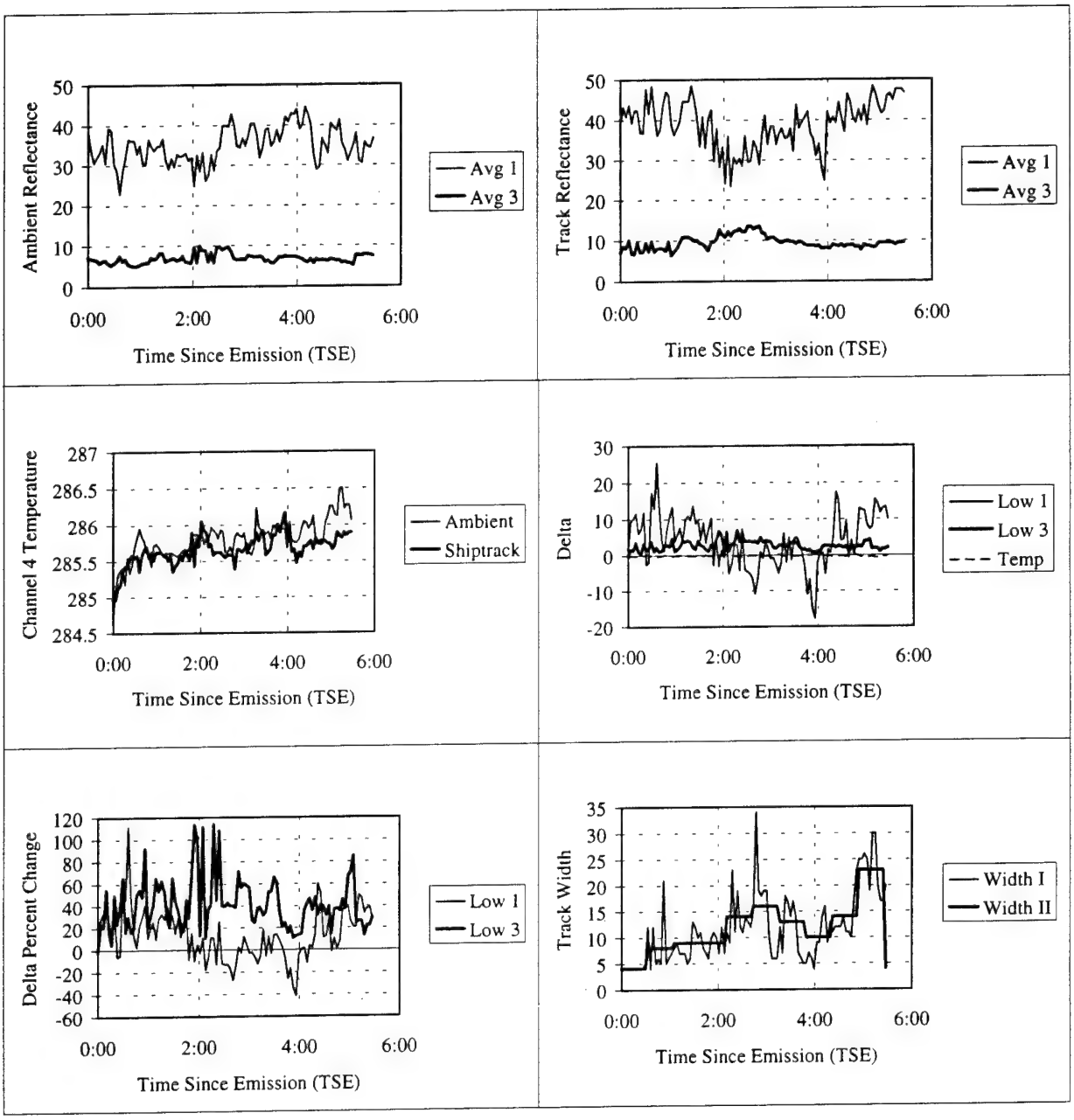

Figure A.4.a. TSE for Hercules Highway (JKOW) 13 June 1994 1653 UTC

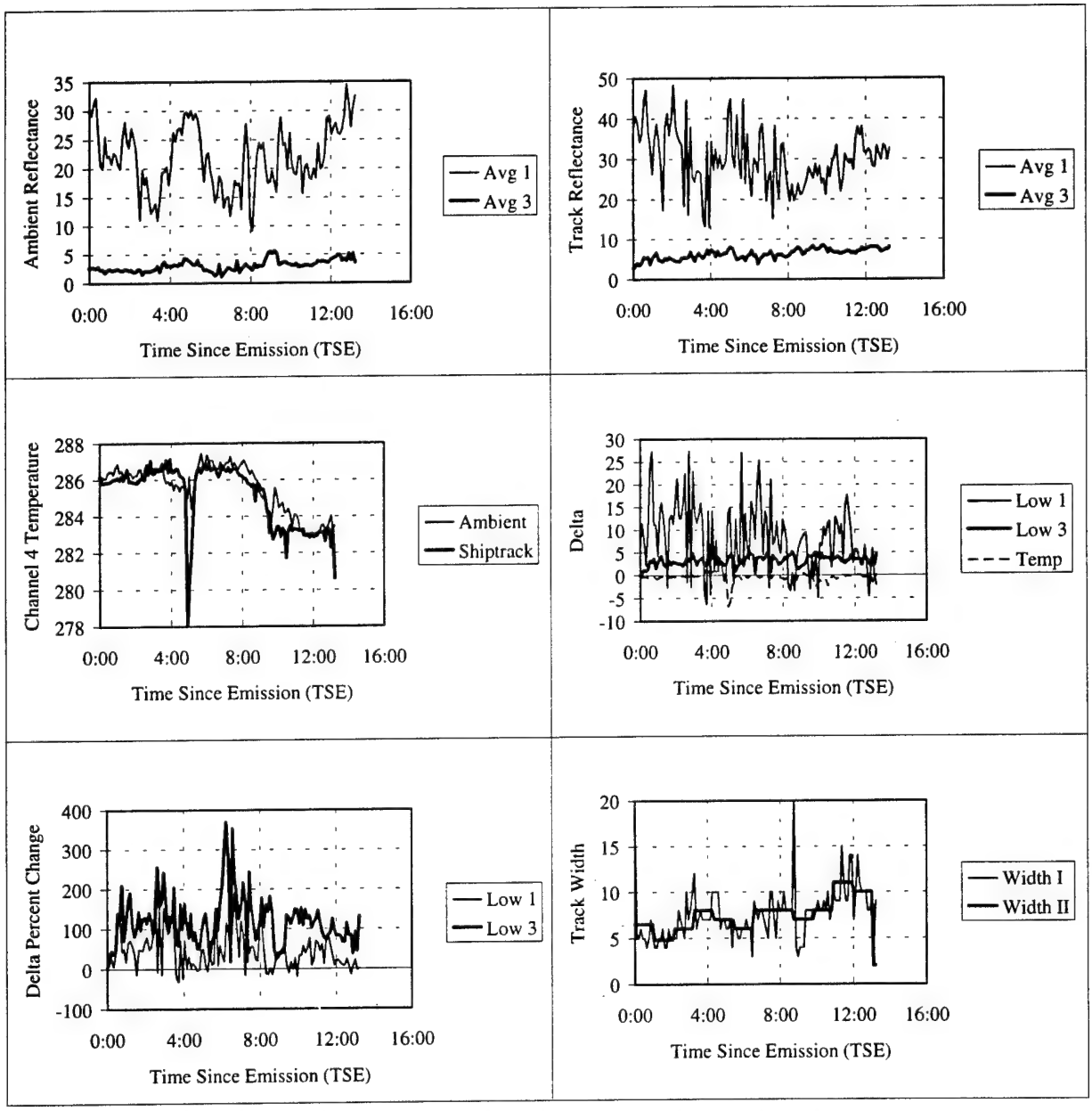

Figure A.4.b. TSE for Hercules Highway (JKOW) 14 June 1994 0047 UTC

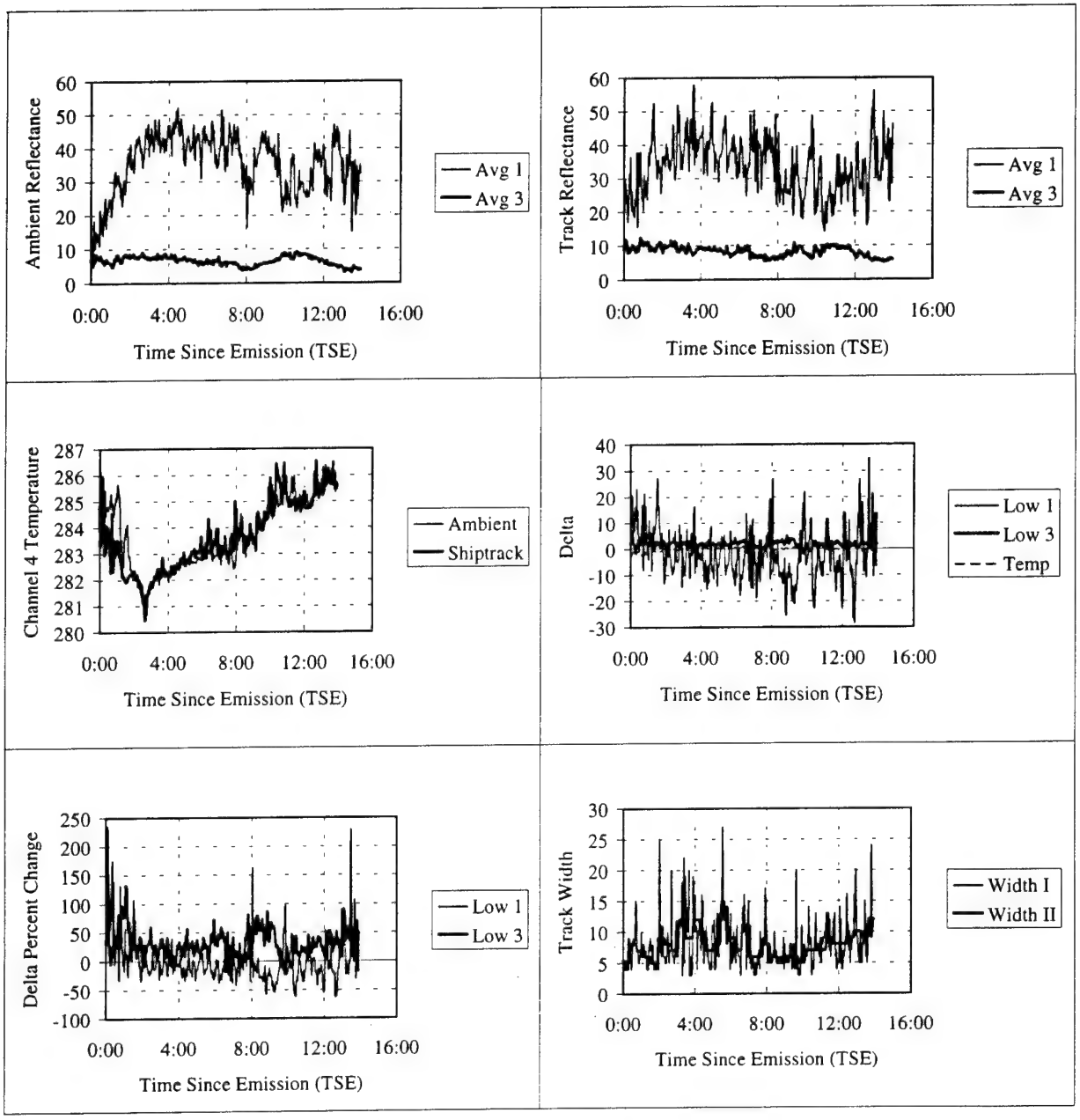

Figure A.4.c. TSE for Hercules Highway (JKOW) 14 June 1994 1720 UTC

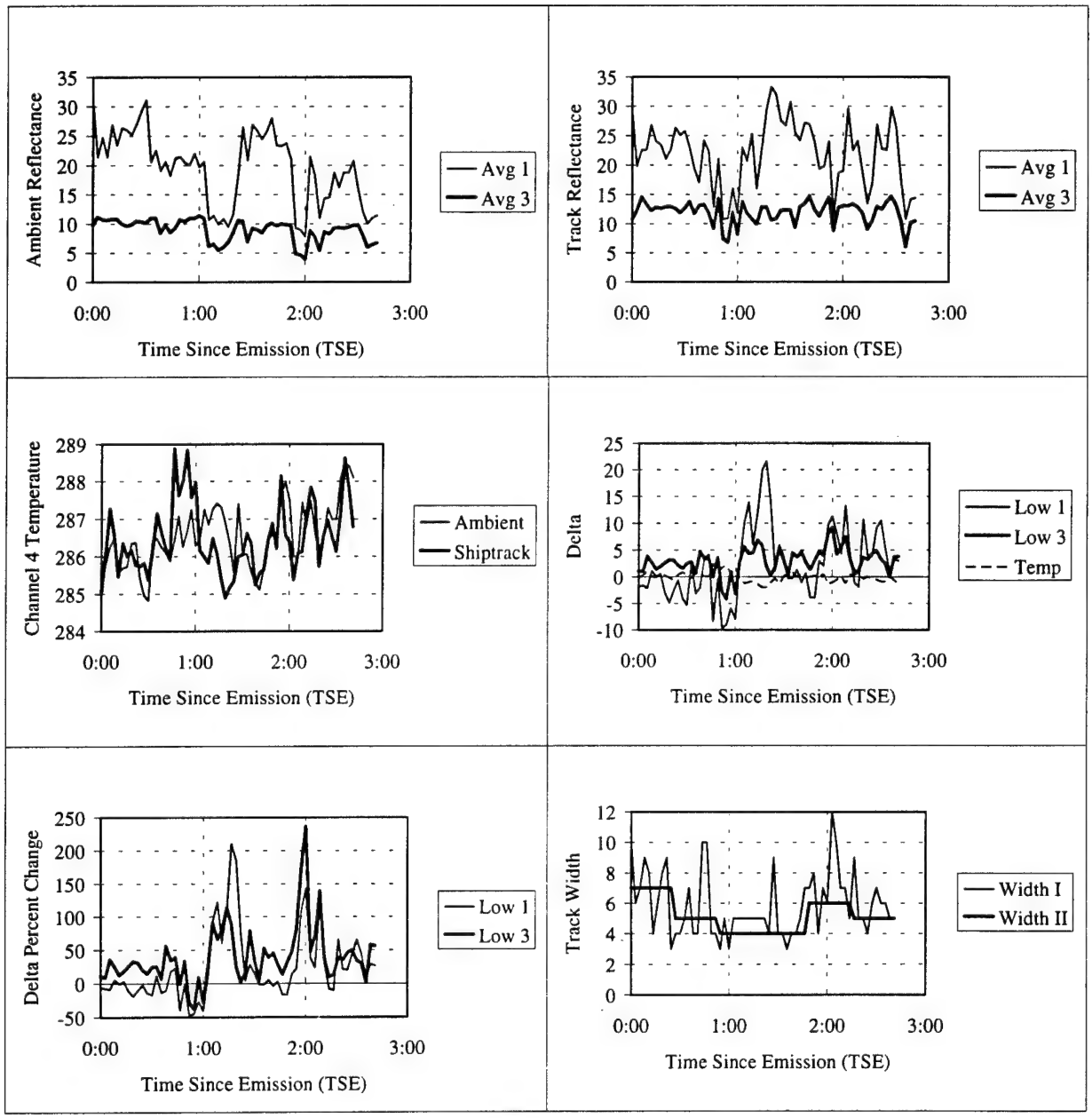

Figure A.4.d. TSE for Hercules Highway (JKOW) 15 June 1994 0035 UTC

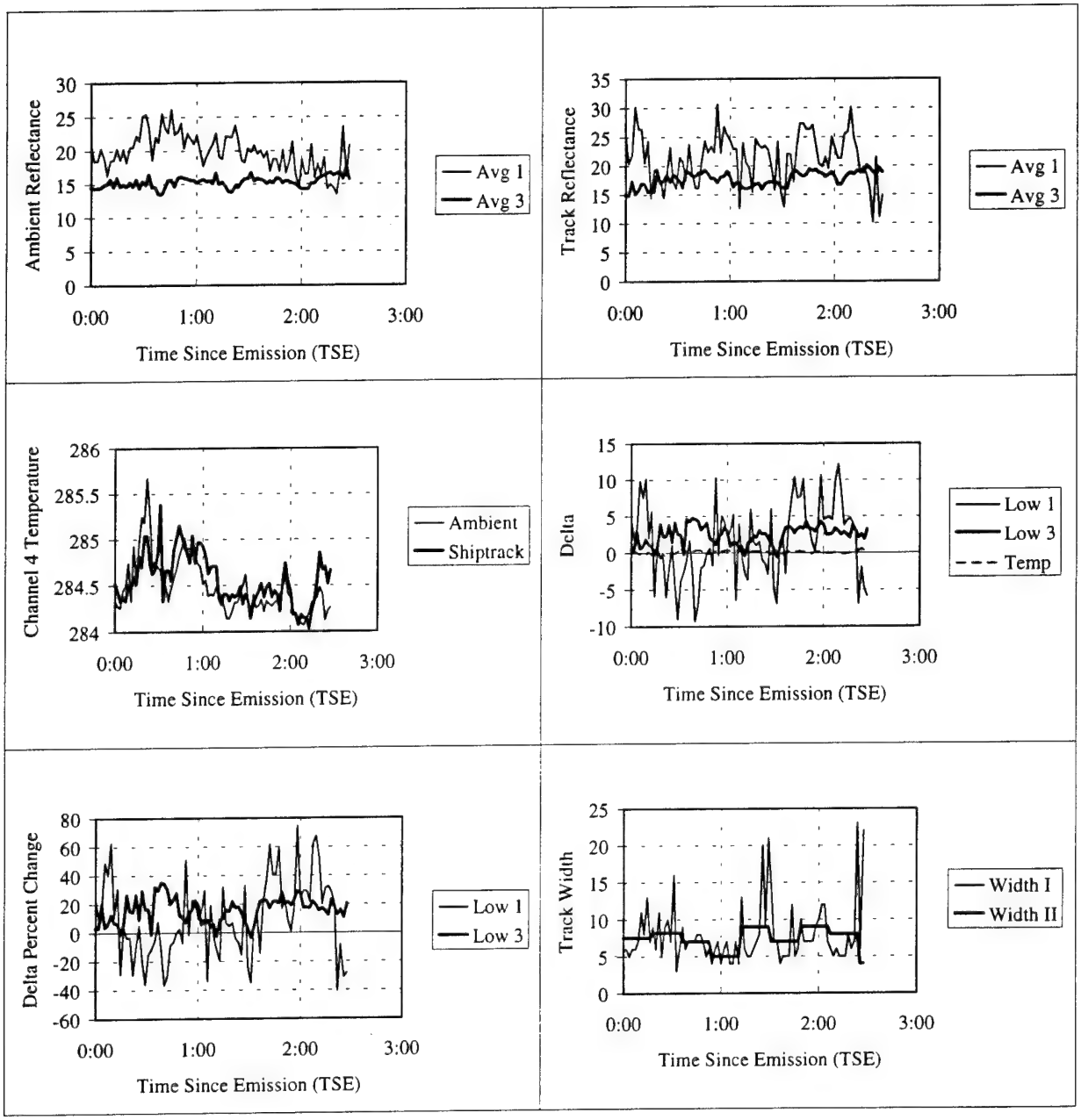

Figure A.4.e. TSE for Hercules Highway (JKOW) 15 June 1994 1707 UTC

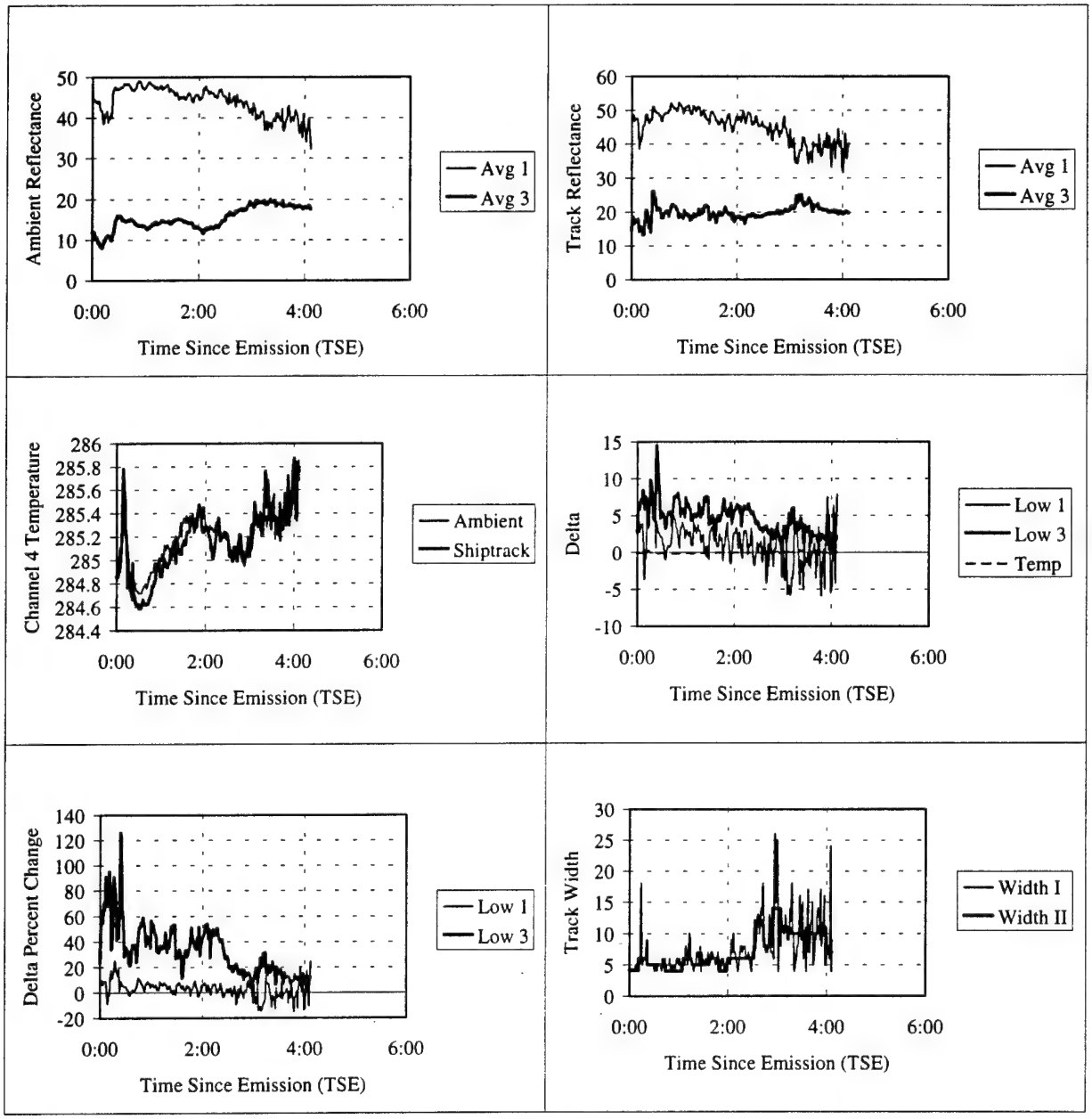

Figure A.5.a. TSE for Sea-Land Consumer (WCHF) 12 June 1994 1535 UTC

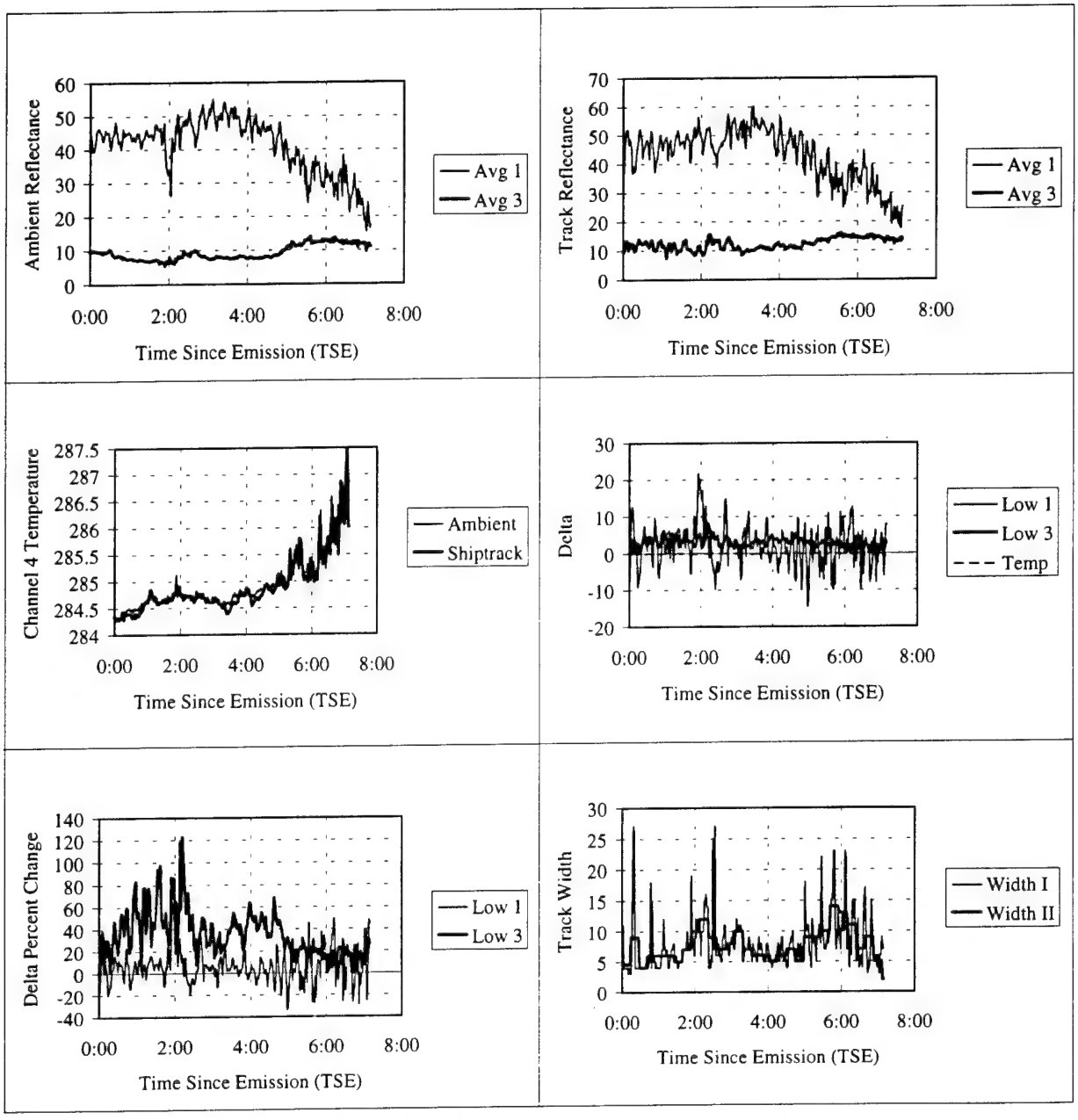

Figure A.5.b. TSE for Sea-Land Consumer (WCHF) 12 June 1994 1745 UTC

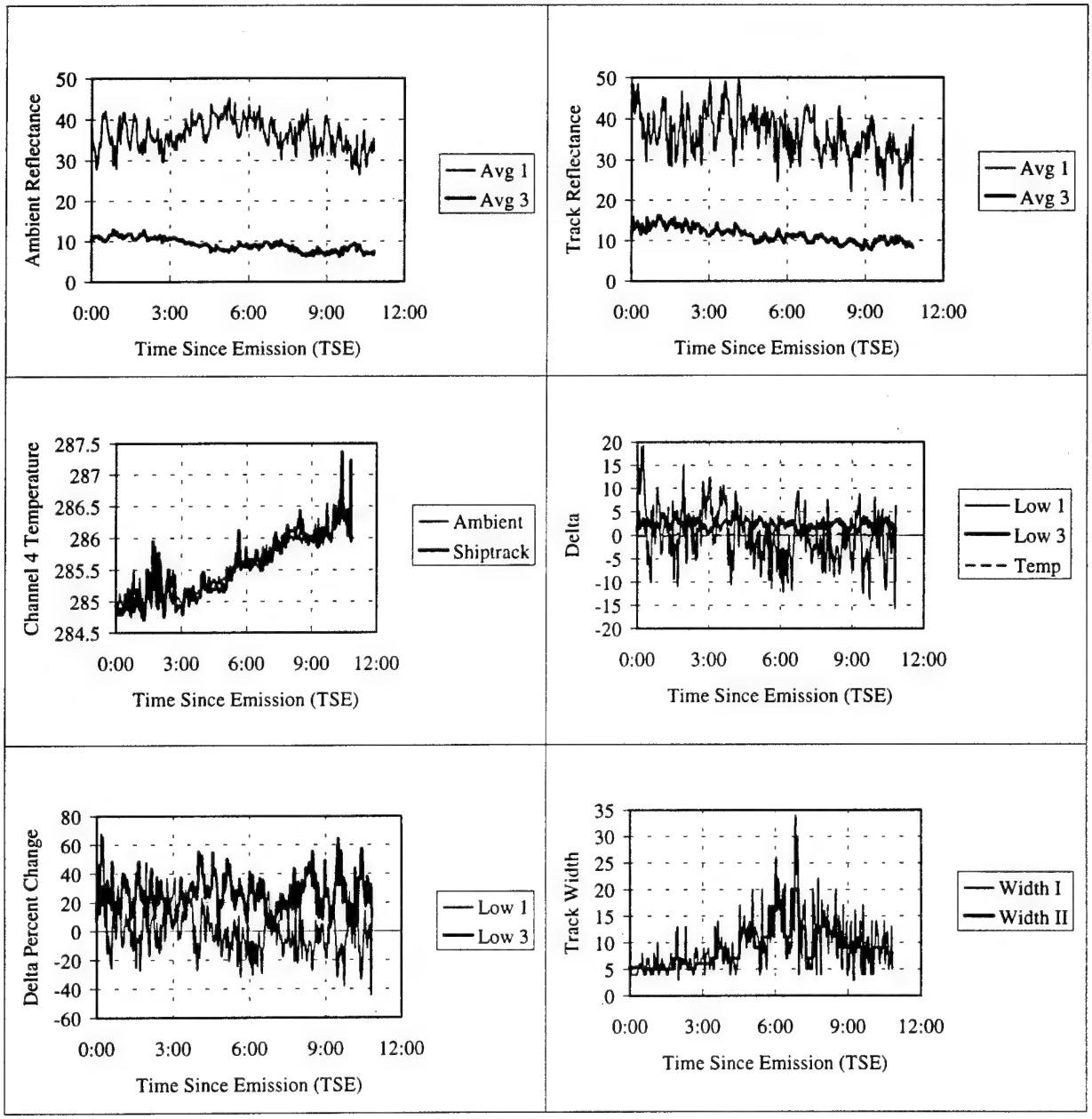

Figure A.5.c. TSE for Sea-Land Consumer (WCHF) 13 June 1994 0054 UTC

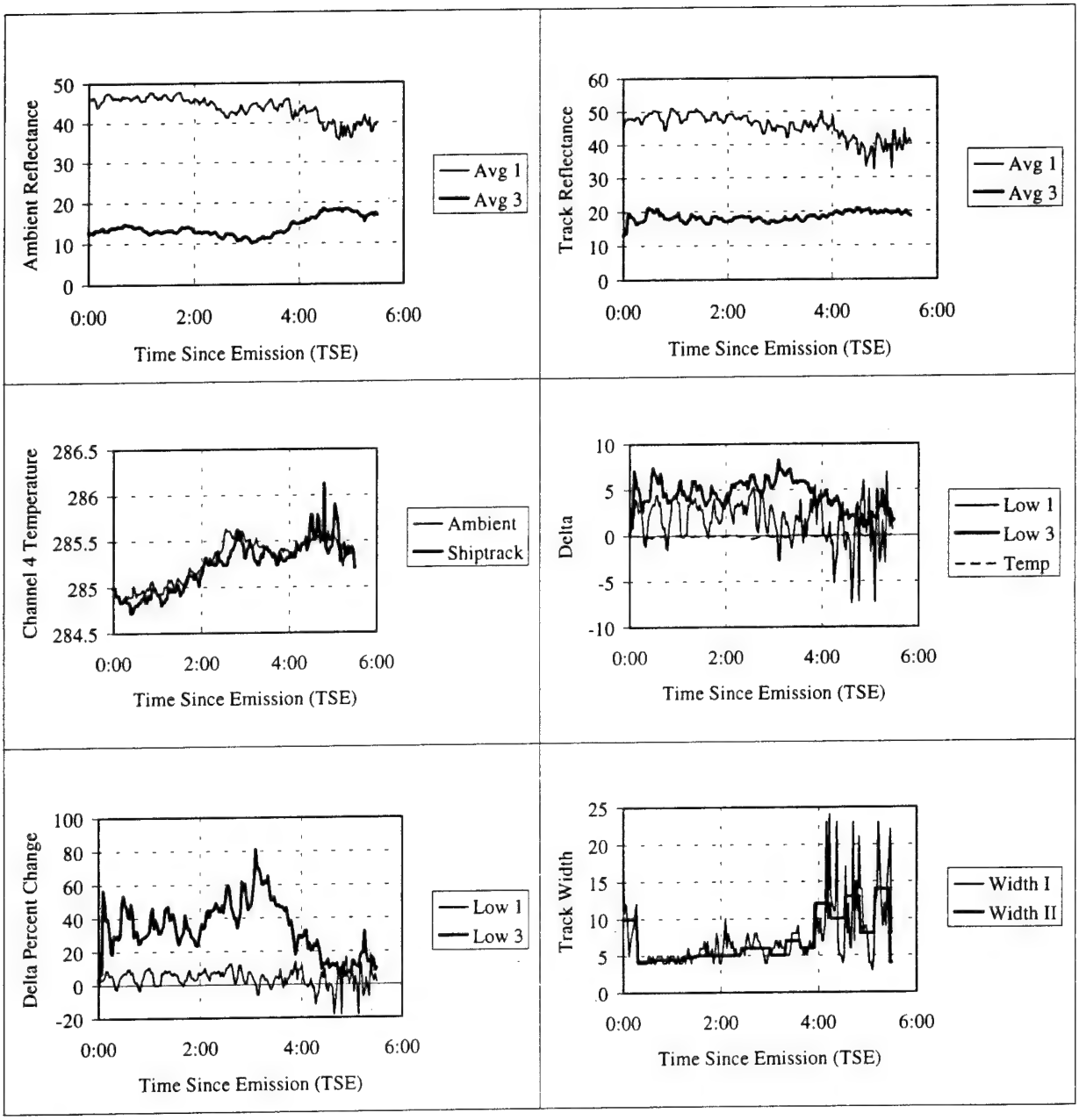

Figure A.6.a. TSE for Manulani (KNIJ) 12 June 1994 1535 UTC

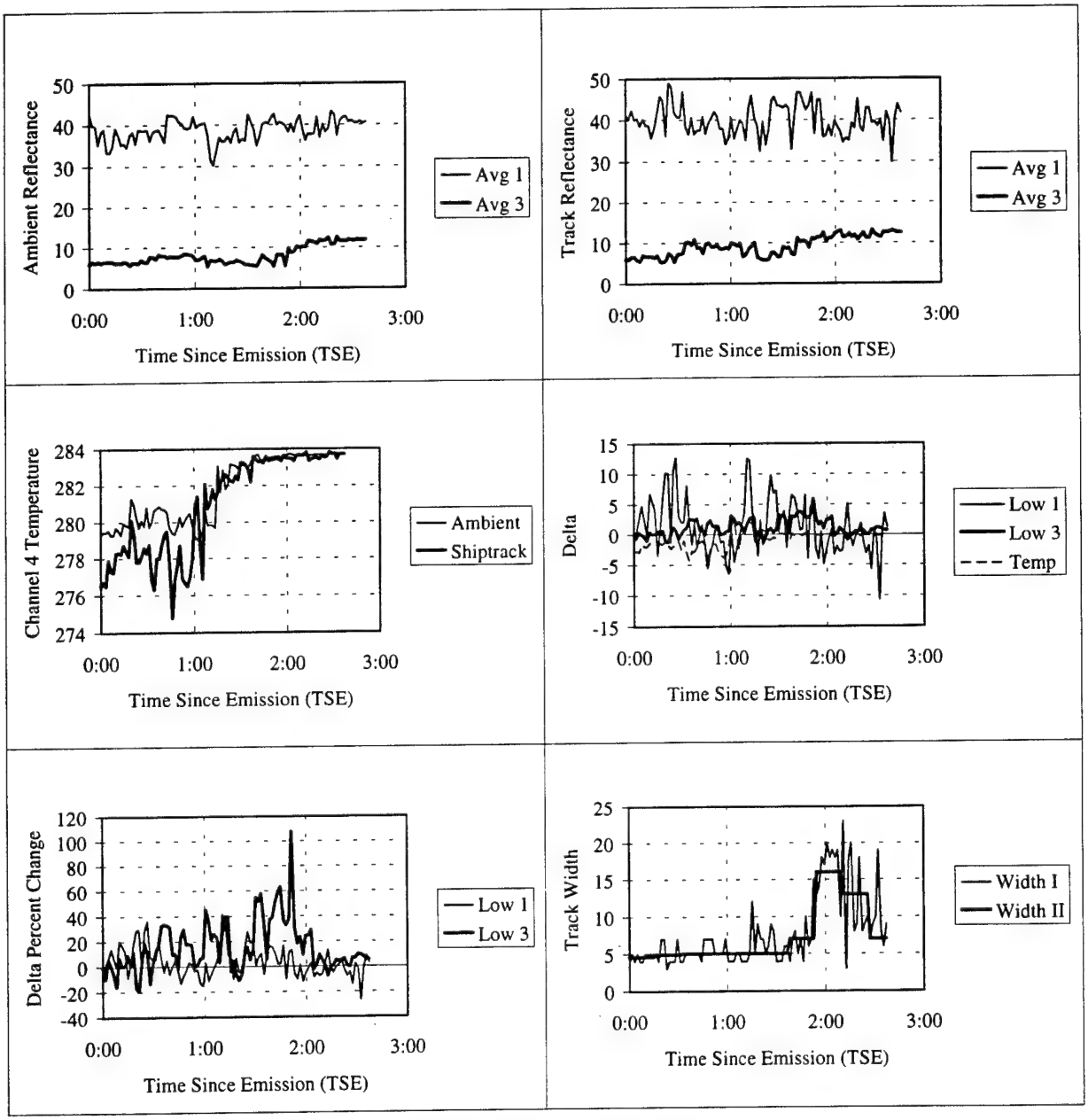

Figure A.6.b. TSE for Manulani (KNIJ) 12 June 1994 1745 UTC

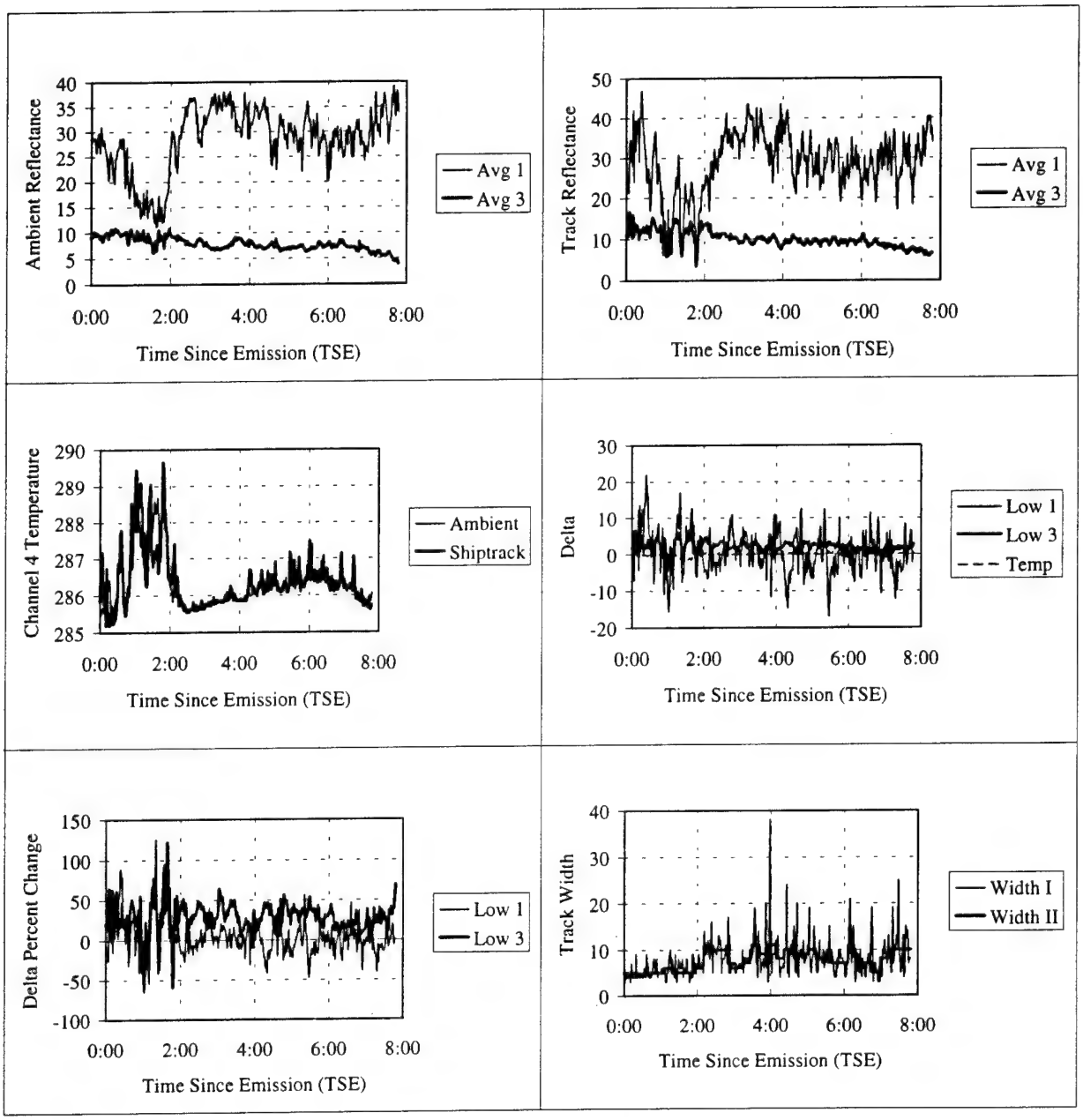

Figure A.6.c. TSE for Manulani (KNIJ) 13 June 1994 0054 UTC

LIST OF REFERENCES

Albrecht, B.A., 1989: Aerosols, cloud microphysics and fractional cloudiness. Science, 245, 1227-1230.

Brenner, J. R., 1994: Continental Aerosol Effects on Stratocumulus Microphysics During MAST 1994. M.S. Thesis, Naval Postgraduate School, Monterey, CA, 60pp.

Charlson, R.J., S.E. Schwartz, J.M. Hales, R.D. Cess, J.A. Coakley Jr., J.E. Hansen and D.J. Hofman, 1992: Climate forcing by anthropogenic aerosols. Science, 255, 423-430.

Charlson, R.J., J.E. Lovelock, M.O. Andreae, and S.G. Warren, 1987: Oceanic phytoplankton, atmospheric sulphur, cloud albedo, and climate. Nature, 326, 655-661.

Coakley, J.A. Jr., R.L. Bernstein and P.A. Durkee, 1987: Effect of ship-stack effluents on cloud reflectivity. Science, 237, 1020-1022.

Conover, J.H., 1966: Anomalous Cloud Lines. J. Atmos. Sci., 23, 778-785.

Durkee, P.A., 1994: Monterey Area ShipTrack Experiment [CNO Project K-1420] Science Plan. 42pp.

Evans, M.E., 1992: Analysis of shiptracks in cloudiness transition regions. M.S. Thesis, Naval Postgraduate School, Monterey, CA, 93pp.

Gifford, F. A., 1980: Smoke as a Quantitative Atmospheric Diffusion Tracer. Atmospheric Environment, 14, 1119-1121.

King, M.D., T. Nakajima and L.F. Radke, 1990: Optical properties of marine stratocumulus clouds modified by ship track effluents. Preprints of 1990 Meeting of the American Meteorological Society, San Francisco, CA, 396-400.

Mays, D., 1993: Shiptrack database analysis. M.S. Thesis, Naval Postgraduate School, Monterey, CA, 60pp.

Mikkelsen, T., 1983: The Borris Field Experiment: Observations of Smoke Diffusion in the Surface Layer over Homogenous Terrain. Risø-R-479. 61 pp.

Millman, T., 1992: A temporal analysis of east Pacific and east Atlantic shiptracks. M.S. Thesis, Naval Postgraduate School, Monterey, CA. 69pp.

Office of Naval Research, 1994: Monterey Area ShipTrack Experiment [CNO Project K-1420] Operations Plan, pp. 1.1 - B12.

Pettigrew, J.C., 1992: Surface meteorological parameters of identified shiptracks. M.S. Thesis, Naval Postgraduate School, Monterey, CA, 71pp.

Radke, L.F., J.A. Coakley, Jr. and M.D. King, 1989: Direct and remote sensing observations of the effects of ships on clouds. Science, 246, 1146-1149.

Trehubenko, E. J., 1994: Shiptracks in the Californian Stratus Region: Dependency on Marine Atmospheric Boundary Layer Depth. M.S. Thesis, Naval Postgraduate School, Monterey, CA, 87pp.

Twomey, S., 1968: On the composition of cloud nuclei in the northeasten United States. J. Rech. Atmos., 3, 281-285.

INITIAL DISTRIBUTION LIST

		No. Copies
1.	Defense Technical Information Center Cameron Station Alexandria, Virginia 22304-6145	2
2.	Library, Code 52 Naval Postgraduate School Monterey, California 93943-5002	2
3.	Chairman Code MR Department of Meteorology Naval Postgraduate School Monterey, California 93943-5002	1
4.	Chairman Code OC Department of Oceanography Naval Postgraduate School Monterey, California 93943-5002	1
5.	Professor Philip Durkee Code OC/De Department of Oceanography Naval Postgraduate School Monterey, California 93943-5002	1
6.	Professor Kenneth Davidson (Code MR/DS) Department of Oceanography Naval Postgraduate School Monterey, California 93943-5002	1
7.	Mr. Bob Bluth Code 4513 Office of Naval Research Room 522 800 North Quincy St. Arlington, Virginia 22217-5000	1

8. Mr. David Johnson — 1
Code 1243 Office of Naval Research
Room 522
800 North Quincy St.
Arlington, Virginia 22217-5000

9. Oceanographer of the Navy — 1
Naval Observatory
34th and Massachusetts Avenue NW
Washington, DC 20390-5000

10. Commander — 1
Naval Meteorology and Oceanography Command
Stennis Space Center, Mississippi 39529-5000

11. Chief of Naval Research — 1
800 North Quincy Street
Arlington, Virginia 22217

12. Commanding Officer — 1
Fleet Numerical Meteorology and Oceanography Center
Monterey, California 93943

13. LCDR Andrew Brown III — 2
Naval Pacific Meteorology and Oceanography Facility
NAS North Island, Bldg. 14
San Diego, California 92135-7076